Volume 51
Number 22
21 November 2022
Pages 9177–9426

Chem Soc Rev

Chemical Society Reviews

rsc.li/chem-soc-rev

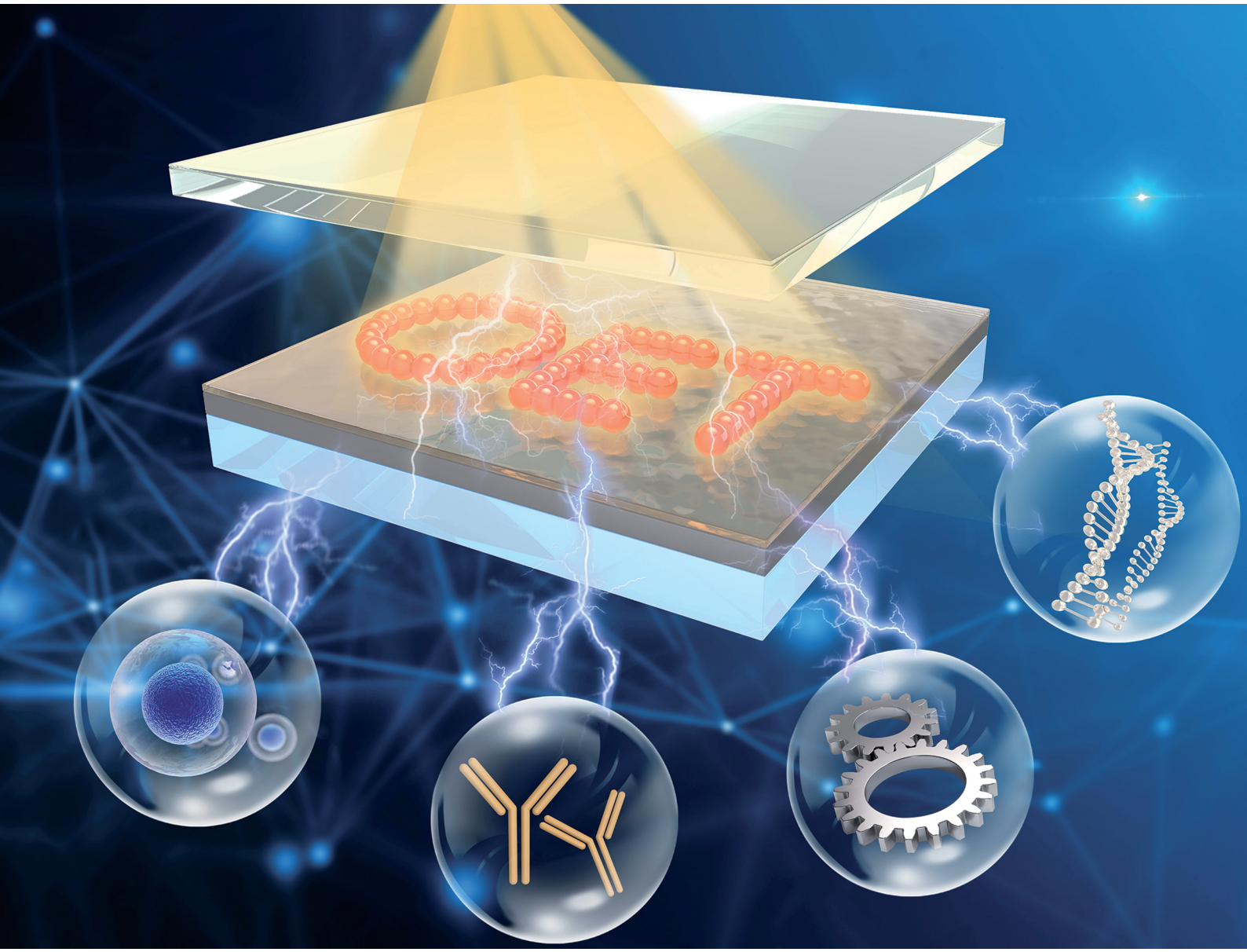

ISSN 0306-0012

ROYAL SOCIETY OF CHEMISTRY

REVIEW ARTICLE

Shuailong Zhang *et al.*

Optoelectronic tweezers: a versatile toolbox for nano-/micro-manipulation

Chem Soc Rev

REVIEW ARTICLE

View Article Online
View Journal | View Issue

Cite this: *Chem. Soc. Rev.*, 2022, 51, 9203

Optoelectronic tweezers: a versatile toolbox for nano-/micro-manipulation

Shuailong Zhang,[*abc] Bingrui Xu,[ab] Mohamed Elsayed,[de] Fan Nan,[f] Wenfeng Liang,[g] Justin K. Valley,[h] Lianqing Liu,[ij] Qiang Huang,[abc] Ming C. Wu[k] and Aaron R. Wheeler[del]

The rapid development of micromanipulation technologies has opened exciting new opportunities for the actuation, selection and assembly of a variety of non-biological and biological nano/micro-objects for applications ranging from microfabrication, cell analysis, tissue engineering, biochemical sensing, to nano/micro-machines. To date, a variety of precise, flexible and high-throughput manipulation techniques have been developed based on different physical fields. Among them, optoelectronic tweezers (OET) is a state-of-art technique that combines light stimuli with electric field together by leveraging the photoconductive effect of semiconductor materials. Herein, the behavior of micro-objects can be directly controlled by inducing the change of electric fields on demand in an optical manner. Relying on this light-induced electrokinetic effect, OET offers tremendous advantages in micromanipulation such as programmability, flexibility, versatility, high-throughput and ease of integration with other characterization systems, thus showing impressive performance compared to those of many other manipulation techniques. A lot of research on OET have been reported in recent years and the technology has developed rapidly in various fields of science and engineering. This work provides a comprehensive review of the OET technology, including its working mechanisms, experimental setups, applications in non-biological and biological scenarios, technology commercialization and future perspectives.

Received 6th May 2022

DOI: 10.1039/d2cs00359g

rsc.li/chem-soc-rev

1. Introduction

Optical micromanipulation is a family of technologies that use light to trap and actuate tiny objects. The first optical micromanipulation technology, later named optical tweezers, was invented by Arthur Ashkin in the 1980s.[1–3] Since then, optical tweezers have been widely used in many fields of physical,[4–11] chemical[12–15] and biological sciences,[16–21] fundamentally shaping the experimental study in the microscopic world. In 2018, the Nobel Prize in Physics was awarded to Arthur Ashkin for the invention of optical tweezers,[22] demonstrating the significance of this technology and its scientific impact. Although optical tweezers are a useful and powerful tool, there exist several challenges. For example, optical tweezers are only capable of reliably actuating small objects (from nanometer size up to a few tens of microns); this fundamental limit is a result of the diminutive forces of optical tweezers, which are on the order of picoNewtons (10^{-12} N). Additionally, optical tweezers can only manipulate objects that are transparent to the light beam, which sets a firm limit on the materials of the objects. Last but not least, optical tweezers require the use of high numerical aperture lens and sophisticated beam-shaping optics, and also

[a] School of Mechatronical Engineering, Beijing Institute of Technology, Room 711, Building No 6, Science and Technology Park, 5 Zhongguancun South St, Haidian District, Beijing, 100081, China. E-mail: shuailong.zhang@bit.edu.cn; Tel: +86-010-68917730
[b] Beijing Advanced Innovation Center for Intelligent Robots and Systems, Beijing Institute of Technology, Beijing, 100081, China
[c] Key Laboratory of Biomimetic Robots and Systems (Beijing Institute of Technology), Ministry of Education, Beijing 100081, China
[d] Institute of Biomedical Engineering, University of Toronto, Toronto, ON, M5S 3G9, Canada
[e] Donnelly Centre for Cellular and Biomolecular Research, University of Toronto, Toronto, ON, M5S 3E1, Canada
[f] Institute of Nanophotonics, Jinan University, Guangzhou 511443, China
[g] School of Mechanical Engineering, Shenyang Jianzhu University, Shenyang, 110168, China
[h] Berkeley Lights, Inc, 5858 Horton Street #320, Emeryville, CA 94608, USA
[i] State Key Laboratory of Robotics, Shenyang Institute of Automation, Chinese Academy of Sciences, Shenyang 110016, China
[j] Institutes for Robotics and Intelligent Manufacturing, Chinese Academy of Sciences, Shenyang 110016, China
[k] Department of Electrical Engineering and Computer Sciences, University of California, Berkeley, California 94720, USA
[l] Department of Chemistry, University of Toronto, Toronto, ON, M5S 3H6, Canada

can induce a detrimental photothermal effect in biological samples. These challenges are substantial and are at least part of the reason that optical tweezers are still mostly used for niche and high-end applications in research labs.

Inspired by optical tweezers and also driven by the need to overcome the aforementioned challenges, substantial research efforts have been devoted to the development of other optical micromanipulation technologies, including optothermal tweezers,[23–28] plasmonic tweezers,[29–34] optoacoustic tweezers,[35,36] and optoelectronic tweezers (OET).[37–43] Among these technologies, OET is a promising one that has shown superior performance in many aspects,[37–43] and attracted much attention since its invention by Ming C. Wu and co-workers (Pei-Yu Chiou, Aaron T. Ohta) in 2005.[44] OET is a powerful opto-electro-fluidic technology that utilizes light-induced electrokinetic force to control and actuate nanoscale and microscale objects. OET combines the merits of photonics and electronics, and provides a user-friendly tool that enables flexible and parallel micromanipulation. Different from optical tweezers which rely on coherent laser light sources, a standard LED light source combined with a digital micromirror device (DMD) is mainly used in OET systems. DMD can modulate the LED light and generate programmable/animated light patterns on demand. By using an optical microscope, the light patterns can be projected onto a photoconductive substrate of an OET device. In the dark, the photoconductive substrate has high impedance and behaves like a resistor; when light is projected onto the photoconductive substrate, its impedance drops significantly due to the photoelectric effect and it can be seen as a conductor. Therefore, "light-induced virtual electrodes" can be formed by projecting light patterns to create illuminated and dark regions on the photoconductive substrate of an OET device. The "light-induced virtual electrodes" can generate a non-uniform electric field in the liquid medium to interact with the samples, producing electrokinetic force that controls their

Shuailong Zhang

Shuailong Zhang received his BS from Beijing Institute of Technology, Beijing, China in 2010, and his PhD degree from the University of Strathclyde, Glasgow, United Kingdom, in 2015. He joined the University of Glasgow and worked as a postdoctoral researcher from 2015 to 2016. In 2017, he moved to Canada and joined the University of Toronto as a postdoctoral fellow. In August 2021, Shuailong Zhang moved to Beijing Institute of Technology and was appointed as a full professor. His current research interests include optoelectronic tweezers, micro/nano robotics, and digital microfluidic technologies.

Bingrui Xu

Bingrui Xu received her BS from China Agricultural University in 2022, majoring in mechanical engineering. She received the Beijing Excellent Undergraduate Award for her bachelor thesis on using an optoelectronic tweezer system to study living microorganisms. She is currently a PhD student at Beijing Institute of Technology working with Prof. Shuailong Zhang. Her research topics include optoelectronic tweezers, microfluidics and their applications for live cell manipulation.

Mohamed Elsayed

Mohamed Elsayed received his BS and MEng degrees in Electrical Engineering from the University of Toronto, in 2011 and 2012, and his MSc degree in Nanotechnology from the American University of Cairo in 2017. From 2012 to 2018, he worked as a Research Assistant at Assiut University, Zewail City of Science and Technology and the American University in Cairo. In 2018, he returned to the University of Toronto to start his PhD degree at the Institute of Biomedical Engineering. He is interested in biological applications of optoelectronics and microfluidics.

Lianqing Liu

Lianqing Liu received his BS degree in Industry Automation from Zhengzhou University, China, in 2002, and his PhD degree in pattern recognition and intelligent systems from the Shenyang Institute of Automation, Chinese Academy of Sciences, China, in 2009. He is currently a Professor at Shenyang Institute of Automation. His research interests include micro/nanorobotics, biosyncretic robotics, and intelligent control.

positions. More importantly, the distribution of the non-uniform electric field can be directly controlled by the light patterns projected on the photoconductive substrate, which allows flexible and rapid manipulation of many targets simultaneously. Compared to optical tweezers, OET supports massively parallel manipulation (*e.g.* 10 000 traps at the same time),[44] and in addition can exert a much stronger manipulation force for a given intensity of light.[44,45] Therefore, OET can be used for applications that optical tweezers typically can not be used, such as massively parallel manipulation of many targets simultaneously and moving objects with a big size range from several tens of nanometers to several hundreds of micrometers. In addition, OET does not require a coherent light source and can work with a low light power density (less than 1 W cm^{-2}). This feature makes OET an ideal tool to manipulate heat-sensitive biological samples compared with other heat-assisted optical micromanipulation technologies. To date, there are demonstrations of OET manipulation of many different kinds of nano-/micro-objects for important applications in biology, chemistry and engineering physics.[37–43]

Here in this work, we present a comprehensive review of the fundamentals, recent advances and state-of-the-art applications of OET technology. As shown in Fig. 1, we first summarize OET devices based on different photoconductive materials and explain their working mechanisms. Second, we introduce the use of OET for the assembly of non-biological objects for applications in sensing and fabrication. Third, we describe the use of OET for different biomedical research. Next, we summarize the integration of OET with microfluidic technologies and platforms. Finally, we overview the recent progress in the commercialization of OET technology for pharmaceutical applications, and discuss its current challenges and future perspectives.

2. Fundamentals of OET

OET can trap and manipulate nano/micro-scale objects *via* locally generated electrokinetic force by imaging light patterns on semiconductor photoconductive substrates. Over the past decade, substantial research efforts have been devoted to develop OET with different materials, structures, and functions, making them a highly versatile manipulation toolbox for different applications and scientific studies. In this section, we will introduce OET technology with different device structures, diverse experimental setups, and different working mechanisms.

2.1 Categories of OET devices

OET devices can be classified into two main categories based on their operating principles. The first category is known as the standard OET device, which requires the use of an external voltage supply; the second category is known as photovoltaic OET (PVOET), which does not require an external voltage supply. More details of the standard OET and PVOET will be presented in the following section.

2.1.1 Standard OET device. Standard OET can be further classified into two sub-categories, vertical OET (VOET) devices and lateral OET (LOET) devices,[46] as shown in Fig. 2(a) and (b), respectively. A VOET device consists of two plates, which are glass slides deposited with an indium tin oxide (ITO) layer. The bottom plate has an extra layer made of a photoconductive material on top of the ITO and the two plates are assembled together *via* a spacer to form a chamber [Fig. 2(a)]. After applying an external bias across the two plates, a vertical electric field is formed inside the device chamber (vertical to the device substrate), in which the micromanipulation is performed. VOET devices are widely used for OET research and over 90% of the published work on OET is based on VOET devices (unless otherwise specified, OET in this review article refers to VOET). Shown in Fig. 2(b) is a schematic of an LOET device, which consists of two plates. The top plate is a glass substrate (without an ITO layer) and the bottom plate is a glass substrate coated with ITO and a photoconductive layer. Different from VOET, the ITO on the bottom plate of the LOET device is patterned into interdigitated structures. An external bias is

Qiang Huang

Qiang Huang received his BS and MS degrees from the Harbin Institute of Technology, Harbin, China, in 1986 and 1989, respectively, and his PhD degree from Waseda University, Tokyo, Japan, in 1996. In 1996, he joined the Mechanical Engineering Laboratory, Tsukuba, Japan. He was with the University of Tokyo, Tokyo, Japan, from 1999 to 2000. He is currently the Executive Director of Beijing Advanced Innovation Center for Intelligent Robots and Systems, Beijing Institute of Technology, Beijing, China. His current research interests include bio-robotic systems, human–robot fusion systems, and micro/nano robotics.

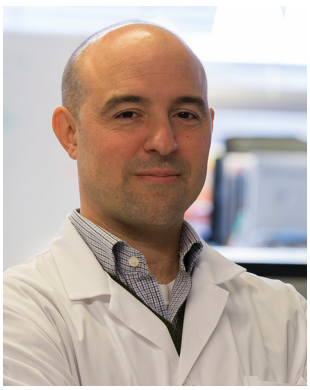

Aaron R. Wheeler

Aaron R. Wheeler completed his PhD at Stanford University in 2003. After a postdoctoral fellowship at UCLA, he joined the faculty at the University of Toronto in 2005, with a primary appointment in Chemistry, with cross appointments in the Institute of Biomedical Engineering and the Donnelly Centre for Cellular and Biomolecular Research. Wheeler was promoted to Associate and Full Professor in 2010 and 2013, respectively; he is the Tier One Canada Research Chair in Microfluidic Bioanalysis, and serves as Editor-in-Chief of the journal, Lab on a Chip.

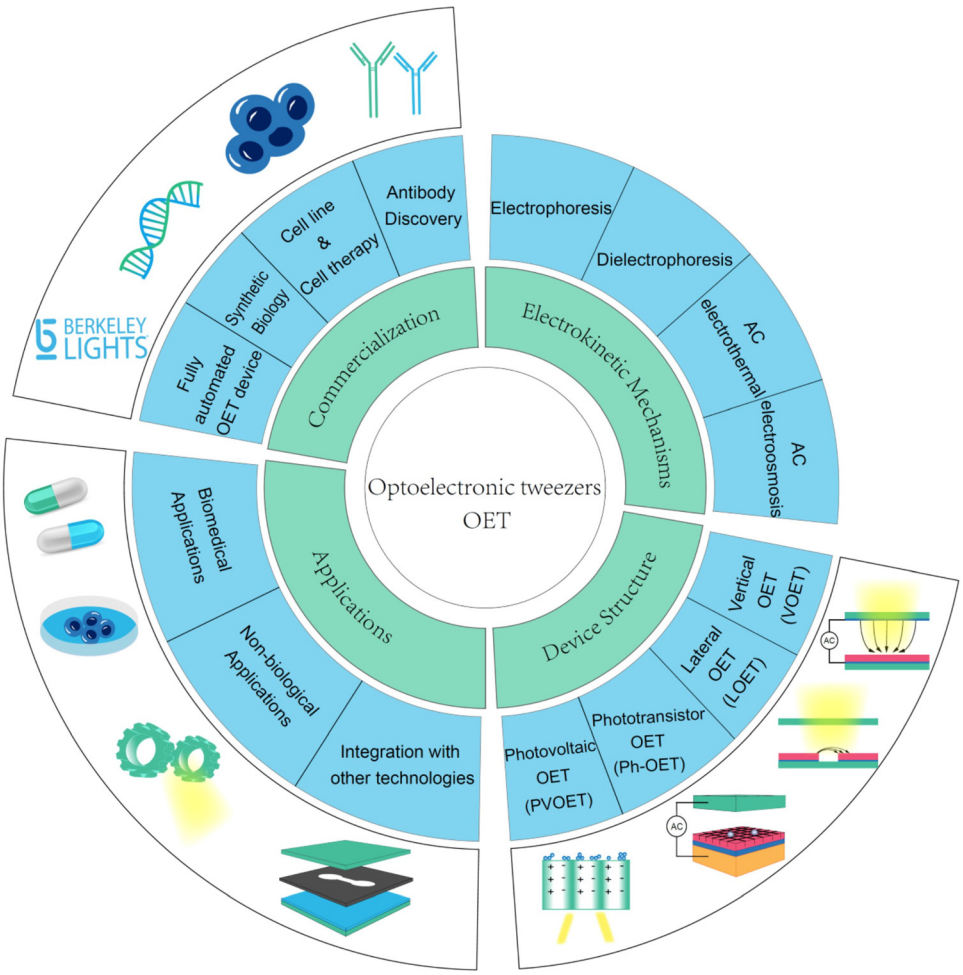

Fig. 1 Schematic illustration of four aspects of OET, including electrokinetic mechanisms, device structures, applications and the commercialization of the technology.

applied between the interdigitated ITO structures on the bottom plate and the induced electric field is oriented parallel to the device substrate (*i.e.*, laterally).[46–49] This lateral electric field provides micromanipulation force in the LOET device. Compared with VOET, LOET devices require additional microfabrication of the interdigitated electrodes and also have a small working area due to the limited space between the interdigitated electrodes. More importantly, light can only change the distribution of the electric field adjacent to the interdigitated electrodes in LOET devices, making it difficult to move objects freely in the *XY* plane. Therefore, most research studies on OET use VOET devices instead of LOET devices. However, for some specific applications such as nanowire manipulation,[49] LOET devices are used because the LOET electric field polarizes the nanowires along the *XY* plane and make them lay on the LOET bottom plate. In this case, the nanowires can be easily visualized and rotated along the *XY* plane.[49]

OET relies on the unique features of the photoconductive layer, which are made of different photoconductive materials. Due to the photoelectric effect, photoconductive materials can absorb light and harvest the photonic energy and transfer it into electric energy. During this process, the electron and hole pairs are generated in the illuminated region of the photoconductive materials, leading to a drop in its conductivity. Therefore, to some extent, the illuminated region of the photoconductive materials can be regarded as a conductor while the dark region of the photoconductive materials can be regarded as an insulator. The conductivity differences between the two regions lead to the generation of the DEP manipulation force in the OET system. As shown in Fig. 2(a), hydrogenated amorphous silicon (a-Si:H) can be used to form the photoconductive layer of an OET device. a-Si:H is a silicon-based inorganic semiconductor material that is widely used for photovoltaic applications. It can be deposited *via* plasma-enhanced chemical vapor deposition (PECVD) in a cleanroom facility. Apart from a-Si:H, organic photoconductive materials, such as titanyl phthalocyanine (TiOPc)[50–52] and bulk heterojunction (BHJ) polymer,[53–55] were also explored for OET research, as shown in Fig. 2(c). These organic photoconductive materials can be dissolved in organic solvent and spin-coated on ITO substrates to form the photoconductive layer of the OET device. OET devices based on

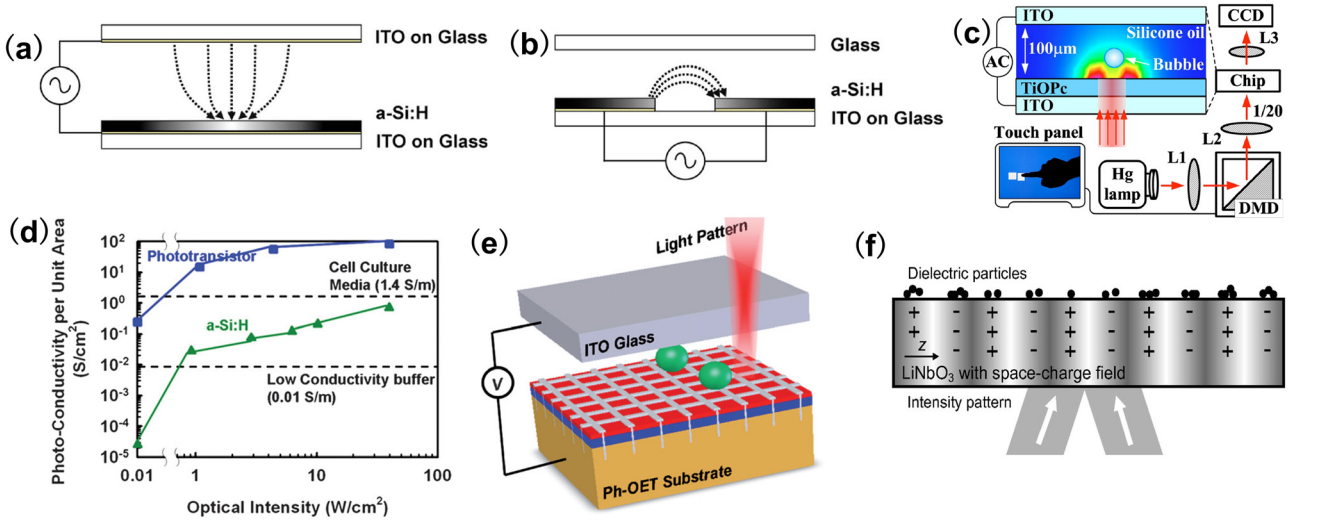

Fig. 2 OET structures. (a) Schematic of a vertical OET device (with a thin layer of a-Si:H). (b) Schematic of a lateral OET device (with a thin layer of a-Si:H). (a and b) Reproduced from ref. 46 with permission from IEEE, copyright 2009. (c) Schematic of an OET device with a thin photoconductive layer made of TiOPc. Reproduced from ref. 51 with permission from American Institute of Physics, copyright 2011. (d) Photoconductivity per unit area of the phototransistor and the a-Si:H as a function of optical intensity. (e) Schematic of a phototransistor-based OET device. (d and e) Reproduced from ref. 56 with permission from Royal Society of Chemistry, copyright 2010. (f) Schematic of a photovoltaic OET device. Reproduced from ref. 59 with permission from American Institute of Physics, copyright 2007.

organic photoconductive materials are cost-effective and easy to fabricate in a cleanroom-free environment, but suffer from larger surface roughness and lower photo/water-stability.

Although OET devices based on a-Si:H or other organic photoconductors have been demonstrated for many useful applications, these devices cannot directly work with a high-conductivity medium due to the limitation of photoconductivity. For example, if an OET device based on a-Si:H is used to work with a typical cell culture medium (conductivity around 1.4 S m^{-1}), most voltage drop would occur on the a-Si:H layer (photoconductivity $<$ 0.01–0.1 S m^{-1}), making it difficult to generate the required non-uniform electric field in the cell culture medium for micromanipulation. This is a major bottleneck of OET, especially for biological applications requiring the use of physiological buffer solutions with high conductivity. To solve this problem, phototransistor-based OET (Ph-OET) devices were developed.[56,57] The NPN junctions of Ph-OET can amplify the surface photocurrent induced by light, leading to a big conductivity difference between the illuminated and dark regions. Fig. 2(d) shows the measured photoconductivity per unit area for the phototransistor and the a-Si: H layer as a function of light intensity. It is demonstrated that the photoconductivity of a phototransistor is more than 500 times higher than that of a-Si:H. More importantly, the conductivity of the phototransistor in the dark state is lower than the conductivity of the cell culture medium, but the conductivity of the phototransistor in the illuminated state is larger than the conductivity of the cell culture medium. Therefore, Ph-OET can effectively manipulate cells in high-conductivity physiological buffers. Fig. 2(e) shows the schematic structure of the Ph-OET device. This device was demonstrated for manipulating HeLa and Jurkat cells in Phosphate Buffered Saline (PBS) and Dulbecco's Modified Eagle Medium (DMEM) with 5 W cm^{-2} light intensity.[56] Another type of Ph-OET was later invented by Chiou's group[58] which can perform automatic trapping of cells in the dark state and releasing of the trapped cells in the illuminated state. As an important technology breakthrough, Ph-OET plays a key role in the process of technology transfer and commercialization of OET, which will be discussed in detail in Section 5. Although Ph-OET is important for many applications, the device requires many steps of microfabrication and semiconductor ion implantation, making it difficult and expensive to fabricate, and inaccessible to most research labs. While organic photoconductive materials are cheap and easy to fabricate, they suffer from larger surface roughness and lower photo/water-stability. Therefore, given the advantages of material stability, robustness, fabrication simplicity and cost, a-Si:H is by far the most widely-used photoconductive material for OET research.

2.1.2 Photovoltaic OET device. In contrast to the aforementioned standard OET devices, photovoltaic OET (PVOET) is a special type of OET device which can work without the use of an external voltage supply. PVOET relies on the bulk photovoltaic effect, in which light is projected to photorefractive crystal materials to induce net directional carrier transport along the crystal's polar axis.[59–62] The directional drift of light-induced charge carriers gives rise to a space–charge field along the polar axis in the crystal [Fig. 2(f)], producing a highly inhomogeneous electric field on the crystal surface which serves as the source of actuation force for PVOET. Among different photorefractive crystal materials with a bulk photovoltaic effect, lithium niobate ($LiNbO_3$) with impurity doping (*e.g.* Fe and Cu) is the main material choice for PVOET due to its superior performance in generating a strong internal electric field (up to several kV mm^{-1}).[61–65]

To date, $LiNbO_3$-based PVOET has been used to pattern/assemble many different kinds of nano-/micro-materials for engineering physics and biology research.[62–68] PVOET has the advantage of generating a space–charge electric field without an external power supply, but directing and localizing electric carriers with low light power densities (the order 1–10 mW cm^{-2}) to generate the electric field takes a relatively long time (several minutes).[68] This influences the temporal resolution of PVOET and sets a firm limit on its ability for real-time micromanipulation using a low light power. For real-time manipulation of particles and droplets with PVOET, the required light power intensities are much higher[69–71] (in the order of 1–100 W cm^{-2}), making the technology challenging to handle light-sensitive and heat-sensitive biological samples. It is expected that photorefractive crystal materials that can work with low light power and have a more rapid response time to form spontaneous electric field would facilitate more powerful PVOET for micromanipulation applications. More details of the PVOET technology can be found in previously published review articles[72,73] and this paper will not present in-depth overview of the technology.

2.2 Experimental setup

Many different experimental setups have been built for OET research. Shown in Fig. 3(a) is a standard OET setup,[74] which consists of a DMD projector, an upright microscope (with a camera, filters, and a motorized positioning stage), a function generator, an amplifier and a computer. The DMD projector is controlled *via* a computer interface to generate light patterns, which are projected through the objective of the microscope onto the photoconductive layer of the OET device. Long pass and short pass filters are used to allow enough light power to be projected onto the OET device and manipulated objects are clearly viewed through the microscope. The function generator provides an AC signal which is amplified by the amplifier to drive the OET device. A motorized positioning stage is used to control the position of the OET device. The position of the trapped object in the OET device can be controlled by generating relative translation between the light pattern and the OET device. This can be done by using animated light patterns while keeping the OET device stationary, or by keeping the light pattern stationary while moving the OET device through the motorized positioning stage. The former approach only allows the manipulation of objects within the field of view, while the later approach allows the manipulation of objects beyond the field of view. In addition, motorized positioning stage allows accurate control of the translational speed of the trapped object,[75–77] which is important to study the exerted manipulation force by the OET system. In some cases [Fig. 3(a)], light patterns are projected onto the OET device from the top of the device, which shares the same objective lens for observation and bright-field illumination. In other cases [Fig. 3(b)], light patterns are projected onto the OET device from the bottom of the device, which is located on the opposite position to the objective lens for observation and bright-field illumination.[78,79] In the case of the OET devices based on a-Si:H, TiOPc, and BHJ on ITO-coated glass substrates, both the setups in Fig. 3(a) and (b) are applicable, mainly due to the semi-transparent properties of these photoconductive materials in the visible spectrum. However, only the setup in Fig. 3(a) can be used for the phototransistor-based OET device, because it is fabricated on an opaque silicon substrate, which blocks the light coming from the bottom.

Light source is a key component for the OET setup. Since OET does not require coherent light sources and can work with a low optical density (around 1 W cm^{-2}), many different kinds of light sources were used for OET research. Commercially-available DMD projector and liquid crystal display (LCD) projector are the

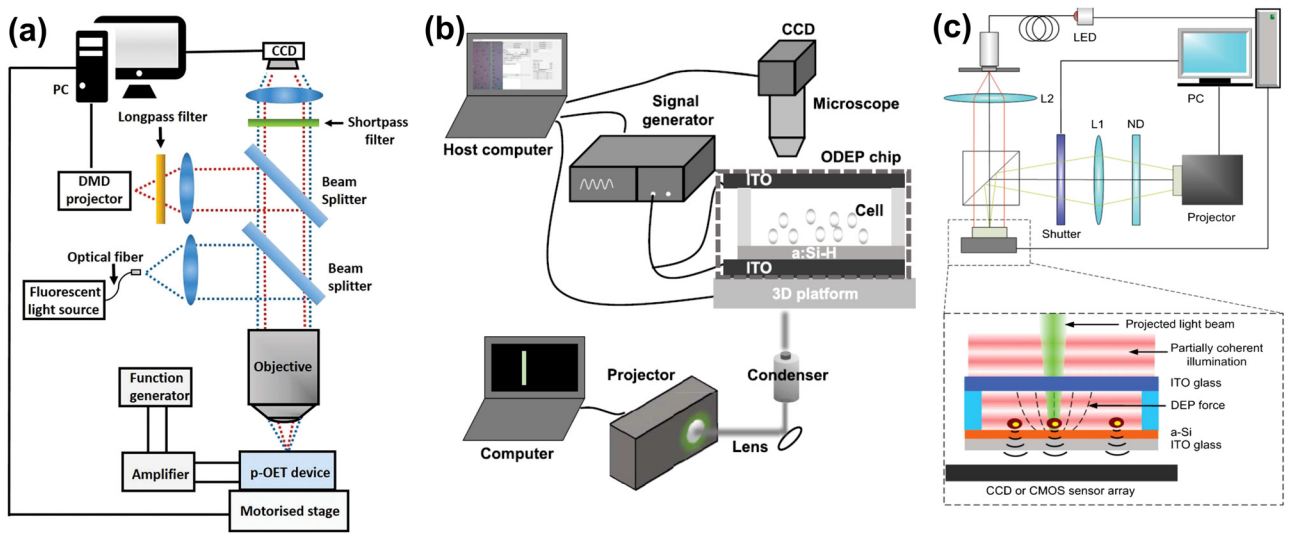

Fig. 3 Experiment setup for OET. (a) Schematic OET setup with light patterns projected from the top of the device. Reproduced from ref. 74 with permission from John Wiley and Sons, copyright 2018. (b) Schematic OET setup with light patterns projected from the bottom of the device. Reproduced from ref. 78 with permission from IEEE, copyright 2020. (c) Schematic OET setup based on a lens-free holographic microscope. Reproduced from ref. 96 with permission from Royal Society of Chemistry, copyright 2013.

commonly used light sources for an OET platform.[74–82] Self-built optical systems consisting of a DMD chip and a light source (*e.g.* LED, laser, and Hg lamp) have also be used for OET research.[44,83–85] These light sources are essentially optical displays which are capable of projecting animated light patterns on the OET device to generate "light-activated virtual electrodes" for programmable manipulation. Apart from optical display, a focused laser can project a light spot onto the OET device for particle and cell manipulation.[45,86–88] In addition, Dawson's group reported the use of a miniaturized self-emissive optical device based on micro-LEDs for OET manipulation and fluorescence cell imaging.[89,90] These systems are useful, but require a bulky and complicated optical setup, thus not applicable for portable applications. To address this problem, an OET setup that fitted within a briefcase was built.[91] In this setup, a small projector, a simple microscope built from optomechanics, and a battery powered function generator were used. Park's group also reported a simplified OET setup by directly interfacing LCD display with the OET device.[92] This approach does not require any optical components between the light source and the OET device, and the LCD display can be a screen of a mobile phone or tablet. However, this lens-free approach causes blurred images on the OET device due to diffraction of light, influencing the performance of the OET system. Therefore, a solution that can simplify the OET setup while maintain desirable manipulation performance was proposed, which is to use an LCD display or micro-LEDs together with a simple optical lens to interface with the OET device.[93–95] Shown in Fig. 3(c) is another simplified OET system, which was built using a lens-free holographic microscope.[96] This system allows effective manipulation of thousands of single cells and micro-particles over a large field of view (*e.g.* 240 mm^2). It is also worth mentioning that, in some cases, the experimental setup for OET includes not only micromanipulation functions but also detection and fabrication features. To date, laser-based Raman sensing system,[97] ultraviolet (UV) patterning system,[98] and microfluidic system[99] have integrated with OET platforms for different applications and scientific studies. These hybrid systems are also important and will be presented in detail in Sections 3–5.

2.3 Working mechanisms

Shown in Fig. 4(a) is a schematic of a typical OET device, which will be used to explain its working mechanism. This OET device consists of two plates, both of them ITO-coated glass substrates. The bottom plate is coated with an additional layer of a-Si:H, which is projected with light patterns. Electrical leads were interfaced with the ITO electrodes on the two plates [Fig. 4(b)]. OET device was assembled by joining the top and bottom plate by adhering them to spacer to form an enclosed chamber [Fig. 4(c)]. Liquid medium containing nano-/micro-objects was pipetted into the chamber of the OET device.[100] An AC voltage was applied to the OET device through an external power supply and the waveform of the AC bias voltage can be a sine function, square wave, or triangle wave. It is demonstrated that, with the same peak-to-peak voltage and frequency, an OET device powered by an AC bias with square waveform can produce the highest manipulation force.[101] The used frequency of the AC bias normally ranges from several kHz to several hundreds of kHz, depending on the dielectric and conductive properties of the liquid medium and the samples.[102] For a-Si:H and other photoconductive materials (TiOPc, BHJ, and phototransistors), the wavelength of the used light can range from violet to red, which is due to the wide absorption spectra of these photoconductive materials.[54,101] However, the absorption coefficients of these photoconductive materials are different at different wavelengths. For example, a-Si:H has larger absorption coefficients at shorter wavelengths (violet–blue region), indicating that it can generate more electron–hole carriers and exhibit larger conductivity when shining with a shorter-wavelength light.[101,103] Therefore, the electric field in an OET device is enhanced and stronger manipulation force can be generated.

The photoconductive layer (in Fig. 4, a-Si:H) of an OET device has unique characteristics. Without light illumination, a-Si:H has high impedance, resulting in a drop of the AC potential mainly across this layer. When illuminated with light, the impedance of a-Si:H drops significantly (due to its photoconductive characteristic), such that the voltage drops predominantly across the liquid medium above the illuminated area.[103] As a result, a non-uniform electric field is produced in the liquid medium above the illuminated and dark a-Si:H, which interacts with the samples in the liquid medium and produces the manipulation force. The manipulation force in an OET device is based on different electrokinetic mechanisms such as dielectrophoresis (DEP), electrophoresis (EP),

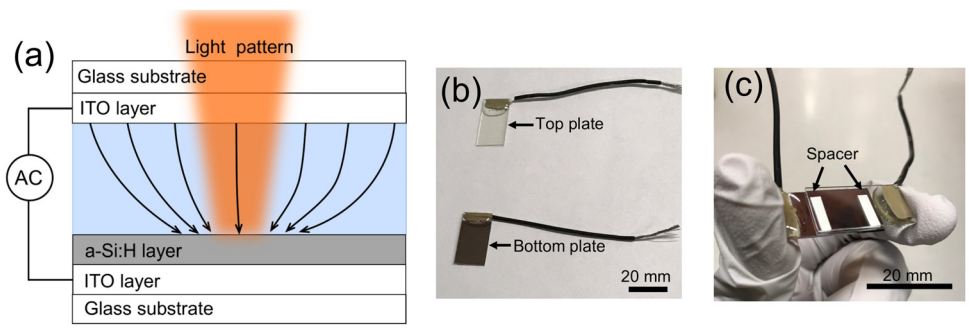

Fig. 4 OET device. (a) Schematic of an OET device. (b) Picture of the top and bottom plates of an OET device. (c) Picture of an assembled OET device. (b and c) Reproduced from ref. 100 with permission from John Wiley and Sons, copyright 2019.

AC electroosmosis (ACEO) and AC electrothermal (ACET), which will be discussed in the following sections.

2.3.1 Dielectrophoresis effect. Dielectrophoresis (DEP) is a phenomenon that polarizable particles experience electrokinetic force in a non-uniform electric field. In DEP, the particles do not need to be charged and the used electric field is mostly AC (from several kHz to several hundreds of kHz). The strength of the DEP force depends on the frequency and magnitude of the electric field, on the electrical properties of the medium and the particle, and on the particle's physical properties such as shape and size. Since the DEP force in OET is induced by projected light patterns, it is also known as optically induced dielectrophoresis (ODEP). The most widely-used method to calculate the DEP force in OET is using classic dipole approximation and the force acting on a spherical particle is given by[39,104]

$$F_{\mathrm{DEP}} = 2\pi r^3 \varepsilon_{\mathrm{m}} \mathrm{Re}[\mathrm{CM}] \nabla |E|^2, \tag{1}$$

where r is the radius of the particle, ε_{m} is the medium permittivity, E is the applied electric field, and Re[CM] is the real part of Clausius–Mossotti (CM) factor which is described as below:[39,104]

$$\mathrm{CM} = \frac{\varepsilon_{\mathrm{p}}^{'} - \varepsilon_{\mathrm{m}}^{'}}{\varepsilon_{\mathrm{p}}^{'} + 2\varepsilon_{\mathrm{m}}^{'}}, \tag{2}$$

where $\varepsilon_{\mathrm{p}}^{'}$ and $\varepsilon_{\mathrm{m}}^{'}$ are the complex permittivity of the particle and medium, which can be expressed as

$$\varepsilon_{\mathrm{p}}^{'} = \varepsilon_{\mathrm{p}} - j\frac{\sigma_{\mathrm{p}}}{\omega} \tag{3}$$

$$\varepsilon_{\mathrm{m}}^{'} = \varepsilon_{\mathrm{m}} - j\frac{\sigma_{\mathrm{m}}}{\omega}, \tag{4}$$

where ε_{p} and ε_{m} are the permittivity of the particle and medium, respectively; σ_{p} and σ_{m} are the conductivity of the particle and medium, respectively; and ω is the angular frequency. CM is a measure of polarizability and it determines whether DEP force is positive or negative. Re[CM] > 0 refers to positive DEP, *i.e.*, particles are more polarisable than the surrounding medium and will be attracted to the illuminated region, where the electric field is relatively higher than that in the dark region. In contrast, Re[CM] < 0 refers to negative DEP, *i.e.*, particles are less polarisable than the surrounding medium and will be repelled from the illuminated region. In the case of cells with a cytoplasm and cell membrane that will differ greatly in conductivity and permittivity; eqn (1) still applies but CM needs to be adjusted based on the core–shell model, in which a highly conductive core is surrounded by a single shell of low conductivity material.[105,106] In addition, some cells have an elliptical structure and the core–shell model needs to take this into consideration.[107,108]

While eqn (1) is intuitive and leads to the direct understanding of how various experimental factors affect the DEP force, it is valid under certain restrictions and leads to qualitative results. For example, it assumes that the particle size is much smaller than the scale of field non-uniformity and the DEP force acts equally on this particle. However, we often observe different results in the experiments.[75,109] A more accurate model for the DEP force on an object can be derived from Lorentz law forces by using Maxwell stress tensor as follows:[76,109–112]

$$\sigma_{ij} = \varepsilon_0 E_i E_j + \frac{1}{\mu_0} B_i B_j - \frac{1}{2}\left(\varepsilon_0 |E|^2 + \frac{1}{\mu_0}|B|^2\right)\delta_{ij}, \tag{5}$$

where σ_{ij} is the ijth element of the second rank Maxwell stress tensor, ε_0 and μ_0 are the vacuum permittivity and permeability, respectively, E and B are the electric and magnetic fields, respectively, and δ_{ij} is the Kronecker's delta. By integrating the Maxwell stress tensor of the electromagnetic field (over the surface area of the volume),[76,109–112] the manipulation force exerting on a dielectric object inside an electromagnetic field can be calculated as follows:

$$F_{\mathrm{DEP}} = \int_s \sigma \cdot n \mathrm{d}S, \tag{6}$$

where S represents the surface enclosing the bead and n represents the unit vector.

2.3.2 Electrophoretic effect. Electrophoresis (EP) refers to the movement of charged micro-objects relative to a fluid under the influence of an electric field at DC or low frequency (*i.e.* $<$10 Hz). EP is originated from Coulomb force, which can be described as follows:[39]

$$F_{\mathrm{Coulomb}} = Eq, \tag{7}$$

where E is the electric field, and q is the net charge of the micro-object. In general, most cells and biological molecules have a negative charge. This is the basis of capillary or gel EP, for example, to separate different DNA segments. In OET, EP force only needs to be accounted for when driven by DC or AC signal with frequencies lower than 10 Hz.

2.3.3 Electroosmotic effect. In OET, the application of an electrical potential on an ionic fluid results in the formation of an electric double layer (EDL) due to the accumulation of ions at the interface between the OET bottom plate and the liquid medium. In response to the tangential component of light-induced electric field, ions in EDL will move, which exerts an electrostatic force on the boundary between the OET bottom plate and the liquid medium, inducing a fluid flow at a slip velocity. In an AC electric field, this fluidic flow caused by the motion of ions is known as AC electroosmosis (ACEO). While for ACEO in OET, it is also known as light-induced AC electroosmosis (LACE).[103,113] Due to LACE, particles can move toward to the illuminated region in OET and their moving speeds are determined by the ACEO flow around the illuminated region. The flow has a rectified slip velocity and is defined by the Helmholtz–Smoluchowski equation:[103,113]

$$v_{\mathrm{SLIP}} = -\frac{\varepsilon_{\mathrm{m}} \zeta E_{\mathrm{t}}}{\eta}, \tag{8}$$

where ζ is the EDL's zeta potential, ε_{m} is the medium permittivity, E_{t} is the tangential electric field, and η is the viscosity of fluid. The optimal frequency for the ACEO flow ranges from

several hundred Hz to several kHz, and it can be described as:[113]

$$f_{\mathrm{OPT}} = \frac{\sigma_{\mathrm{m}}\lambda_{\mathrm{d}}}{2\pi\varepsilon_{\mathrm{m}}D}, \quad (9)$$

where σ_{m} is the conductivity of the medium, λ_{d} is the thickness of EDL, ε_{m} is the permittivity of the medium, and D is the thickness of the liquid chamber. In OET, ACEO flow can be controlled by the light-induced electric field and push micro-objects towards the illumination center. Since the ACEO flow magnitude decreases along the vertical direction from the OET bottom plate, the micro-objects would finally be concentrated and located at the illumination center on the OET bottom plate. It is demonstrated that ACEO can move objects that are far away from the illuminated region (several mm away).[90,114] In addition, ACEO is more effective to move smaller objects.[115] Therefore, ACEO can be used to sort particles of different sizes[93] and manipulate objects that are otherwise difficult to control with ODEP forces, such as nanoparticles and biomolecules.[113]

2.3.4 Electrothermal effect. OET relies on the use of light to generate a non-uniform electric field in the liquid medium. However, light illumination can also induce temperature gradient on the surface of the OET bottom plate, mainly due to the phonon generation in the photoconductive layer. Light absorption in the photoconductive layer will transfer its energy not only to electron–hole pairs (*i.e.* photoconduction) but also to phonons (*i.e.* heat). As a result, illuminated regions can have a higher temperature than dark regions, which leads to spatial gradients in the fluidic permittivity and conductivity. When the fluid with these permittivity and conductivity gradients is placed in an AC electric field, a fluidic motion is induced due to a net body force.[116–118] This flow phenomenon is known as AC electrothermal (ACET), which can be defined by the following equation:[103,118]

$$F_{\mathrm{ET}} = \frac{1}{2}\mathrm{Re}\left[\frac{\sigma_{\mathrm{m}}\varepsilon_{\mathrm{m}}}{\sigma_{\mathrm{m}} + i\omega\varepsilon_{\mathrm{m}}}(\kappa_{\varepsilon} - \kappa_{\sigma})(\nabla T \cdot E)E^{*}\right] - \frac{1}{2}|E|^{2}\kappa_{\varepsilon}\kappa_{\sigma}\nabla T \quad (10)$$

where σ_{m} is the medium conductivity, ε_{m} is the medium permittivity, ω is the angular frequency of the AC electric field, T is the thermal field, E is the electric field, E^{*} is the complex conjugate of the electric field, κ_{σ} and κ_{ε} are constants which represent the variations of the conductivity and permittivity per-unit temperature. The ACET effect strongly depends on the optical power density, which determines the temperature gradient. For typical OET setup in which a low-power light source (<100 W cm^{-2}) is used, ACET has limited contribution to the overall manipulation force.

In summary, the OET manipulation force relies on these electrokinetic mechanisms. Depending on the frequency of the electric field, the dominant mechanism can be different.[103] In typical cases, DEP is the dominant manipulation force in OET. However, forces based on ACEO and ACET also play a role in OET manipulation. For example, ACEO and ACET can bring a particle over a long distance to the illuminated region, where it is trapped by strong DEP force at the center of the light pattern. However, not all forces are beneficial for OET manipulation. Non-specific surface–particle adherence[119,120] and electrostatic particle–particle interactions[121] can undermine the manipulation performance of OET. To minimize these effects, various methods were developed, such as using a chemical surfactant,[77] antifouling coating,[119] lipid bilayer,[83] and novel device structure.[120] It is also worth mentioning that the OET manipulation force for a specific target can be adjusted by a variety of parameters, such as optical power density, light pattern distribution, medium conductivity, frequency and magnitude of applied electric field. Because of this, OET is a flexible and versatile manipulation tool, which have been demonstrated for many applications as presented in the following sections.

3. OET for non-biological applications

In this section, we will overview the use of OET to manipulate a variety of non-biological nano/micro-objects for applications in micro-assembly and microfabrication.

3.1 Manipulation and assembly of nanoscale objects

OET has been used to manipulate and assemble a variety of nanomaterials, including semiconductor and metallic nanowires,[84,87,122,123] carbon nanotubes,[124,125] graphene nanoplatelets,[100,126,127] conductive nanoparticles,[83,86,114,115,127,128] and metal ions.[129–132] The size of the manipulated nanoparticles ranges from a few tens of nanometers to a few hundreds of nanometers. Fig. 5(a)–(c) show the microscope images of using a laser spot to trap an individual silicon nanowire in OET.[84] The silicon nanowire undergoes Brownian motion when no voltage is applied (Fig. 5(a)). Once a voltage is applied, the silicon nanowire's long axis aligns with the electric field (Fig. 5(b)) and the nanowire moves into the laser trap (Fig. 5(c)). It was demonstrated that silver nanowires experience stronger DEP force and thus move faster in an OET system compared with silicon nanowires under the same experimental conditions. This is mainly due to the high polarizabilities of silver nanowires in an electric field. Therefore, it is possible to separate/sort silver and silicon nanowires by adjusting the scanning speed of the trapping laser, keeping the silver nanowires captured while leaving the silicon nanowires behind.[84] In addition, the positions and orientations of silver and silicon nanowires trapped in OET can be preserved using a photocurable polymer solution. This process is achieved by polymerizing the solution with UV light to immobilize the trapped nanowires.[84] Fig. 5(d) shows the simultaneous and parallel trapping of multiple silver nanowires in the OET to form a nanowire array, demonstrating the potential of using an OET for large-scale assembly of nanowires. The nanowires in an OET always align in the direction of the applied electric field. For example, in a VOET device with a vertical electric field,[84,87] the nanowires align vertically and form ''bottom-up'' structures; in an LOET device with a lateral electric field,[48,49] the nanowires

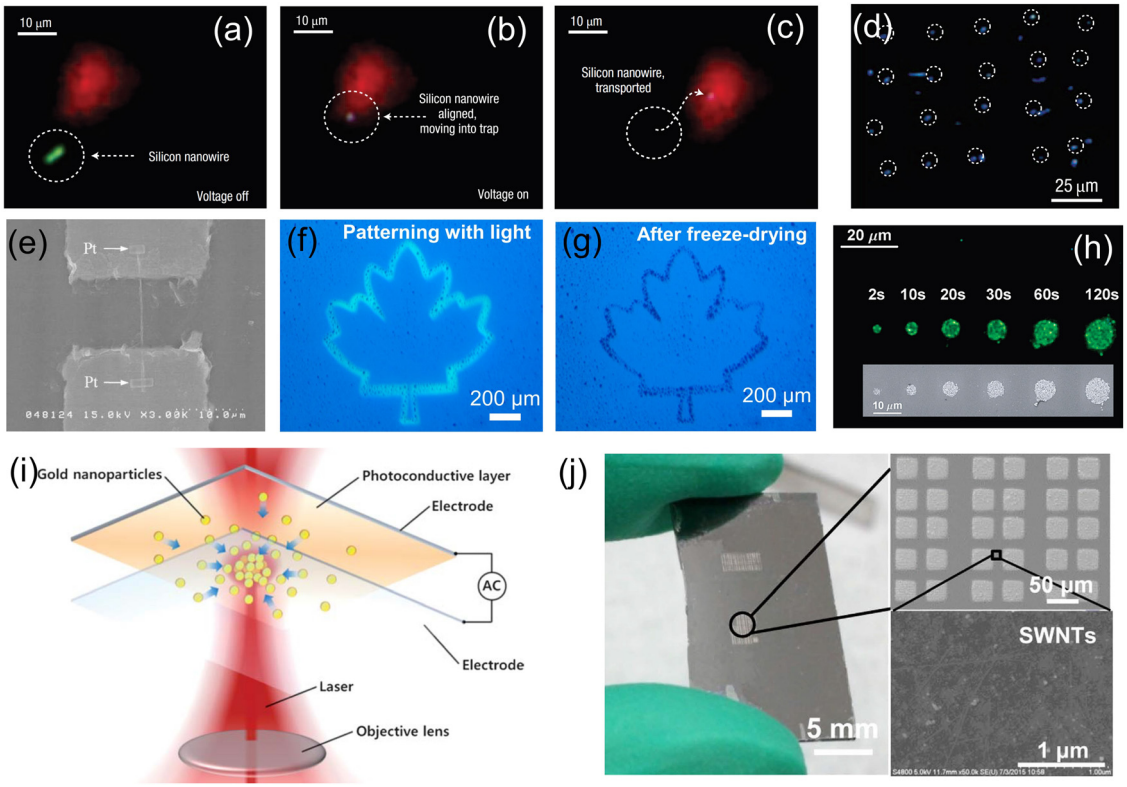

Fig. 5 OET manipulation and assembly of nanoscale objects. (a) The silicon nanowire undergoes Brownian motion when no voltage is applied. (b) The long axis of the silicon nanowire aligns with the electric field when a voltage is applied. (c) The silicon nanowire moves into the laser trap. (d) Assembly of a silver nanowire array in OET. (a–d) Reproduced from ref. 84 with permission from Springer Nature, copyright 2008. (e) SEM image of an electrochemical sensor based on a single silicon nanowire. Reproduced from ref. 122 with permission from OPTICA Publishing Group, copyright 2014. (f) The illumination of a suspension of graphene nanoplatelets with a light pattern depicting a positive "maple leaf" image. (g) The formed "maple leaf" pattern made of graphene nanoplatelets after freeze-drying. (f and g) Reproduced from ref. 100 with permission from John Wiley and Sons, copyright 2019. (h) The use of 'Nanopen' to assemble gold nanoparticles into different micro-patterns. Increasing the exposure time expands the patterned area of gold particles. Reproduced from ref. 114 with permission from American Chemical Society, copyright 2009. (i) Schematic setup of OET-integrated SERS platform, in which a single laser source can be used for the assembly of gold nanoparticles and the *in situ* detection of SERS signal. Reproduced from ref. 86 with permission from Royal Society of Chemistry, copyright 2011. (j) Optical and SEM images of the fabricated field-effect transistor consisting of silver electrodes and carbon nanotubes in between. Reproduced from ref. 130 with permission from Springer Nature, copyright 2016.

aligns laterally and form "lying-down" structures. Fig. 5(e) shows the scanning electron microscope (SEM) image of a pH electrochemical sensor based on a single silicon nanowire.[122] This nanowire is controlled by ODEP force in an OET device and can be placed close to a pair of Pt metal electrodes. The electrodes can be turned on and exert conventional DEP force to the nanowire, making it to bridge and connect the electrodes, thus forming the electrochemical sensor.[122] Carbon nanotubes[124,125] and graphene nanoplatelets[100,126,127] also experience strong DEP force in OET and behave similar to silver nanowires. Fig. 5(f) and (g) show the microscope images of using OET to pattern graphene nanoplatelets to form a "maple leaf" structure.[100] In this case, freeze-drying is used to safely remove the liquid and keep the assembled structure in place.

Micro-assembly of conductive nanoparticles is an important application of OET technology. As shown in Fig. 5(h), OET can be used as a 'NanoPen'[114] to assemble gold nanoparticles to form the desired micro-patterns, which can be used as Surface Enhanced Raman spectroscopy (SERS) hot spots with enhancement factors exceeding 10^7 and picomolar concentration sensitivities. Fig. 5(i) shows an OET-integrated SERS platform, which can be used to assemble gold nanoparticles and detect SERS signal simultaneously.[86] Using a single laser source, this platform can be used to assemble SERS hot spots at specific regions and detect target molecules in a tiny amount of liquid sample with SERS signal. Apart from applications on SERS sensing, conductive nanoparticles can also be assembled by OET to form electrodes and used for chemical sensing.[115,128] Another method to fabricate electrodes with an OET is using light-activated 'virtual electrodes' to deposit metal ions through an electrochemical reaction.[129–132] In this case, metal ions in the liquid medium react with the trapped electrons on the surface of the illuminated region in an OET. Under the effects of dynamic electron transfer,[132] the metal ions are reduced to atoms, which then crystallize and form metallic structures. This OET-based electrochemical deposition method can be used to fabricate highly-conductive microelectrode with the desired layout and smooth surface within a few seconds.[129] In addition, the heights of electrodes can be controlled by adjusting the deposition time and solution concentration. In some studies,

OET was used to fabricate microelectrodes by the electrodeposition of metal ions as a first step. After that, OET was further used to assemble other nanomaterials in between the prefabricated microelectrodes to form microelectronic devices. One such example is shown in Fig. 5(j),[130] in which silver electrodes were first fabricated using OET and carbon nanotubes were then assembled in between the prefabricated silver electrodes, finally forming a field-effect transistor. Using similar methods, OET has been used to fabricate field-effect transistors based on metal electrodes and a variety of semiconductor materials including MoS_2 thin-film,[81] ZnO thin-film[130] and CuO nanowires.[131] These results demonstrate that OET is a useful tool for the assembly, integration and fabrication of microelectronic devices made of nanomaterials.

3.2 Manipulation and assembly of microscale objects

OET has also been used to manipulate a variety of microscale objects on the order of several microns to a few hundreds of microns, including dielectric/metallic microparticles,[44,45,50,53–55,75–77,80,89,91–94,96,100–103,109,120,121,127,133–143] oil/water droplets,[144–149] gas bubbles,[51] and electronic/photonic components.[47,77,110,127] For the OET research, the most commonly used microscale objects are polystyrene spherical microbeads, which have desirable shapes and dielectric properties to work in OET systems. In addition, classic theories and equations (such as those in Section 2.3) can be applied to explain/characterize the behaviors of polystyrene microbeads under OET manipulation. Therefore, polystyrene microbeads have become a standard test sample for OET research. For example, polystyrene microbeads were used to characterize the performance of OET devices with different structures and made of different materials;[44,45,50,53–55] to optimize OET systems based on different experimental hardware;[89,91,92,94,96,120,127,133] and to study the electrokinetic physics in an OET system under different experimental conditions.[75,80,93,101–103,109,121,134–139,142,143]

Shown in Fig. 6(a) and (b) are microscope images of multiple and single 15 μm-diameter polystyrene microbeads undergoing OET manipulation, respectively. For the parallel manipulation of multiple microbeads, a dynamic "Roulette" light pattern was used to rotate the microbeads while the motorized microscope

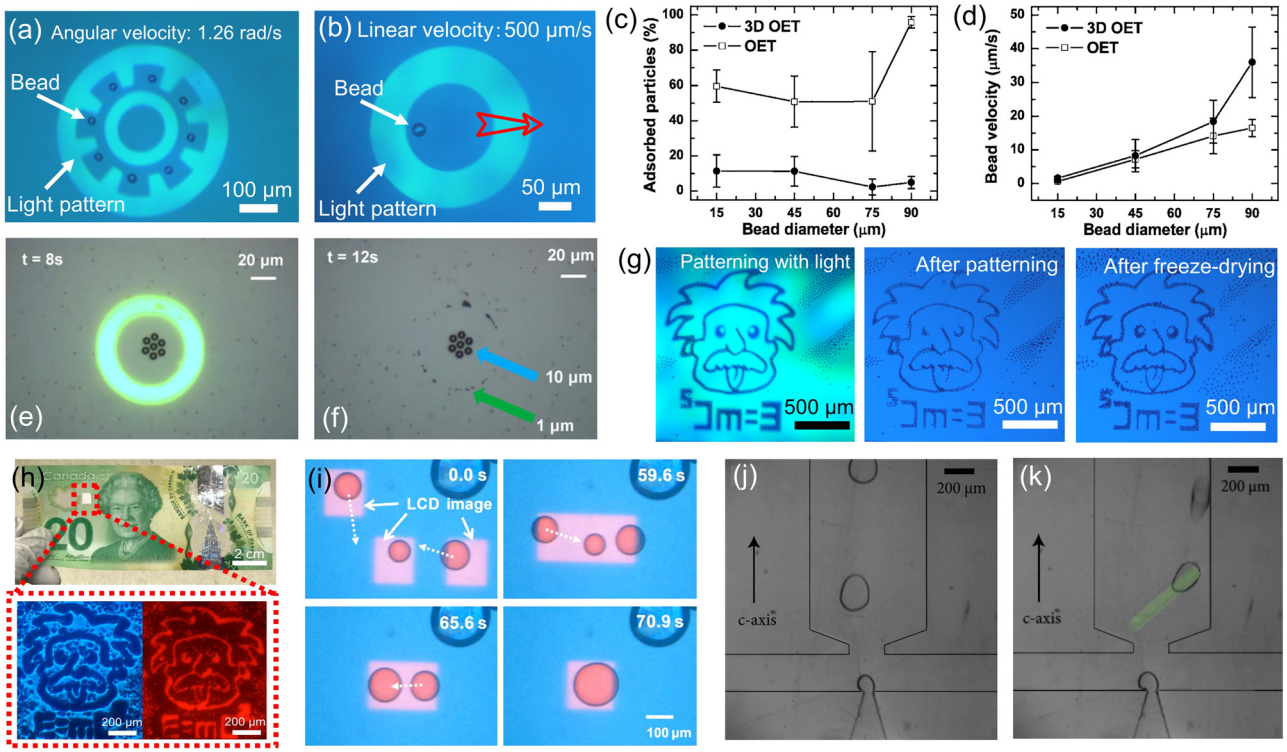

Fig. 6 OET manipulation and assembly of microscale objects. (a) The use of a "Roulette"-shaped light pattern to rotate 15 μm-diameter polystyrene microbeads. (b) Moving a 15 μm-diameter polystyrene microbead at a linear velocity of 500 μm s^{-1} using a "doughnut"-shaped light pattern. (a and b) Reproduced from ref. 130 with permission from the OPTICA Publishing Group, copyright 2019. (c) Percentage of absorbed polystyrene microbeads and (d) velocity of polystyrene microbeads according to their diameters in the conventional OET and 3D OET devices. (c and d) Reproduced from ref. 120 with permission from American Institute of Physics, copyright 2008. (e and f) Separation of 10 μm and 1 μm polystyrene microbeads in OET with a "doughnut"-shaped light pattern. (e and f) Reproduced from ref. 134 with permission from Elsevier, copyright 2013. (g) Bright-field microscope images showing (left) the illumination of the polystyrene microbead suspension with a light pattern depicting a stylized caricature of Albert Einstein with the mass energy equation, (middle) the assembled Einstein TMP in suspension, and (right) the assembled Einstein TMP after freeze-drying. (h) Image of a Canadian $20 bill modified with a red-fluorescent TMP. (g and h) Reproduced from ref. 100 with permission from John Wiley and Sons, copyright 2019. (i) Manipulation, transport and merging of multiple water-in-oil droplets with light patterns in an OET. Reproduced from ref. 144 with permission from American Institute of Physics, copyright 2009. (j and k) Droplet manipulation using a PVOET-based optofluidic droplet router. Reproduced from ref. 148 with permission from John Wiley and Sons, copyright 2015.

stage was kept stationary. For the manipulation of a single microbead, the ''doughnut'' light pattern was kept stationary, while the microscope motorized stage was programmed to move linearly. With the motorized stage to control the speed of the microbead, it was found that the manipulation force imposed on the different-sized polystyrene microbeads did not increase proportionally to the bead volume, primarily due to the electric field's non-uniform distribution above the photoconductive layer of the OET device.[75] This size-scaling mechanism also applies to cells of different sizes.[75] In addition, it was found that the polystyrene microbeads experience strong vertical DEP force in an OET, which enabled the understanding of a new ''hopping'' mechanism for particle-escape from the OET trap.[109,143] Fig. 6(c) and (d) show the measured percentage of absorbed polystyrene microbeads and their moving velocities according to bead diameters in a conventional OET device and a novel 3D OET device composed of two photoconductive layers. Using polystyrene microbeads, it was demonstrated that the 3D OET device shows a higher particle trapping efficiency and less particle absorption rate.[120] Polystyrene microbeads of different sizes may behave significantly different in an OET.[134–139] As shown in Fig. 6(e) and (f), under an applied AC voltage of 20 Vpp at 80 Hz, 1 μm polystyrene beads experience positive DEP force in an OET device and get trapped in the illuminated region of the 'donut shaped' light pattern; while 10 μm polystyrene beads experience negative DEP force in an OET device and get repelled to the dark center of the 'donut shaped' light pattern.[134] This is mainly due to different CM factors of polystyrene microbeads of different sizes.[134,135] In other cases, different-sized polystyrene microbeads experience negative DEP force but with different magnitudes, allowing them to have different moving speeds.[137–139] Therefore, it is possible to separate and sort polystyrene microbeads of different sizes in an OET device. Polystyrene microbeads can also be assembled into a variety of topographical micropatterns (TMPs) in OET.[100,127] As shown in Fig. 6(g), 10 μm polystyrene microbeads were assembled to form a TMP featuring stylized caricature of Albert Einstein. After the assembly, a method based on freeze-drying was developed to safely remove the liquid medium while keep the assembled TMP in place. During this freeze-drying process, the aqueous medium is flash-frozen, after which it sublimates directly to the vapor phase. This process allows good preservation of the TMP, while in a preliminary study with room-temperature evaporation, the fluidic forces were found to be substantially more disruptive.[100] After freeze-drying, the assembled TMP can be transferred to alternate substrates using double side tape with the potential to serve as anti-counterfeiting markers, as presented in Fig. 6(h). Similar results were also reported for TMP assembled by OET but preserved *via* photopolymerization.[127] Apart from polystyrene microbeads, OET was also used to manipulate magnetic microbeads and study their electrokinetic behaviors,[150,151] which is useful for the concentration and purification of biological substances that can attach to magnetic microbeads. OET can also be applied to manipulate gas and liquid phases, such as gas bubbles,[51] water-in-oil and oil-in-water droplets.[144–147] Shown in Fig. 6(i) are microscope images of multiple water droplets transported and merged in an oil medium using OET.[144] In addition, an opto-fluidic droplet router was developed based on a PVOET device integrated with microfluidic channels.[148] As shown in Fig. 6(j) and (k), the droplets of Novec 7300 in a collinear stream of tetradecane initially flow in the middle but can change direction toward the right-hand side due to positive DEP force. These results demonstrate that OET can manipulate not only a variety of micro-objects in single-phase systems but also droplets and bubbles in two-phase systems.

3.3 Fabrication of functional devices

An important application of OET is to assemble microscale electronic and photonic components into functional devices. Fig. 7(a) illustrates an ''OET'' pattern formed by $Sn_{62}Pb_{36}Ag_2$ solder microbeads attracted to the illuminated region.[76] These solder beads experience positive DEP force in OET and can be manipulated by circular light traps, as shown by the microscope images in Fig. 7(b). At an applied bias of 25 V at 15 kHz, the bead can move at a max velocity of 2500 μm s^{-1}, corresponding to a DEP manipulation force of 2.9 nN. It is worth mentioning that the solder bead experiences a very high DEP force in the region of several nanoNewtons (10^{-9} N), which is over one order of magnitude stronger than the DEP force exerted to similar-sized dielectric beads under the same experimental conditions.[76] This is mainly due to the influence of the bead's metal surface on the surrounding electric field. Fig. 7(c) shows the simulated electric field around a metallic bead. As shown by the simulation results, strong electric fields appear in the region between the metallic bead and the OET bottom plate, creating a large gradient of the electric field just next to the bead and hence a large DEP force.[77] With the strong DEP force, it was demonstrated that the solder beads can be positioned with sub-micron accuracy.[76] Fig. 7(d)–(f) show the process of using an OET to assemble solder beads into a straight line to connect two isolated metal electrodes.[140] After the assembly process, freeze-drying was used to remove the liquid medium and keep the assembled solder beads in place. Then, the assembled solder beads were heated and melted to connect with each other. After heating the solder beads, the surfaces of the beads became rough and physical connections formed to bridge adjacent solder beads. Fig. 7(g) shows the *I–V* characteristic of the isolated metal electrodes connected by solder beads after heating.[140] The resistance between the two electrodes was measured to be 11.6 Ohm, suggesting the assembled solder beads bridge an effective conductive path between the metal electrodes. Similar results were also achieved for solder beads assembled by a PVOET device.[141] Apart from solder beads, OET can also be used to assemble electronic and photonic components, such as capacitors[77,127] and microlasers.[47,110] Fig. 7(h) shows the use of an OET to manipulate a standard Fabry–Pérot InP semiconductor laser.[110] The laser die is 250 μm across and 100 μm thick, which can be placed and rotated in an OET with a positional and angular accuracy of 2.5 ± 1.4 μm and 1.4 ± 0.4°. The laser has a large volume, which is difficult to move with other optical

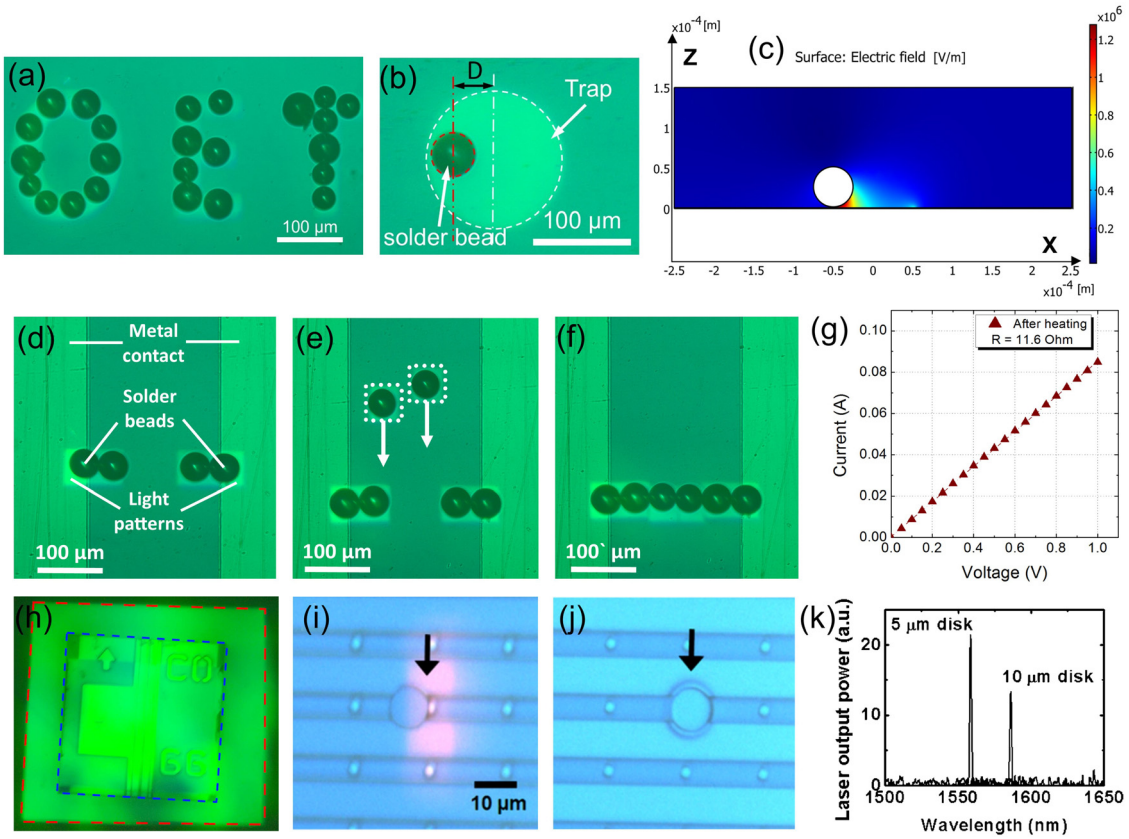

Fig. 7 OET assembly of electronic and photonic devices. (a) "OET" pattern formed by solder beads attracted to the illuminated region. (b) Moving a solder bead at 900 μm s^{-1} with a 140 μm-diameter circular light pattern. (a and b) Reproduced from ref. 76 with permission from American Institute of Physics, copyright 2016. (c) Simulated electric field distribution in an OET device with a metallic bead. Reproduced from ref. 77 with permission from Springer Nature, copyright 2016. (d–f) Assembly of solder beads to form a straight line to connect two isolated metal electrodes. (g) *I*–*V* characteristic of the isolated metal electrodes after heating the assembled solder beads. (d–g) Reproduced from ref. 140 with permission from Springer Nature, copyright 2017. (h) Picture of a standard Fabry–Pérot InP laser die (blue dashed contour) inside an OET trap (red dashed contour). Reproduced from ref. 110 with permission from OPTICA Publishing Group, copyright 2016. (i and j) Placing a 10 μm-diameter InGaAsP microdisk laser on top of a Si pedestal. (k) Lasing spectra of assembled microdisk lasers. (i–k) Reproduced from ref. 47 with permission from Springer, copyright 2009.

micromanipulation techniques. Shown in Fig. 7(i) and (j) are microscope images of using a LOET device to place a 10 μm-diameter InGaAsP microdisk laser on top of a Si pedestal.[47] The positioning accuracy is 0.13 μm in the horizontal direction and 0.25 μm in the vertical direction. Similar results were also achieved for 5 μm-diameter InGaAsP microdisk lasers.[47] After assembly, the optical characteristics of the microdisk lasers were investigated and the threshold pump powers were found to be 0.85 and 2.5 mW for the 5 and 10 μm microdisk lasers, respectively. More importantly, pre-assembled and the assembled microdisk lasers show no significant difference in terms of threshold pump power, indicating that the assembly process does not influence the performance of the microdisk lasers. Shown in Fig. 7(k) are the spectra of the assembled microdisk lasers. For the 5 and 10 μm microdisk lasers, the peak lasing wavelengths are measured to be 1558.7 and 1586 nm, respectively. In addition, both lasers can work in the single-mode. These results demonstrate that OET is a promising assembly tool for the manipulation, alignment and integration of semiconductor photonic components over a wide range of sizes (from a few microns to a few hundreds of microns).

4. OET for biological applications

Since being invented, OET has been used for a variety of biomedical applications such as cell sorting, cell analysis, DNA transfection, *etc.* In this section, we will review the use of OET for these biomedical applications and introduce the related working mechanisms.

4.1 Concentration control of biological samples

OET has been used to manipulate DNA molecules directly, as shown in Fig. 8(a). By patterning the fluorescence excitation illumination light with an iris ring, λ-phage DNA molecules can be attracted to the illuminated region in the OET device.[113] In addition, the electric conductivity of DNA molecules can be estimated by comparing the frequency-dependent moving velocities of DNA with its CM factor.[152] Apart from directly manipulating DNA molecules, OET can be used to manipulate DNA at a single molecule level using a microbead.[153] As illustrated in Fig. 8(b), the ends of a single DNA molecule are bound with a microbead, which is then manipulated by an OET. This allows the single DNA molecule to be indirectly

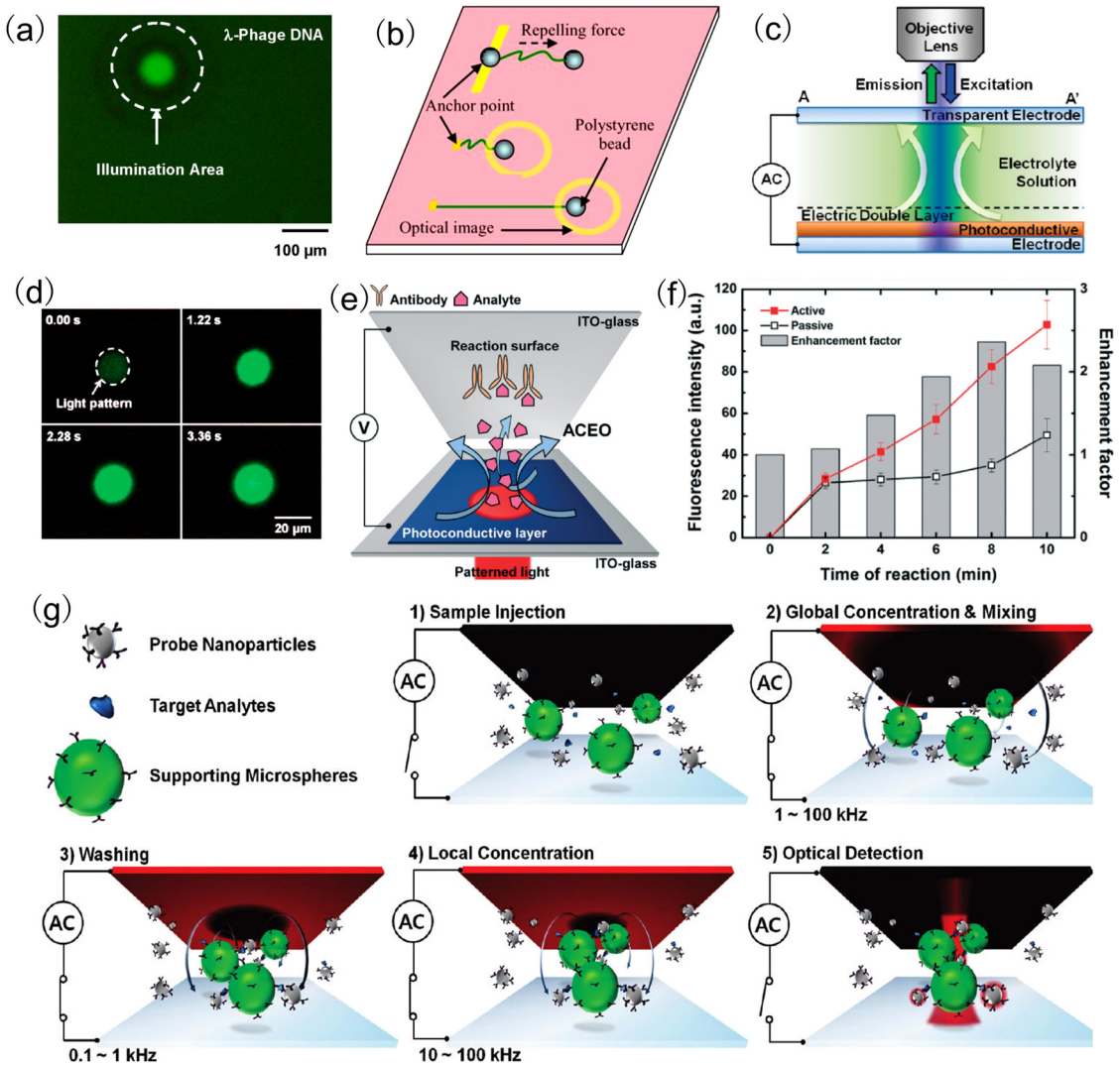

Fig. 8 OET manipulation of biomolecules and biochemical substances. (a) Fluorescence microscope images of concentrated λ-phage DNA molecules. Reproduced from ref. 113 with permission from IEEE, copyright 2008. (b) Schematic images of stretching a single DNA molecule using microbeads. Reproduced from ref. 153 with permission from OPTICA Publishing Group, copyright 2009. (c) Schematic setup of using an OET to tune the local molecular concentration. (d) Fluorescence microscope images showing the increase in the FITC-dextran concentration in the illuminated area of the OET device after applying an AC voltage of 10 Vpp at 1 kHz. (c and d) Reproduced from ref. 154 with permission from American Chemistry Society, copyright 2009. (e) Schematic illustration of an OET-based immunoreaction system. In the system, light-induced ACEO flow transports analytes to the assay spot on the OET top plate to enhance the immunoreaction rate. (f) Fluorescence immunoreaction results of active and passive modes. The enhancement factor indicates the ratio of fluorescence intensity between to the active and passive modes. (e and f) Reproduced from ref. 156 with permission from the Royal Society of Chemistry, copyright 2016. (g) Schematic procedures of immunoassay based on antibody-conjugated microbeads in an OET system. Reproduced from ref. 97 with permission from American Chemistry Society, copyright 2010.

manipulated by the OET. Two types of manipulation modes, specifically DNA elongation and rotation, were successfully demonstrated and characterized. It was found that the maximum stretching force for a single DNA molecule can be as high as 61.3 pN using a 10.1 μm microbead. OET was also implemented to manipulate other biochemical substances, such as polysaccharides, protein, and fluorophores.[154] In these studies, an OET device is placed on the stage of an epi-fluorescence microscope and blue fluorescence excitation light is focused onto the photoconductive layer of the OET device, as shown in Fig. 8(c).[154] The blue light for fluorescence excitation was applied for not only detection but also modulation of the molecular concentration in the liquid sample. Shown in Fig. 8(d) are microscope images illustrating the temporal change of the chemical concentration of fluorescein isothiocyanate (FITC)-labeled dextran in the illuminated region of the OET device. With an application of a 10 Vpp AC voltage at 1 kHz, a combination of different electrokinetic mechanisms including ACEO, DEP and electrostatic interactions can converge FITC-dextran from the dark region into the illuminated region, inducing a sudden increase of the fluorescence signal due to the increase of molecular concentration. Frequency-dependent concentration of

the FITC-dextran in an OET was also investigated.[154] When the frequency of the AC signal was set to 1 kHz and the light was turned on, FITC-dextran was attracted to the illuminated region and showed strong fluorescence intensities. When the light was turned off, the concentration of FTIC-dextran showed a sudden drop, indicating that the attraction force is weakened without light illumination. When the frequency of the AC signal increased from 1 to 10 kHz, it was found that there was a significant decrease in the concentration of FTIC-dextran, mainly due to the weaker ACEO flow around the illuminated area at the high-frequency range. When the frequency of the applied AC signal increased to 100 kHz, no obvious change of the concentration of FTIC-dextran was found, very similar to the case with no applied voltage. This was due to the frequency characteristics of ACEO, which normally exists at the low frequency range below 10 kHz. Similar results were also demonstrated for fluorescein-conjugated bovine serum albumin (BSA) undergoing OET manipulation.[154] Therefore, dynamic modulation of the local concentration of biochemical substances can be achieved in a temporal and spatial manner by controlling the applied AC signal and the light pattern. Apart from concentrating biochemical molecules as demonstrated in Fig. 8(d), OET can also be used to reduce molecular concentration within the illuminated region, creating a molecular depletion area.[155] For example, it was demonstrated that a sudden decrease in FTIC-dextran concentration occurred within the illuminated region in the OET after applying a 10 Vpp AC voltage at 100 Hz.[155] After turning off the voltage, the dispersed molecules start to diffuse into the molecular depletion region, resulting in the recovery of the fluorescence signal. On the basis of these phenomena, *i.e.*, the fluorescence recovery in the molecular depletion area, diffusion coefficients of various dextran molecules were successfully measured.[155] Therefore, OET is capable of controlling the local molecular concentration, which is useful for several applications such as molecular patterning as well as studies on molecular aggregation, molecular mobility and molecular diffusion kinetics.

4.2 Immunoreaction analysis

Apart from controlling chemical concentrations, OET has been used as an immunoreaction platform for biological assays. Fig. 8(e) shows the schematic of the OET-based immunoreaction system.[156] The OET top plate consists of capture antibodies and is employed as an antibody-immobilized assay spot. When a light pattern is projected onto the assay spot under an AC voltage, a non-uniform electric field is formed, which can induce ACEO flow and thus generate counter-rotating vortices to transport analytes from the bulk solution to the assay spot. This configuration significantly increases the binding efficiency of antibody–analyte and overcomes the slow reaction problem of the standard immunosensing system based on the diffusion effect. To investigate the enhancing effect, heterogeneous immunoassays were performed using immunoglobulin G (IgG) and anti-IgG. The IgGs were conjugated with quantum dots for fluorescence detection. Fig. 8(f) shows the fluorescence immunoreaction results for the passive and active modes. Under the passive mode, molecules in the chamber were transported *via* random diffusion. Therefore, the analyte depletion caused by diffusion limitation became intensified as time passed, resulting in a low reaction rate. Meanwhile under the active mode, OET can induce strong ACEO vortices to transport analytes to the assay spot. Since the analytes were continuously transported to the assay spot, the problem for a slow reaction due to the limitation of random diffusion in the passive mode was solved. As a result, OET can enhance the immunoreaction rate by a factor of 2.52 at 10 min compared to the diffusion-based passive mode, as shown in Fig. 8(f). It was also demonstrated that multiple assay spots can be fabricated in a microarray format on the OET top plate, while light-induced ACEO flow caused by a microarray-patterned light can transport analytes to these assay spots simultaneously to improve the assay efficiency.[157] Using this configuration, the immunoreaction time was reduced from more than 30 min to 10 min. More importantly, detection of multiple proteins using different IgGs was successfully demonstrated, which proves that multiple assays could be performed simultaneously on this microarray-integrated OET immunoreaction platform.[157] In addition to surface-based immunoassays, OET can be used for immunoassays based on antibody-conjugated microbeads.[97,158] Fig. 8(g) shows the schematic procedures for the microbead-based immunoassay in an OET system. There are five steps in the assay,[97] including (1) sample injection; (2) global concentration of antibody-conjugated microbeads and mixing of the samples; (3) washing of free analytes and probe nanoparticles; (4) local concentration of the immunocomplexes; and (5) SERS detection of the probe nanoparticles on the immunocomplexes. Apart from step 1, other steps were performed using a light pattern and an AC voltage with different frequencies. At different AC frequencies, dominant electrokinetic mechanisms are different in the OET system, which can implement different assay steps.[97] Based on the microbead-based immunoassay, quantitative and automatic detection of alphafetoprotein (a human tumor biomarker) has been conducted in a 500 nL sample droplet. The lower detection limit is around 0.1 ng mL^{-1} and the whole assay can be accomplished within 5 min. These results demonstrate that OET is a powerful optoelectrofluidic immunoreaction platform, which is capable of performing fast and highly-sensitive detection of biochemical substances in tiny sample volume.

4.3 Cell sorting

A major application of OET is for cell manipulation and this field has attracted considerable research in recent years. Fig. 9(a) shows the use of 'doughnut'-shaped light patterns to manipulate MCF-7 cells (human breast cancer cells) and ARPE-19 cells (human retinal pigment epithelial cells).[74] MCF-7 cells and APRE-19 cells were prelabelled green and red using the CellTracker dye, respectively. As illustrated, a single MCF-7 cell and a single ARPE-19 cell were positioned next to each other after moving the two traps together. In addition, randomly distributed MCF-7 cells and ARPE-19 cells were pushed together after shrinking the OET trap. These results demonstrate OET is

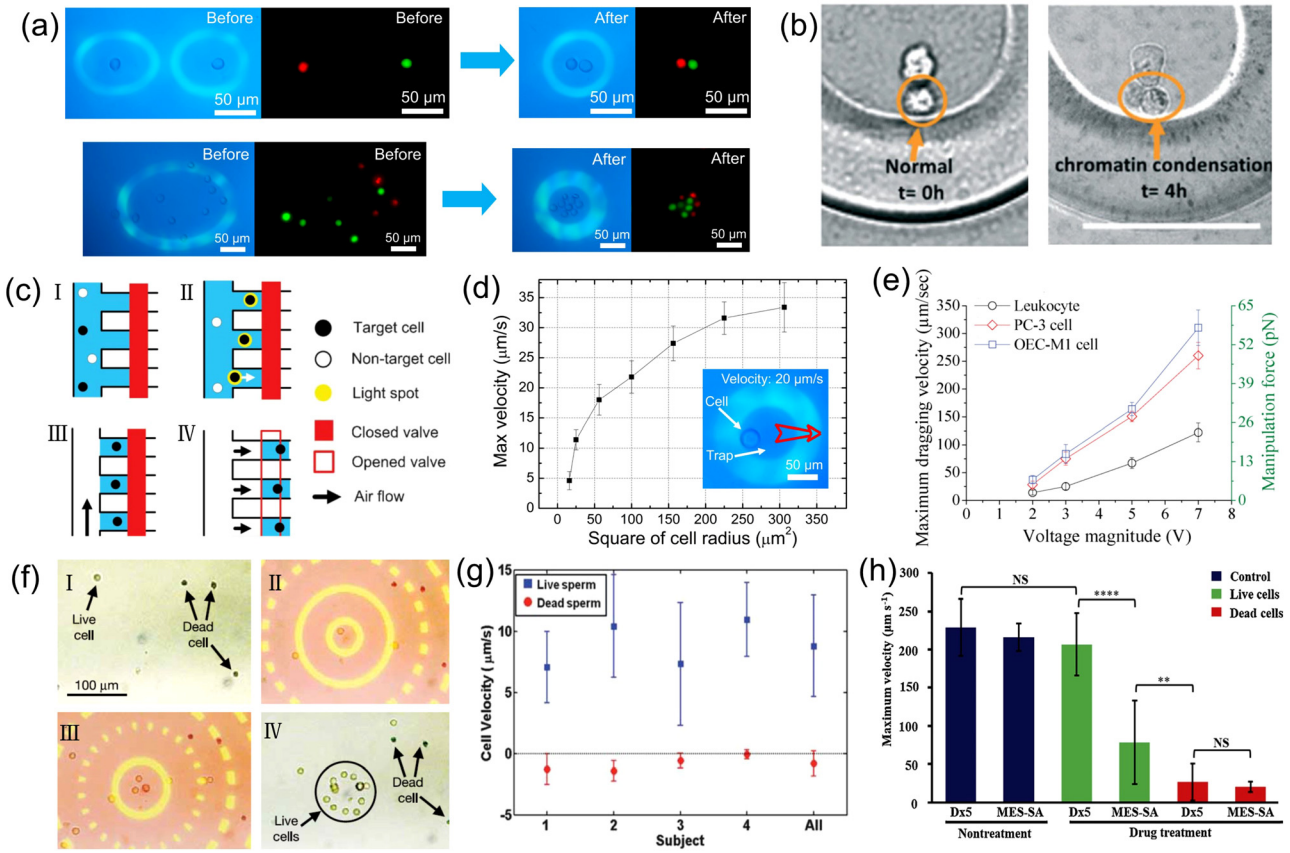

Fig. 9 OET for manipulation and separation of cells. (a) Bright-field and fluorescence microscope images showing the use of an OET to manipulate MCF-7 human breast cancer cells (pre-labelled green) and ARPE-19 human retinal pigment epithelial cells (pre-labelled red). Reproduced from ref. 74 with permission from John Wiley and Sons, copyright 2018. (b) After moving a natural killer cell in direct contact with a target cell using an OET, the target cell shows a normal morphology at t = 0 h, and chromatin condensation at t = 4 h. Reproduced from ref. 52 with permission from Royal Society of Chemistry, copyright 2018. (c) Schematic process of using an OET to extract target cells in a microfluidic channel. Reproduced from ref. 164 with permission from Royal Society of Chemistry, copyright 2013. (d) Measured moving velocities of MCF-7 cells *versus* the square of cell radius. Reproduced from ref. 75 with permission from OPTICA Publishing Group, copyright 2019. (e) Measured moving velocities and manipulation force of PC-3 cells, OEC-M1 cells and leukocyte cells at different bias voltages. Reproduced from ref. 170 with permission from Royal Society of Chemistry, copyright 2013. (f) Selectively concentrating live human B cells from a mixture of live and dead cells. Reproduced from ref. 44 with permission from Springer Nature, copyright 2005. (g) Measured moving velocities of live and dead sperms. Reproduced from ref. 88 with permission from Royal Society of Chemistry, copyright 2010. (h) Maximum moving velocities of live MES-SA and Dx5 cells before they were treated with drug (control); maximum moving velocities of live and dead MES-SA and Dx5 cells after they were treated with drug (5.0 μg ml^{-1} doxorubicin for 48 h) (NS: no significance, ****: $p < 0.0001$, **: $p < 0.01$). Reproduced from ref. 99 with permission from Elsevier, copyright 2019.

capable of controlling single cell and multiple cells using dynamic light patterns. Similar results were also demonstrated for HeLa cells[56] and human leukemia cell lines, including K562 and Jurkat cells.[57] OET can also be used to manipulate cells to achieve direct cell–cell contact, which is very useful to study the interaction between immune cells and other cells for real-time analysis of immune cells' behavior. Fig. 9(b) shows the study on immune cell cytotoxicity by moving a natural killer cell (NK-92MI cell line) in direct contact with a target cell (K562-EGFP cell line) using an OET.[52] When NK cells came into contact with the target cell, the target cell showed apoptotic characteristics (*i.e.* cell shrinkage, blebbing and then death within a few hours). It was also demonstrated that the percentage of target cells killed by the NK cells based on the OET method was almost twice those of the traditional assays.[52] This is mainly due to the advantage of OET, which can ensure direct cell–cell interaction, whereas in traditional methods different cells are mixed and interact with each other randomly. Therefore, OET showed a great potential to enhance NK cell activity and to study cell interactions in a controllable manner. OET was also used to manipulate different cell types and study how these cells behave under different experimental conditions.[82,95,105,137,159,160] In other studies, cells were used as test samples to characterize and improve the performance of different OET systems.[46,58,89,90,94,96,119,135,161–163] These studies are important for the development of OET as a toolbox for cell manipulation.

The capability to manipulate cells make an OET an important tool for application in cell sorting and cell separation. Fig. 9(c) shows the use of an OET-integrated microfluidic device to sort target cells from cell mixtures, in which the target cells are fluorescent labelled.[164] In this process, cells were visually

checked under a fluorescence microscope (step 1) and targets cells were identified based on their fluorescence and moved into branch channels using light spots (step 2). Then, airflow is used to flush the main channel to generate nanoliter droplets (step 3). Finally, the pneumatic valve is opened and the main channel is flushed again with airflow. As a result, the airflow generates air pressure in the branch channels that can push the droplets to the outlets parallelly for highly-efficient extraction (step 4). After extracting the target cells, downstream analyzing techniques such as polymerase chain reaction (PCR) and DNA sequencing can be used for cell analysis.[164] This sorting scheme relies on selectively labelling target cells with a fluorescent dye so that the target cells in the cell mixtures can be identified in the first place and then sorted using an OET. Using this scheme, immunofluorescence-stained circulating tumor cells (CTCs) were successfully extracted and purified from blood samples with 100% purity for gene expression analysis.[165,166] There are other methods to distinguish cells based on their morphology and intrinsic physical properties such as size.[167] OET can also perform label-free sorting of different cells based on their sizes. Shown in Fig. 9(d) are the measured velocities of MCF-7 human breast cancer cells as a function of cell size under OET manipulation.[75] Under the same experimental conditions, the OET manipulation force is proportional to the cell volume (*i.e.* $F_{DEP} \propto r^3$). Therefore, larger cells experience stronger manipulation force and thus can move faster under OET manipulation.[75,168,169] Fig. 9(e) shows the moving velocities and manipulation forces for cells of different species.[170] PC-3 prostate cancer cells and OEC-M1 human oral cancer cells have large sizes than leukocyte cells, thus experiencing strong manipulation force and showing larger moving velocities. Therefore, OET systems can be used to effectively separate cells of different species based on their size. For example, OET light patterns can be designed to trap larger CTCs and allow smaller leukocyte cells to escape, extracting CTCs in a label-free and highly pure manner.[170–172] In addition, cells of different species may have different polarization properties due to their distinct morphology and dielectric features (*i.e.* permittivity and conductivity), resulting in different CM factors under specific frequency conditions. This can cause differences in the manipulation force (*i.e.* $F_{DEP} \propto$ Re[CM]) and be used to separate cells of different species.[108] OET can also be used to separate live and dead cells. As shown in Fig. 9(f), live human B cells were selectively concentrated from a mixture of live and dead cells.[44] This is due to different polarization properties of live and dead cells based on their distinct membrane properties. For live cells, their cell membranes function normally and are selectively permeable. This means live cells can maintain an ion concentration difference for intracellular environments and extracellular environments through their cell membranes. However, the cell membranes of dead cells cannot function properly. Therefore, if placed in a medium with a low ion concentration, the ions inside the dead cells will diffuse into extracellular environments and the interior of dead cells will have similar electrical properties to those of the isotonic medium. This results in a difference between the polarization properties of live and dead cells. Because of this, live cells experience strong manipulation force in OET, while dead cells experience a much weaker manipulation force.[44,173,174] Based on this principle, live and dead cells (or abnormal cells with damaged cell membrane) can be effectively separated.[44,173–175] Fig. 9(g) showed the measured velocities of live and dead human sperms, in which the live sperms demonstrated a higher velocity than the dead ones.[88] In this work, OET was used to sort sperms and predict sperm viability based on their kinetic response.[88] More importantly, OET is capable of sorting and separating drug-treated cancer cells with different levels of drug resistance gene.[99,176] Cancer cells with different levels of drug resistance gene suffer different damage after drug treatment, resulting in differences in the integrity and permeability of the cell membrane. Because of this, the polarization properties are different for cancer cells with different levels of drug resistance gene after drug treatment, resulting in different magnitudes of OET manipulation force and moving speeds.[99] Fig. 9(h) shows the measured velocity of doxorubicin-treated Dx5 (*i.e.*, cells with drug resistance) and MES-SA (*i.e.*, cells without drug resistance) cancer cells under OET manipulation. Dx5 cells have much larger moving velocity than MSE-SA cells after drug treatment, allowing the effective separation of the two cell species.[99,173] For cells of the same type (*i.e.*, drug-treated Dx5 cells), the results demonstrate that OET was capable of separating them based on different cell viabilities (because these cells have different drug resistance capabilities). The sorting capability is useful for clinical applications and fundamental research. In addition to cells, bacteria can also be manipulated and sorted using OET.[177,178] For example, OET was used to detect *Escherichia coli* heteroresistance and select minor resistant strain within a bacterial clone.[178] The working principle is similar to that of the work on sorting drug-treated cancer cells, which is based on the different magnitudes of OET manipulation force exerted on the bacteria with different viabilities. The viability differences of bacteria are mainly due to different levels of antibiotic resistance.[178] More recently, OET was also used to enrich and collect cell-released, membrane-encapsulated extracellular vesicles for disease diagnosis and drug delivery applications.[179]

4.4 Cell analysis

OET is useful for cell analysis based on cell's kinetic response under different experimental conditions. For example, many cells exhibit unique self-rotation behaviors in OET systems, which can be used as a label-free biomarker to rapidly identify and characterize cells of different kinds.[180–182] Although the mechanism responsible for self-rotation of cells in OET still remains debatable,[181–188] it is demonstrated that the rotation is determined by the electric field (*i.e.*, frequency and field intensity) and polarization properties of cells. Fig. 10(a) shows self-rotational speeds of four kinds of cells (MCF-7 cells, HEK-293 cells, L929 cells, and C2C12 cells) with respect to the applied AC frequencies at a kept bias voltage of 10 V.[180] Imaging-matching algorithms were developed to measure the self-rotational speeds of these cells.[183,189,190] As illustrated in

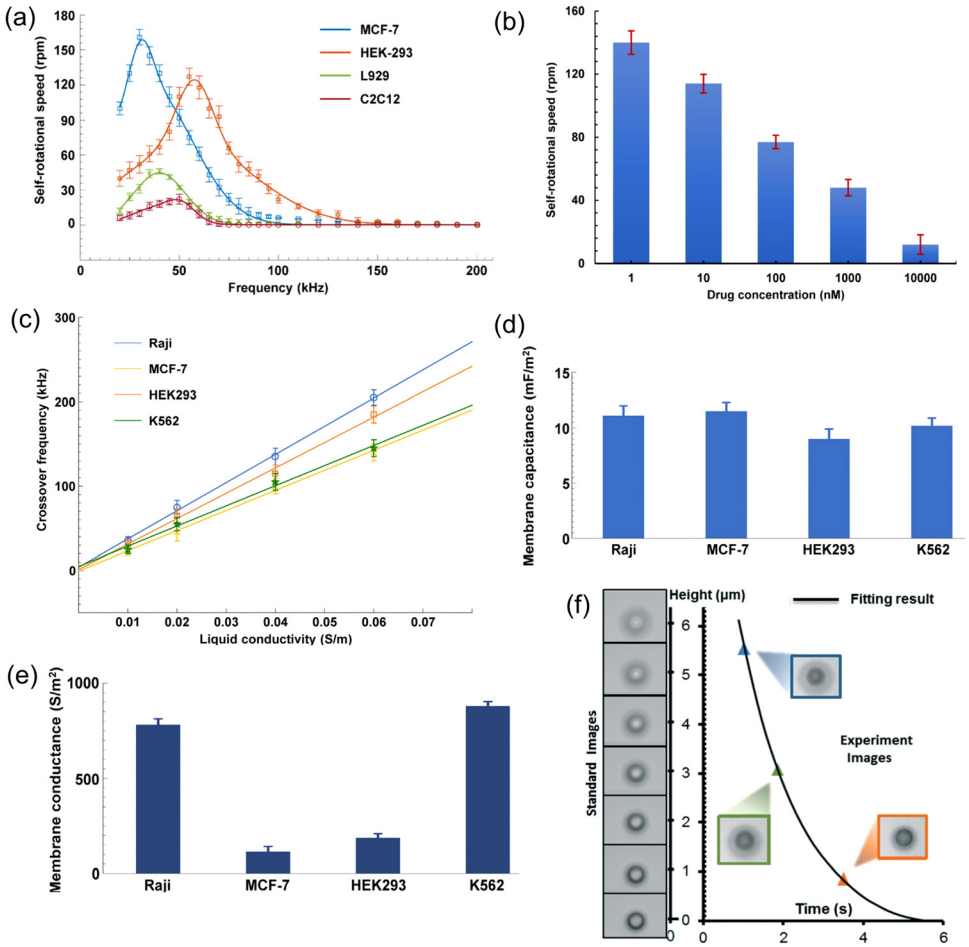

Fig. 10 OET for cell analysis. (a) Self-rotational speeds of MCF-7, HEK-293, L929, and C2C12 cells *versus* applied AC frequencies at a bias potential of 10 V. (b) Self-rotational speeds of drug-treated MCF-7 cells *versus* drug concentration. (a and b) Reproduced from ref. 180 with permission from OPTICA Publishing Group, copyright 2020. (c) Measured crossover frequencies for Raji, MCF-7, HEK293, and K562 cells as a function of liquid conductivities. Extracted (d) cell membrane capacitance and (e) conductance (c) of Raji, MCF-7, HEK293, and K562 cells. (c–e) Reproduced from ref. 193 with permission from Cell Press, copyright 2017. (f) Comparison between standard images of polystyrene beads with known heights and dynamics images of a moving bead during sedimentation to extract its motion with time. Reproduced from ref. 196 with permission from Royal Society of Chemistry, copyright 2014.

Fig. 10(a), four kinds of cells showed different self-rotational spectra, which can be used for cell identification. The differences in self-rotational spectra are mainly caused by the intrinsic dielectric parameters of cells (*e.g.* cell-membrane/cytoplasm/nucleus capacitance and conductance), which result in different polarization properties among different cell species. In addition, the self-rotational behaviors of MCF-7 cells treated with different drug concentrations were investigated,[180] as shown in Fig. 10(b). The self-rotational speeds of MCF-7 cells decreased with the increase of drug concentration, which is mainly due to the influence of drug on the cell membrane. Higher drug concentration is more likely to induce more severe damage to the cell membrane, affecting the polarization properties of cells. Consequently, the MCF-7 cells treated with a higher drug concentration show lower self-rotational speeds. Based on a similar principle, the self-rotational behaviors of red blood cells (RBCs) were used to evaluate the quality of blood samples stored at different storage times.[191] It was demonstrated that the self-rotational speeds of RBCs decreased significantly when the storage time was over three weeks, indicating that the qualities of RBCs that were stored for more than three weeks were different from those that were preserved for a shorter storage time. The decrease in the self-rotation speeds of RBCs is primarily due to the change of polarization properties of RBCs, caused by the depletion of adenosine triphosphate (ATP) and 2,3-diphosphoglycerate (DPG).[191] Therefore, OET-induced self-rotational behaviors of RBCs can be used to monitor and evaluate the qualities of banked blood. Although self-rotational behaviors were widely observed for many different cell species in OET,[180–183,190,191] not all cells exhibit self-rotational behavior. For example, it was demonstrated that non-pigmented cells (*e.g.*, A549 alveolar epithelial cells and HaCaT keratinocyte cells) rarely rotate under OET manipulation, very different from pigmented cells (*e.g.* Melan-A melanocytes cells and B16 cells).[186] It was also found that the melanin content in pigmented cells played an important role in the cell's self-rotational behavior.

For example, macrophages exhibit no self-rotating behaviors in OET. However, after seeding melanin into macrophages, they exhibit strong self-rotation behaviors.[186] Apart from melanin, nano/microparticles (*e.g.* polystyrene microparticles and gold nanoparticles) can also induce self-rotational behaviors of cells after the cells uptake the particles.[186,192] Although conclusive mechanism for this phenomenon is still under investigation, a reasonable guess is that the polarization properties of cells get changed after the cells uptake foreign substances, which increase the electrokinetic responses of cells in OET, making them rotate faster.

OET can also be used to calculate the capacitance and conductance of cell membrane, which are key parameters to assess cellular phenotype and state. In terms of OET-based cell manipulation, changed AC frequency can lead to a positive or negative DEP force exert to cells, resulting in attracted movement or repulsive movement of cells relative to the illuminated region. The frequency that leads the DEP force shift from positive to negative is known as the crossover frequency. At the crossover frequency, the real part of the CM factor is zero (*i.e.*Re[CM = 0]) and the cell experiences no manipulation force. Using the core–shell model, the relationship between cell membrane and conductance and other parameters (*e.g.* crossover frequency and liquid conductivity) can be expressed as follows:[193,194]

$$f_{\text{crossover}} = \frac{\sqrt{2}}{2\pi r C_{\text{mem}}}\sigma_{\text{medium}} - \frac{\sqrt{2}G_{\text{mem}}}{8\pi r C_{\text{meme}}} \tag{11}$$

in which $f_{\text{crossover}}$ is the crossover frequency, σ_{medium} is the liquid conductivity, and C_{men} and G_{men} are the capacitance and conductance of the cell membrane, respectively. Since G_{men} is much smaller than C_{men}, eqn (11) can be simplified as:

$$f_{\text{crossover}} = \frac{\sqrt{2}}{2\pi r C_{\text{mem}}}\sigma_{\text{medium}} \tag{12}$$

According to eqn (12), cell's crossover frequency would increase linearly with the increase of the medium conductivity. Based on this linear relationship, a slope and an $f_{\text{crossover}}$-axis intercept can be extracted and the capacitance of cell membrane can be expressed as follows:

$$C_{\text{mem}} = \frac{\sqrt{2}}{2\pi r \times \text{slope}}, \tag{13}$$

and cell membrane conductance can be expressed as follows:

$$G_{\text{mem}} = -\frac{4 \times \text{intercept}_{f_{\text{crossover}}}}{r \times \text{slope}}. \tag{14}$$

Shown in Fig. 10(c) are the measured crossover frequencies of four different kinds of cells (Raji, MCF-7, HEK293, and K562) at different liquid conductivities.[193] The crossover frequencies of cells have linear relationships with the liquid conductivities. According to the data in Fig. 10(c) and eqn (13) and (14), the capacitance and conductance of cell membrane can be extracted, as shown in Fig. 10(d) and (e), respectively. The effectiveness of this method was further proved by comparing the extracted cell parameters to those presented in other works. It was found that drug-treatment can increase the membrane capacitance of MCF-7 cells. In addition, the cell membrane capacitance increases with the increase of drug concentration.[193] For cells from the same species (*e.g.*, lymphoma cells),[181] it was found that the cell membrane capacitance decreases linearly with the increase of cell diameter. More importantly, an OET system was recently built to characterize the cell membrane capacitance of individual cells automatically.[78] In this system, a visual tracking computer algorithm was used to control the frequency-sweeping range and measure the crossover frequencies and radius of cells. This automated system is capable of measuring cancer cells (T24 and RT4) and normal urothelial cells (SV-HUC-1) at a speed of 1 cell per second, with an accuracy of 0.2 μm for cell size, and an accuracy of 1 kHz for the crossover frequency. By utilizing the dual functions to characterize and manipulate cells, the OET system was used for the detection and isolation of free cancer cells from clinical samples, such as ascites and peritoneal lavages.[195]

Apart from measuring the dielectric properties of the cell membrane, OET can also be used to measure the mass and density of single cells.[196,197] To achieve this, cells are first lifted by vertical OET manipulation force to a certain height and then, "free fall" down to the surface of the OET bottom plate of the cells is allowed, with competing buoyancy, gravitational, and Stoke's drag forces. Then, the mass and density of each cell were rapidly determined using a computer vision algorithm. This vision algorithm can accurately track the trajectory of the moving cells and apply sedimentation theory to the measured cells' trajectory for the calculation of the cell mass and density. To verify the accuracy and validity of this method, a polystyrene microbead with a known mass and density was first tested, as shown in Fig. 10(f).[196] After this, the mass and density of yeast and leukemic cells were determined,[196,197] with results comparable to those reported in other works.

There are other methods that report the use of OET for cell analysis. For example, it was demonstrated that Raji cells and RBCs can be very well distinguished based on their different transient responses under OET manipulation.[198] In addition, OET can be used to study the developmental stage of an embryo based on its translational velocity, which is useful for applications such as *in vitro* fertilization (IVF) and embryonic stem cell harvest.[199] As mentioned previously, OET-based cell analysis is based on the cell's kinetic response (*e.g.* rotational speed, crossover frequency, motion trajectory, translational velocity, *etc.*). Since different cells have different physical (*e.g.* size, shape, density and mass) and dielectric properties (*e.g.* membrane capacitance and conductance), they will exhibit unique kinetic responses in OET systems, which can be used to identify cell of specific phenotype and state or analyze cellular parameters of interest.

4.5 Cell electroporation

OET was also used for light-induced electroporation (LIE) of cells. Electroporation is a widely used membrane poration method, in which temporary permeation of the cellular membrane is achieved by subjecting the cell to an electric field.[46,200,201]

The cell's bi-lipid membrane can be temporarily depolarized by an electric field and small pores can form on the cell membrane. Therefore, reagents, chemicals and molecules in the extra-cellular space can pass through the pores and across the cell membrane based on diffusion. If the field is properly controlled, the pores can reseal (also known as reversible electroporation) and the cell retains its viability. Electroporation has many important biomedical applications such as gene transfection, cell line development and regenerative medicine.

Compared to conventional electroporation methods requiring fixed metal electrodes,[46,200] OET utilize patterned light to create virtual electrodes that can locally concentrate the electric field across the cell, resulting in electroporation. Therefore, OET enable the operator to reconfigure the electrode geometries and positions to perform electroporation in a much more flexible manner, and parallel electroporation can be performed on multiple sites simultaneously. More importantly, OET can be used for both cell manipulation and LIE, and the manipulation function can be easily switched to LIE function by increasing the bias voltage. For example,[202] it was demonstrated that cell electroporation does not occur at low electric fields (below 1.4 kV cm^{-1}), while, in an electric field with a field strength ranging between 1.4 to 2.3 kV cm^{-1}, reversible electroporation occurs. However, if the field strength is above 2.3 kV cm^{-1}, the pores on the cell membrane will not reseal and cell lysis occurs. Therefore, it is important to choose suitable electrical bias for LIE in OET systems. Show in Fig. 11(a) are the bright-field and fluorescent microscope images of using OET to perform LIE, enabling HeLa cells to uptake Propidium Iodide (PI) dye from solution.[202] At a low electric field (0.2 kV cm^{-1}), the system was working in the OET mode and was used to manipulate cells to form a 2 by 2 array. It was found that normal OET operation does not cause cell electroporation as the fluorescent image shows no fluorescence signals inside the cell. When a high electric field is applied (1.5 kV cm^{-1}, 100 kHz, 5 s) and light patterns are projected on the two cells on the diagonal, they were successfully electroporated, as indicated by the fluorescence images. In addition, only cells that were illuminated got electroporated while other cells were unaffected. Finally, the remaining two un-electroporated cells were illuminated and subjected to the electroporation bias. In this case, all four cells showed red fluorescence, indicating successful electroporation. To increase the throughput of LIE, a channel microfluidic device with OET function was developed, which was demonstrated for gene transfection for mammalian cells in continuous fluidic flow.[203] In this work, three DNA fluorescent plasmids were loaded along with different types of mammalian cells. The used DNA plasmids are pEGFPC-1 (pGFP) carrying green fluorescence genes, pDsRed-express-1 (pDsRed) carrying red fluorescence genes, and pECFP-H2B (pECP) carrying blue fluorescence genes; the used cells are mouse bone marrow stromal cells (M2-104B), colon cancer cells

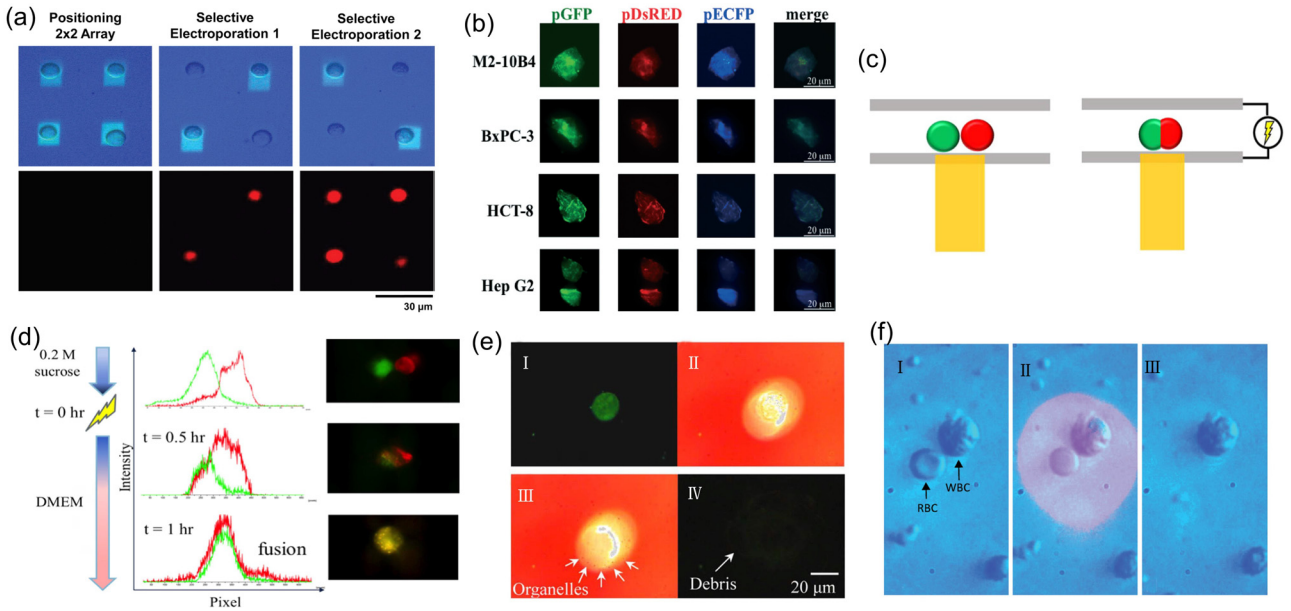

Fig. 11 OET for electroporation, fusion and lysis of cell. (a) Microscope images showing the electroporation process of cells. Bright-field images are shown in the top row. Corresponding fluorescence images are shown in the bottom row. Cells are manipulated to form an array using OET. Then, two cells on the diagonal are subjected to the electroporation bias and light illumination. Finally, the remaining two cells are electroporated, resulting in the fluorescence of all cells. Reproduced from ref. 202 with permission from Royal Society of Chemistry, copyright 2009. (b) Various types of cells were transfected with plasmids carrying triple fluorescence. Reproduced from ref. 203 with permission from Royal Society of Chemistry, copyright 2014. (c) Schematic process of cell fusion using OET. (d) Fluorescence intensity profiles and fluorescence images of a HeLa cell and an A549 cell fusing together in OET. (c and d) Reproduced from ref. 205 with permission from Springer Nature, copyright 2016. (e) A series of images showing the lysis process of a single fibroblast cell. Reproduced from ref. 209 with permission from American Institute of Physics, copyright 2009. (f) Bright-field microscope images showing the use of light to selectively lyse an RBC that is sitting next to a WBC. The RBC is lysed and the morphology of WBC remains unchanged. Reproduced from ref. 213 with permission from John Wiley and Sons, copyright 2014.

(HCT-8), liver cancer cells (HepG2) and human pancreatic cancer cells (BxPC-3). After LIE and culturing, successful transfection of DNA plasmids was verified as green, red and blue fluorescent proteins were expressed in live transfected cells, as shown in Fig. 11(b). To improve the gene transfection efficiency, the experimental conditions were optimized based on the light exposure time and geometry of light patterns. An improved version of microfluidic device with OET function was also developed,[204] which can perform continuous LIE of cells and automatic replacement of culture medium with electroporation buffers. These results demonstrate that OET-based LIE is an effective method to transfect different genes and reagents into various types of mammalian cells.

4.6 Cell fusion and lysis

OET was also used for cell fusion,[205,206] in which different cell types are merged together to form a hybrid cell. Cell fusion has many important biomedical applications such as monoclonal antibody production, cell reprogramming, cancer immunotherapy, and tissue generation.[205–208] To achieve cell fusion in OET, different types of cells are brought together to contact with each other to form a cell pair. Then, the paired cells are illuminated under an AC electric field in OET. This step results in the electroporation of the cells, making the cell membrane highly porous/leaky. The highly porous/leaky cell membrane then permits cross-cellular cytoplasm exchange, inducing cell fusion at the area of cell contact. Fig. 11(c) depicts the schematic process of cell fusion in OET.[205] In this process, OET was first used to manipulate cells to form a cell pair, in which a red cell and a green cell are later fused together to form a hybrid cell. Shown in Fig. 11(d) is the change in fluorescence intensity profile when a HeLa cell and an A549 cell fuse together in OET.[205] After the virtual electrode was generated (t = 0 hour), the peak of green fluorescence (representing HeLa cells) and the peak of red fluorescence (representing A549 cells) were observed to move closer and merge. After a certain period of incubation (t = 1 hour), the two peaks were observed to overlap, indicating successful cell fusion. It is worth mentioning that OET play two roles in this work: (1) manipulation of cells to form a cell pair, and (2) light-induced electrofusion of paired cells to form a single hybrid cell. While in another study, OET only play a single role, *i.e.*, manipulation of cells to form a cell pair.[206] In this case, cell fusion is achieved by applying strong DC pulses between the OET top and bottom plates to produce an electroporation potential across the cellular membrane. To facilitate cell pairing and prevent the paired cells from separating apart, cells were normally moved inside prefabricated 3D micro-reservoirs, in which the cell fusion was performed.[205–208]

Another important application of OET is cell lysis,[46] which is a crucial technique to extract proteins and nucleic acids from inside a cell for a variety of research purposes. As mentioned previously, if the electric field strength is above a certain magnitude (*e.g.* 2.3 kV cm^{-1}), electroporation-induced pores on cell membrane will not reseal and cell lysis occurs. Based on this mechanism, OET was used for light-induced electrolysis of cells.[209–213] Fig. 11(e) shows the lysis process of a single fibroblast cell in OET.[209] Before applying a non-uniform electric field, the cell shows green fluorescence and remains viable. However, when the cell is illuminated with a light beam, the cell membrane is ruptured by the light-induced non-uniform electric field and the cell releases some organelles. Finally, the cell debris is shown, verifying that the cell is disrupted. Although this method physically destroys the cell membrane, it does not damage the nucleus.[209] Furthermore, it is demonstrated that OET can be used to selectively lyse different types of cells that are adherent or non-adherent at a single cell level within a crowded environment.[210] This overcomes a major bottleneck in the analysis of rare cells or targeted populations in complex biological samples. In addition to the standard OET device, a specifically designed microfluidic device with OET function and cell counting function was also developed for cell lysis.[211] In this device, hydrodynamic force can focus the cells in the middle of the microfluidic channel and the integrated optical fibers can be used to count the cells. Then continuous cell lysis was achieved by projecting an optical image to induce an electric field. Experimental data showed that the cells were counted without any miscounts and 93.8% cells were successfully lysed. Apart from lysing cells, OET can also be used to extract nuclei from the lysed cells. To facilitate nucleus extraction, a microfluidic device with OET function and flow control function was developed,[212] which automates the nucleus extraction in three steps: (1) automatically focusing and transporting cells, (2) lysing cells and releasing the nucleus, and (3) separating the nucleus and cell debris based on different OET manipulation force. Therefore, OET was used for both cell lysis and separation of nucleus and cell debris. It was demonstrated that this device can achieve efficiencies of 78.04 $\pm$ 5.70% and 80.90 $\pm$ 5.98% for cell lysis and nucleus separation, respectively. Therefore, an overall efficiency of 58.21 $\pm$ 2.21% can be achieved for nucleus extraction. OET was also used for selective cell lysis based on cell shapes.[213] Shown in Fig. 11(f) are bright-field microscope images of a smaller RBC and a larger white blood cell (WBC) before, during, and after the light and electric field are activated using an OET. In this case, only the RBC is lysed while the morphology of WBC remains unchanged. This phenomenon is mainly caused by the shape of the cells (*i.e.*, biconcave shape for RBC, spherical shape for WBC), which influences the distribution of the electric field. RBCs normally have wide and flat geometry. This leads to a greater deflection and distortion of the electric field lines around the cell surface and a concentration of electric fields to form hotspots surrounding and beneath the RBCs, resulting in a higher chance of electrolysis. Similar shape-dependent cell lysis results were also observed for RBCs mixed with parasites.[213] More importantly, it was demonstrated that this technique can be performed over large areas (several mm^2) to process many hundreds of cells simultaneously.

4.7 Cell patterning

Cell patterning is an important technique for biomedical applications such as regenerative medicine, drug screening and tissue engineering. OET has proved to be a useful tool

for cell patterning,[214] due to its capability to manipulate massive amount of cells simultaneously. Shown in Fig. 12(a) are microscope images of human liver cells patterned in a sucrose buffer in an OET system.[50] Using a programmable light pattern, thousands of human liver cells were patterned into a snowflake shape within a few seconds. Similar results were also demonstrated for other cell types in bio-friendly hydrogel materials.[215] Fig. 12(b) shows the microscope images of chondrocyte-encapsulating hydrogel microbeads with different cell densities.[216] In this work, a microfluidic-based micro-vibrator was used to generate cell-containing hydrogel microbeads, which were later assembled using an OET to form a sheet-like cell culture construct. After the assembly, multiple sheet-like cell culture constructs can be stacked to create a larger cell culture construct, which shows similar 3D cell distribution to that in native articular cartilage. Apart from the direct assembly of cell-containing hydrogel microbeads, a more easy-to-use cell patterning technique is developed based on an OET and a UV-curable poly(ethylene glycol) dicarylate (PEGDA) hydrogel.[217] In this work, OET was used to pattern the cells in PEGDA hydrogel, which was later polymerized using UV light. After UV polymerization, a hydrogel sheet with an encapsulated cell pattern was formed, which can be used for drug screening and tissue engineering. A similar approach was recently developed to assemble topographical micropatterns and an electronic circuit.[127] Fig. 12(c) shows the schematic of a high-throughput microfluidic system that combines high throughput fabrication and assembly of hydrogel microstructures. In this system, PEGDA hydrogel microstructures were fabricated using a maskless photolithography technique based on a DMD projector and a UV laser.[98] The DMD served as the reconfigurable mask that allowed for the dynamic control of UV light to fabricate PEDGA microstructures of different shapes.[98,218–220] After fabrication, the polymerized PEDGA microstructures were transferred to an OET device for manipulation and assembly, as shown in Fig. 12(d). Furthermore, cell-encapsulating PEDGA microstructures were fabricated with

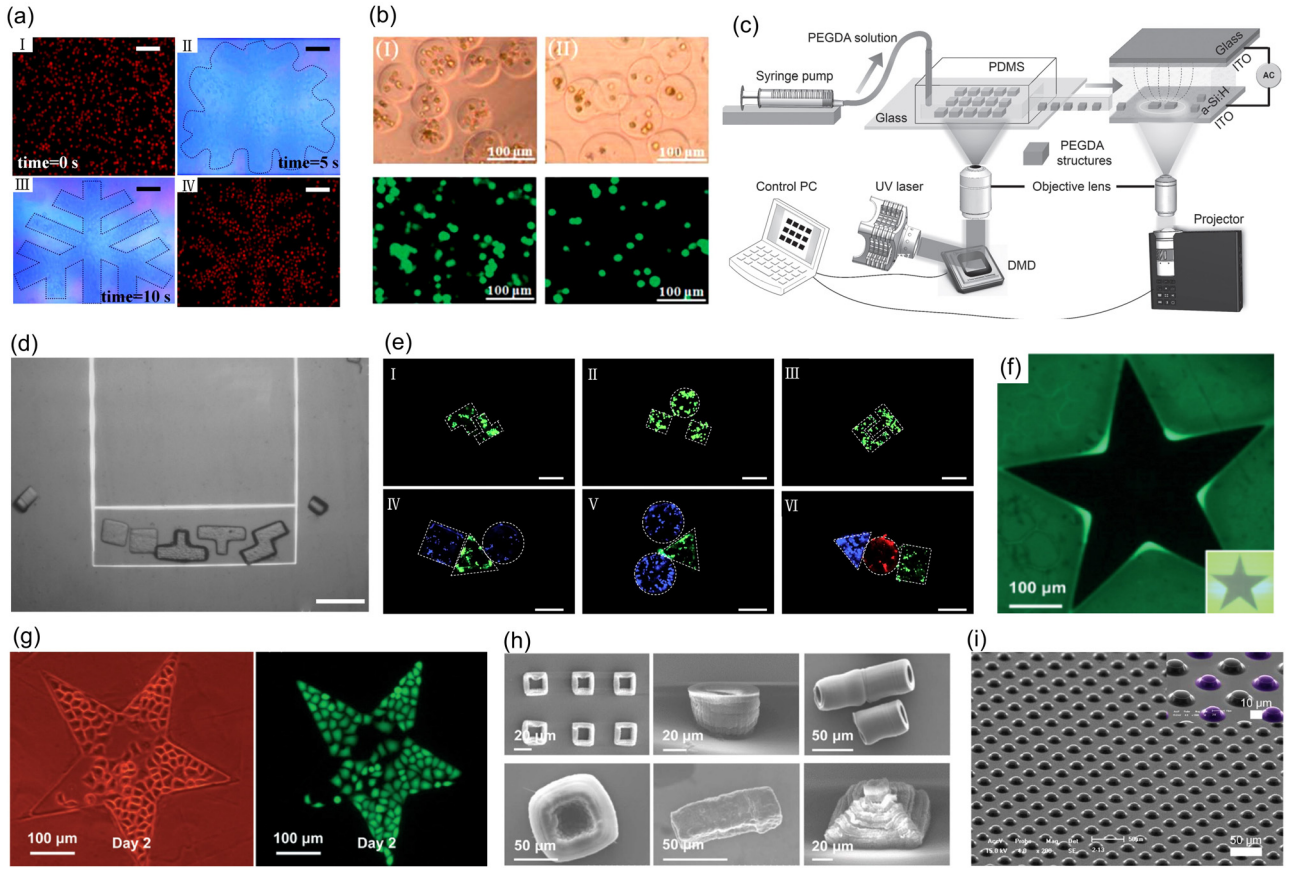

Fig. 12 OET for cell patterning and bio-fabrication. (a) Real-time image recording for liver-cell patterning by using dynamic light patterns in OET. Reproduced from ref. 50 with permission from OPTICA Publishing Group, copyright 2010. (b) Bright-field and fluorescence microscope images of chondrocyte-encapsulating hydrogel microbeads with different cell densities. Reproduced from ref. 216 with permission from Royal Society of Chemistry, copyright 2012. (c) Schematic of the high-throughput fabrication and flexible manipulation system, which consists of two major units: a DMD-based hydrogel fabrication unit and an OET-based manipulation unit. (d) Microscope image showing the use of an OET to construct a line with various PEDGA hydrogel microstructures. (e) Assembly of cell-encapsulating PEDGA hydrogel microstructures. (c–e) Reproduced from ref. 98 with permission from John Wiley and Sons, copyright 2017. (f) Star-shaped PEDGA hydrogel pattern fabricated using an OET. The inset shows the image of the used light pattern. (g) Bright-field and fluorescence microscope images of a star-shaped MCF-7 cell pattern. (fand g) Reproduced from ref. 221 with permission from Royal Society of Chemistry, copyright 2014. (h) SEM images of various 3D PEDGA hydrogel microstructures. Reproduced from ref. 223 with permission from IEEE, copyright 2015. (i) SEM image of a PDMS micro-pillar array. Reproduced from ref. 227 with permission from American Institute of Physics, copyright 2013.

the designed shapes without affecting cell viability and proliferation. These cell-encapsulating micro-gels were later assembled into desired geometries using OET, as shown in Fig. 12(e). Therefore, UV/hydrogel-based fabrication and OET-based assembly demonstrate great potential for creating functional biological structures.

In addition to UV-based polymerization of hydrogel, non-UV based electropolymerization and patterning of hydrogel were demonstrated using an OET.[221–226] This technique operates on the principle of the photoelectric effect in an OET, which can electrochemically trigger the polymerization of the PEDGA hydrogel.[222,223] Briefly, electrons generated from the photoconductive layer of the OET due to the photoelectric effect will combine with the hydrogen ions in the PEDGA hydrogel, making the ions reduce to hydrogen radicals. These hydrogen radicals then trigger the PEGDA polymerization chain reaction and make the hydrogel cross-linked. Using this method, PEDGA hydrogel microstructures with controlled sizes, shapes and thickness were fabricated using non-UV optical images in the OET. As shown Fig. 12(f), a star-shaped light pattern is used to fabricate a star-shaped hydrogel pattern, in which the dark star is the bare a-Si:H surface and the green area (surrounding the dark star) is the cross-linked PEGDA hydrogel.[221] After fabricating the PEDGA hydrogel pattern, it was used as a physical template to pattern cells. As shown in Fig. 12(g), MCF-7 cells only adhere to the a-Si:H surface but not to the hydrogel areas, forming a start-shaped cell pattern. The reason for the cells selective growth is due to the intrinsic properties of PEGDA hydrogel materials, which are resistant to cell adhesion.[221] Therefore, OET can be used to fabricate PEGDA hydrogel microstructures, which can be used to pattern cells into desired geometries. Furthermore, by tuning the light exposure time and light distribution in an OET, complex 3D hydrogel microstructures were successfully fabricated in a layer-by-layer manner with controllable thickness, as shown in Fig. 12(h).[223] Using a similar method, a hydrogel bio-scaffold for tissue growth was created by a series of dynamically modified images to form a 3D mesh-like hydrogel network with tunable pores and gaps.[224] In addition to the fabrication of hydrogel microstructures, OET was also used to rapidly construct organized micro-pillar array from a thin polydimethylsiloxane (PDMS) polymer film, as shown in Fig. 12(i).[227] This work utilizes the electrohydrodynamic instability effect,[227–230] which is induced by the light-induced lateral electric field and thermocapillary flow. Therefore, OET can be used to change a PDMS film into periodic 3D pillar array, with voltage control of the pillar diameter and light pattern control of the pillar position,[227–230] which offers a new method for efficient and simple fabrication of polymer microstructures for many bio-MEMS applications.

5. Integration of OET with other technologies

Many applications described earlier rely heavily on OET integrated with other technologies including microfluidics, conventional DEP, SERS, *etc.* In this section, we will overview the technical details of OET integration with these technologies and explain how the integration benefits relevant applications.

5.1 Integration with microfluidic systems

The importance of integrating OET with channel microfluidic devices has been identified shortly after the invention of OET. Channel microfluidic devices allow precise control and manipulation of fluids that are geometrically constrained in a small channel (typically sub-millimeter). Once being integrated with OET, channel microfluidic devices can continuously deliver and extract sample to the region where OET works, enabling high-throughput OET-based sorting, separation and processing of targets. The key step to integrate channel microfluidic devices with OET is to fabricate a spacer with microchannel features and use the spacer to bring the OET top and bottom plates together, forming an enclosed channel. To fabricate the spacer, different methods were developed. One method is to create microfluidic channels on double-sided adhesive tape,[99,165,166,169–173,178,179,195,203–205,212,231–233] which sandwiches in between the top and bottom plates of the OET device, as illustrated by the schematic in Fig. 13(a). Shown in Fig. 13(b) is an image of the fabricated OET device with microfluidic channels,[170] according on the schematic design in Fig. 13(a). In this work, the hollow structures of microfluidic channels on the doubled-sided tape was created by laser cutting. However, some tapes experience burnt and melted edges after laser cutting. To solve this problem, microfluidic channels on double-sided tape were created using a "cookie-cutter" approach, in which a custom-made metal mold was used to create a hollow structure of the micro-channels on double-sided tape through manual punching.[99,165,166,172] More recently, Xurography – cutting with a blade – is emerging for integrating microfluidic channels with OET devices.[233] Using a high-resolution craft-cutter, microfluidic features can be created on double-sided tape with smaller feature size and smoother cutting edge as compared to laser-cutting and metal mold punching. Generally speaking, these methods of creating hollow structures of microfluidic channels on double-sided adhesive tape are simple, cost-effective and highly-efficient, thus being widely-used for the integration of OET with channel microfluidics.

As an important UV-curable polymer material for microfabrication, SU8 is also used for creating microfluidic channels in OET.[202,206,211,234,235] Fig. 13(c) shows the schematic of an OET device, consisting of a SU8 layer with microfluidic channels sandwiched in between the OET top and bottom plates.[234] This device is fabricated by first creating the SU8 microfluidic channels on the OET bottom plate and then bonding the top plate using epoxy. Shown in Fig. 13(d) is an SEM image of the fabricated SU8 microchannel, integrated with a pair of optical detection fibers.[234] With the optical detection fibers, the SU8-based OET-microfluidic device is capable of interrogating micro-particle size and then sorting micro-particles based on their sizes. Using the same fabrication method, an OET-microfluidic device with optical detection fibers was developed to perform hydrodynamic cell focusing, cell counting and

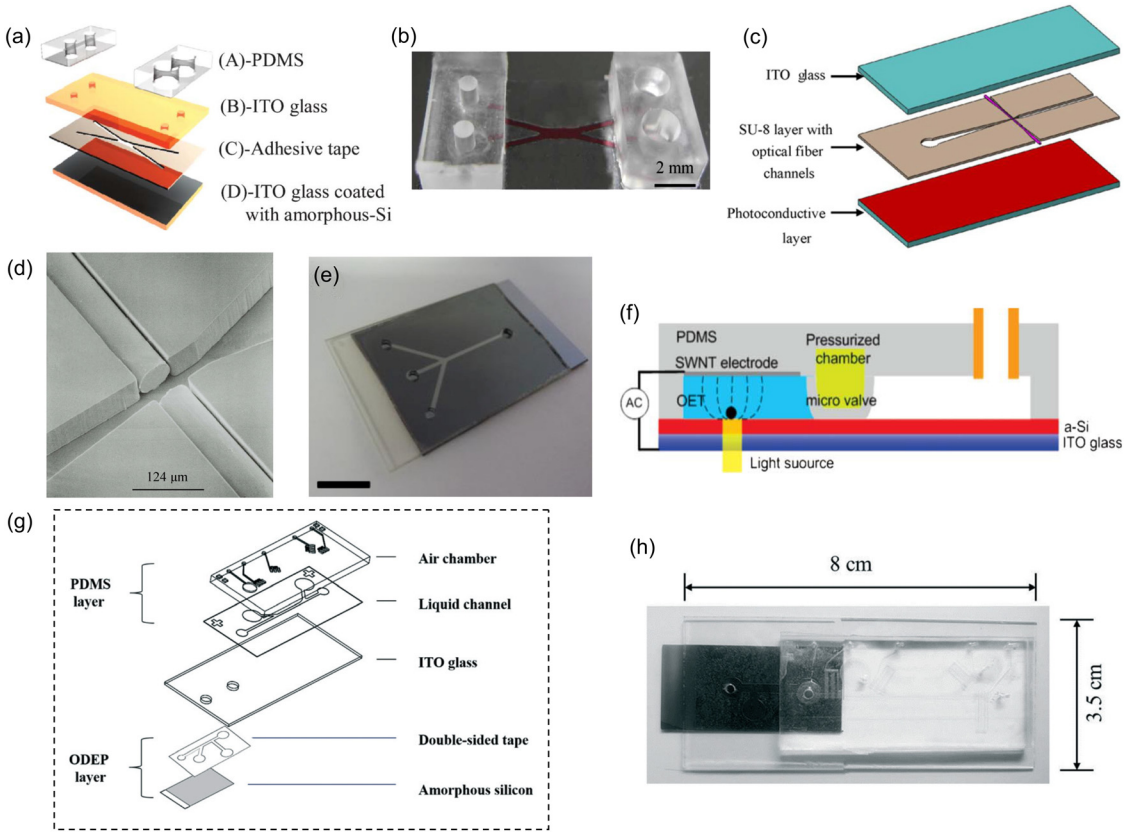

Fig. 13 Integration of OET with channel microfluidics. (a) Schematic design of an OET-microfluidic device based on double-sided adhesive tape with micro-channels. (b) Image of an OET-microfluidic device. The micro-channels in the device were created by laser-cutting a double-sided adhesive tape. (a and b) Reproduced from ref. 170 with permission from Royal Society of Chemistry, copyright 2013. (c) Schematic design of an OET-microfluidic device with SU8 micro-channels and a pair of optical fibers. (d) SEM image of the SU8 micro-channels and the optical fibers. (c and d) Reproduced from ref. 234 with permission from Elsevier, copyright 2008. (e) Image of an OET-microfluidic device with SU8 micro-channels. Reproduced from ref. 235 with permission from IOP Publishing Group, copyright 2020. (f) Schematic design of an OET-microfluidic device with PDMS top plate and PDMS micro-channels. Reproduced from ref. 164 with permission from Royal Society of Chemistry, copyright 2013. (g) Schematic design of a hybrid microfluidic device consisting of PDMS fluidic control module and OET-microfluidic micromanipulation module. (h) Image of a fabricated microfluidic chip consisting of a PDMS fluidic control module and an OET-microfluidic manipulation module. (g and h) Reproduced from ref. 231 with permission from Royal Society of Chemistry, copyright 2014.

continuous cell lysis.[211] A similar fabrication method was developed by fabricating the SU8 layer with microfluidic channels on the OET top plate, and then the OET top plate was adhered to the bottom plate using UV-curable epoxy.[202] The OET-microfluidic device fabricated using this method can move cells and perform selective electroporation of single cells. More recently, a slightly different fabrication method was developed to create SU8 microfluidic channels in an OET device.[235] In this method, the SU8 material is first spin-coated on the OET bottom plate, and then the top plate with inlet and outlet holes is placed on top of the bottom plate. Therefore, a featureless SU8 layer is sandwiched in between the OET top and bottom plates. Afterwards, the SU8 layer is processed with baking and photolithography. Finally, unexposed SU8 is removed by immersing the device in a developer for an extended length of time with agitation/sonication. Using this method, OET-microfluidic devices with different channel heights were fabricated, which were demonstrated for focusing and sorting micro-particles. Fig. 13(e) shows an example of an OET-microfluidic device, fabricated using this method. Although not discussed in this work, the ''extended length of time'' to develop SU8 materials sandwiched in between the OET top and bottom plates can be days or even weeks if the channel geometries are small. Apart from SU8, UV-curable PEGDA polymer materials were also used for creating microfluidic channels in OET devices.[236] The motivation for this work stemmed from the fact that TiOPc is used as the photoconductive layer instead of a-Si:H, and the normal processing for SU-8 materials would damage the TiOPc layer.

Poly(dimethylsiloxane) (PDMS) is a silicon-based organic polymer that is widely used for fabricating microfluidic devices.[237,238] By incorporating a gold mesh or carbon nanotubes on PDMS,[164,239] an OET device with PDMS microfluidic channels was developed. This device is different from other OET-microfluidic devices as normally a spacer with micro-channels is fabricated to bring the OET top and bottom plate together. However, in this work, PDMS structures form both the OET top plate and the spacer,[164] as shown by the schematic in

Fig. 13(f). In addition, with an integrated pneumatic-controlled value, this PDMS-based OET-microfluidic device is capable of isolating and extraction single cells for downstream mRNA analysis. Although this device demonstrates superior device performance, the fabrication process of a PDMS-based OET-microfluidic device is much more complex than the aforementioned fabrication methods with double-sided tape and SU8 materials. To solve this problem, hybrid microfluidic systems were developed by interfacing PDMS microfluidic devices directly with double-sided tape-based OET-microfluidic devices.[179,204,212,231] In this case, PDMS microfluidic devices were used as modules for fluidic control while OET-microfluidic devices were used as modules for target sorting/processing. As shown in the schematic in Fig. 13(g),[231] the two modules were interfaced together by stacking the PDMS microfluidic module on top of the OET-microfluidic module, with the inlet and outlet holes aligning to each other. Fig. 13(h) shows the image of a fabricated microfluidic chip consisting of a PDMS fluidic control module and an OET-microfluidic sorting module,[231] according to the schematic design shown in Fig. 13(g). This device combines the advantage of PDMS microfluidic device in fluidic control and the advantage of OET in micromanipulation, thus offering a powerful platform for continuous cell sorting and processing.

5.2 Integration with digital microfluidics and optoelectrowetting technology

Digital microfluidics (DMF) is a liquid-handling technology that enables individual control over discrete micro-droplets on an array of electrodes,[240] representing an alternative to the conventional paradigm of channel microfluidics in which fluids are transported in enclosed micro-channels. Show in Fig. 14(a) is a schematic structure of the DMF device, which consists of a bottom and a top plate, separated by a spacer. The structure of DMF has some resemblance to that of an OET. As shown in Fig. 14(a), the DMF bottom plate is composed of an array of electrodes, a dielectric layer and a hydrophobic coating. The DMF top plate is an ITO-coated glass slide with a hydrophobic coating, similar to that of an OET device. The working principle of DMF refers to the electrowetting-on-dielectric (EWOD) effect,[240] in which the hydrophobicity of a substrate is controlled by an electrical field. The electric field can control the contact angle of the droplet and create a surface tension force that allows continuous movement of the droplet in the DMF device. In simple words, activating a particular DMF electrode causes the region above the electrode to change from hydrophobic to hydrophilic, attracting nearby micro-droplets. Although well suited for controlling micro-droplets (*e.g.* moving, splitting, merging, and dispensing), DMF is unable to manipulate the micro-objects inside the micro-droplet. Hence, there exists a strong demand to combine DMF and OET together, allowing a single chip to acquire both convenient fluidic control and effective micromanipulation of micro-objects for a variety of applications.

The dielectric layer required for the DMF device is problematic for OET operation. One way to integrate DMF and OET is to partially remove the dielectric layer,[241] as shown in Fig. 14(b). In this case, the bottom plate is identical to the bottom plate of a standard OET device. The top plate contains patterned ITO electrodes for DMF operation, with the dielectric layer selectively removed at one of the electrodes, and at that electrode, the cross section of the device is identical to that of a standard OET device. The cross section of other electrodes is the same as that of a typical DMF device albeit upside-down. This design causes discrete areas of either droplet manipulation by EWOD or particle manipulation by OET.[241] This design was further improved by using a lateral OET device as the bottom DMF plate, allowing simultaneous DMF control and OET manipulation on the same area, as shown in Fig. 14(c). This DMF–OET integration is useful for both droplet control and micro-object manipulation.

Another solution for simultaneous droplet control and micro-object manipulation is to utilize the optoelectrowetting (OEW) effect.[242–244] OEW relies on light-induced 'virtual electrodes', which can selectively change the hydrophobic surface to the hydrophilic surface, thus attracting the nearby micro-droplets. The OEW device is similar to the DMF device in terms of the underlying physics with the only difference being the electrodes in OEW are created by light. Shown in Fig. 14(d) is a schematic of an OEW device, which consists of a top plate and a bottom plate.[245] The top plate of the OEW device is identical to that of a DMF device; the bottom plate of the OEW device is similar to that of an OET device (with an additional dielectric layer and a hydrophobic coating). This device can work under the OEW mode to move droplets [as illustrated in Fig. 14(d)] or under the OET mode to move micro-particles inside the droplet [as illustrated in Fig. 14(e)], depending on the AC frequency and light pattern being used. Just like in OET, organic photoconductors such as TiOPc were also used for OEW to simplify device fabrication and reduce device cost.[246] Single-sided lateral OEW devices (in which electric field is applied laterally) were also developed for the actuation of micro-droplets[247,248] and this approach requires very low light power density (less than 1 W cm^{-2}). Shown in Fig. 14(f) is a schematic of a lateral OEW device, consisting of a flexible PET substrate, two ITO electrodes on the sides, a TiOPc photoconductive layer, a SU8 dielectric layer and a Teflon hydrophobic coating.[249] This single-sided OEW device works by illuminating the whole device and moving the droplet with dark pattern. Using this device, continuous droplet transportation were demonstrated on various 3D terrains such as on flat ($\varphi = 0^\circ$), vertical ($\varphi = 90^\circ$), and upside-down ($\varphi = 180^\circ$) surfaces. In addition, droplets can be moved, merged and splitted on a curved surface, as shown in Fig. 14(g). Using a similar design, a smartphone-integrated OEW device was developed,[250] as shown in Fig. 14(h). In this work, light from a smartphone screen was used to perform OEW based microfluidic operations such as droplet transportation, merging, mixing, and immobilization (in an oil environment), allowing automated sample processing of marine water. Furthermore, the smartphone camera can perform on-chip microscopic evaluation of water quality by measuring the population and fluorescence signals from the target cells in water samples, offering a portable lab-on-a-chip system for

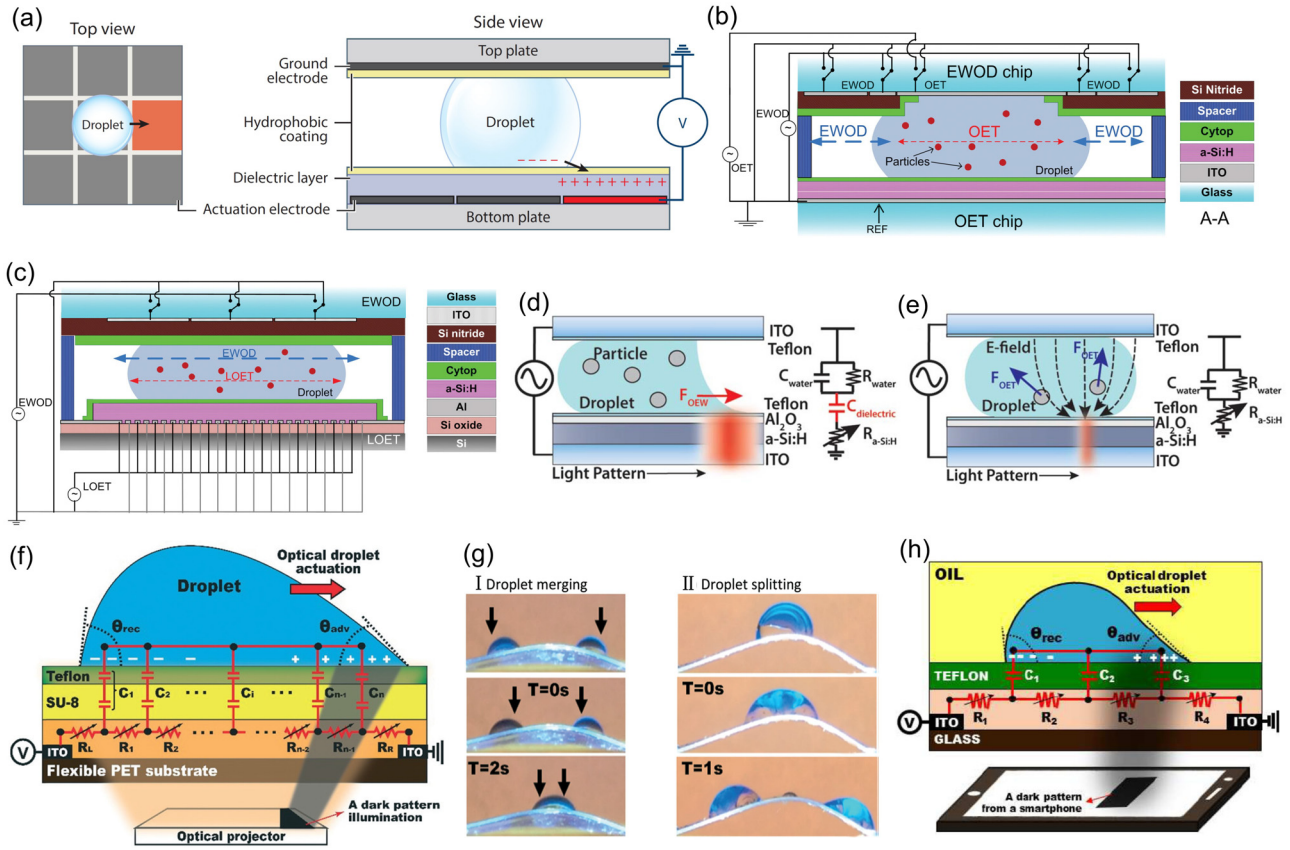

Fig. 14 OET integration with DMF and optoelectrowetting. (a) Left: Top view of the DMF device showing an array of electrodes; right: the cross-sectional view of a DMF device showing its detailed structure. Reproduced from ref. 240 with permission from Annual Reviews Inc., copyright 2015. (b) Cross section of a device integrating OET and DMF operation. The device looks like an upside-down DMF device with the dielectric coating removed at one of the electrodes, enabling OET operation. (c) Using lateral OET as the bottom plate, the integrated device allows OET and DMF operation simultaneously. (b and c) Reproduced from ref. 241 with permission from Royal Society of Chemistry, copyright 2009. (d) Schematic of the device working in the OEW mode ($f < 100$ kHz), causing aqueous droplets in the vicinity to move towards the light pattern. (e) Diagram of the same device operating in the OET mode ($f > 100$ kHz). In this mode, particles within the droplet experience a DEP force when in the vicinity of light illuminated region. (d and e) Reproduced from ref. 245 with permission from Royal Society of Chemistry, copyright 2011. (f) Schematic design of a single-sided OEW device fabricated on a flexible PET substrate and its equivalent circuit and working principle. (g) Image showing the use of a single-sided OEW device for droplet merging and splitting on a curved surface. (f and g) Reproduced from ref. 249 with permission from the Royal Society of Chemistry, copyright 2016. (h) Schematic design of a single-sided OEW device, in which the droplet is driven by the light pattern from a smartphone screen. Reproduced from ref. 250 with permission from Royal Society of Chemistry, copyright 2018.

monitoring water quality. More recently, the same research group developed a TiOPc-based lateral OEW device while incorporating plasmonic nanoparticles into the TiOPc layer to improve its light absorption efficiency,[251] resulting in a droplet movement speed of 12.5 mm s^{-1}. OEW is an emerging new optofluidic technology for droplet control that shares the same advantages as those of OET in simplicity and flexibility. It is expected that OEW technology will be further improved and explored for different uses in the future.

5.3 Integration with other micromanipulation technologies

OET was also used in combination with other micromanipulation technologies for different applications. For example, conventional DEP technology was integrated with OET for nanowire assembly.[122] In this work, a pair of metal electrodes with a 10 μm gap were fabricated on top of the OET bottom electrode. OET was first used to trap the nanowires and move them next to the fabricated metal electrodes. Then, an AC bias was applied to the metal electrodes to generate DEP, which attracted and aligned the nanowires to fill in the gap between the metal electrodes. Another method to integrate conventional DEP with OET is to fabricate patterned optoelectronic tweezers (p-OET).[74] As shown in Fig. 15(a), the photoconductive layer of the p-OET device is patterned to expose the ITO electrode layer, which is different from the conventional OET device with a continuous photoconductive layer. Fig. 15(b) shows the numerical simulations of the p-OET structure, which indicate that strong non-uniform electric fields exist at the edges of the patterned photoconductive layer. Therefore, the outer edges of the patterns on the p-OET's photoconductive layer can generate DEP force to push away unwanted targets from the area of interest. This solves the problem of "particle-crowding" in a conventional OET device and generates a clear field for particle observation and manipulation. In addition, the p-OET

device allows the direct trapping and moving of particles into a physical trap formed by a photoconductor surrounded by an exposed ITO electrode, as shown in Fig. 15(c). Even without light illumination, particles can still stay in these physical traps due to negative DEP generated by the edge of the patterned photoconductor. This feature can minimize the light-induced heating effect in a conventional OET as light needs to be "on" all the time in a conventional OET to maintain the trapping force. Therefore, p-OET is similar to conventional OET in terms of permitting flexible, parallel and reliable manipulation of microparticles, but also has a patterned photoconductive layer that is useful for keeping selected microparticles in place by conventional DEP (even after turning off the light source). Another OET system employing a non-uniform background electric field was recently demonstrated.[252] The electrode layer (beneath the photoconductive layer) of the OET device was patterned to generate a non-uniform background electric field. This background electric field's gradient mainly changes along the specific axis. Influenced by the background DEP force and light-induced DEP force, particles can be trapped along an axis around the edge of the light spot, resulting in an improvement of the manipulation performance in terms of resolution and position accuracy compared with the conventional OET technology.[252]

OET was also integrated with acoustic tweezers (ATs) for particle manipulation and cell lysis.[253,254] To integrate the two technologies together, an OET device with the SU8 microfluidic channel was put on top of a surface acoustic wave (SAW) transducer, as shown in Fig. 15(d) and (e).[253] AT is achieved utilizing the SAW transducer which transmits ultrasound into the OET device and forms a pressure standing wave under resonance conditions. After the integration, the OET–AT system is characterized in terms of coupling of acoustic energy into the chip as well as OET trapping efficiency. The individual control of each technique was demonstrated and applied for sorting of micro-particles by DEP and acoustophoretic forces.[253] In addition, this OET–AT system can be used for continuous cell lysis.[254] Shown in Fig. 15(f) are microscope images of using AT to drive RBCs to form a line and using OET to perform continuous lysis of RBCs. When an electric field is applied, RBCs disappear and get lysed when passing the illuminated area. It was demonstrated that this OET–AT system has a cell lysis efficiency of $>$ 99% for a sample concentration of 10^6 cells per ml.

In addition to direct OET manipulation, OET can also be used to control microrobots, which are in turn used to manipulate secondary objects.[233] Fig. 15(g) shows a representative SEM image of a "cogwheel"-shaped microrobot, bearing a

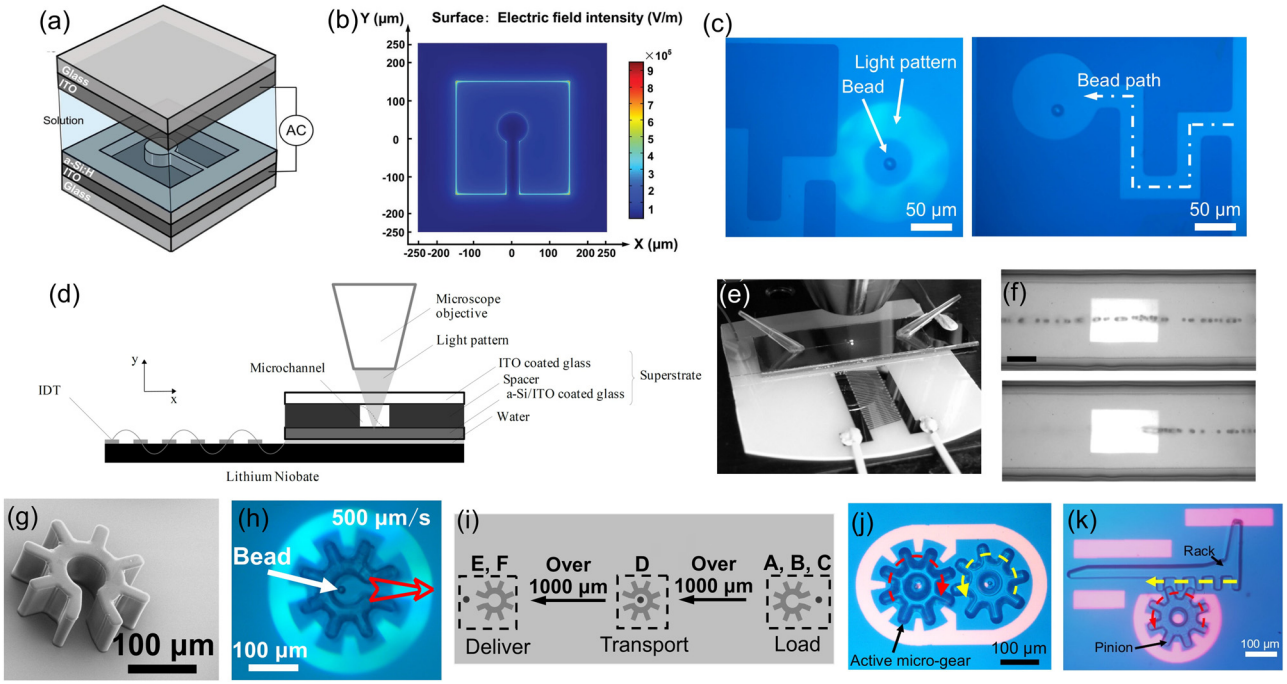

Fig. 15 OET integration with other micromanipulation technologies. (a) Schematic of a p-OET device with a patterned a-Si:H layer on an ITO electrode. (b) Simulations on the electric field and its distribution in a p-OET device (AC voltage: 7 Vpp, 25 kHz). (c) Microscope images showing the use of a p-OET device to manipulate and trap a microbead. (a–c) Reproduced from ref. 74 with permission from John Wiley and Sons, copyright 2018. (d) Schematic of an integrated OET-AT system. (e) Image of an assembled OET-AT system, placed under the objective, containing an OET-microfluidic chip and a SAW device for AT. (d and e) Reproduced from ref. 253 with permission from SPIE, copyright 2012. (f) RBCs lysing under continuous flow (flow from right to left). RBCs are concentrated along the pressure node by AT to form a line. Rectangular light pattern is projected in the microchannel. This is the area where lysis is induced. Scare bar: 50 μm. Reproduced from ref. 254 with permission from SPIE, copyright 2013. (g) SEM image showing the 3D structure of a "cogwheel"-shaped microrobot. (h) Bright-field microscope image of a microrobot that carries a microbead. (i) Payloads can be loaded, translated and delivered using a microrobot. (g–i) Reproduced from ref. 233 with permission from the National Academy of Sciences USA, copyright 2019. (j) Microscope image showing a microgear train in operation. (k) Microscope image showing a micro-rack-and-pinion in operation. (j and k) Reproduced from ref. 256 with permission from Springer Nature, copyright 2021.

semienclosed central chamber with an opening on one side. The microrobot is straightforward to manufacture and can be programmed to carry out sophisticated, multiaxis operations. Shown in Fig. 15(h) is a microscope image of using a light pattern to control a microrobot, which carries a micro-particle. The microrobot can be used to load, transport and deliver a variety of micrometer-dimension payloads, as shown in Fig. 15(i). In addition, parallel and independent manipulation of multiple microrobots is feasible. More importantly, microrobots can be programmed to move and ''scoop up'' mammalian cells such that they can be isolated and evaluated independently. Microrobots programmed in this manner are much gentler on fragile mammalian cells than conventional OET techniques. This OET-based microrobotic system is capable of sorting and isolating single cells for clonal expansion and RNA-sequencing, facilitating cell–cell fusion and interactions, and extraction of precious biomedical samples from complex micro-environment.[233] More recently, automatic control of multiple microrobots to simultaneously collect, transport and deposit microparticles was demonstrated, based on an open-loop algorithm consisting of automated targeting and path planning.[255] These results demonstrate the feasibility of automating the OET-driven microrobots to carry out micromanipulation tasks. In addition to the microrobot technology, OET-driven microgears were also developed. These microgears can be made to work together as microgear train [Fig. 15(j)] and micro-rack-and-pinion [Fig. 15(k)],[256] allowing for 3D particle control, mechanical advantage, and microfluidic valving behaviors to be realized. These multi-component micromechanical systems represent an important step forward for the microsystem community, suggesting great potential for complex OET-driven micromachines and microrobots in the future, for applications in micromanipulation, microfluidics, life sciences and beyond.

6. Commercialization

The commercialization of OET started shortly after the invention of this technology in 2005. Ming Wu, the inventor of OET, founded Berkeley Lights Inc. with Igor Khandros and William Davidow in 2011.[257] This California-based company has successfully commercialized fully automated OET instruments to enable the functional screening and selection of individual cells for antibody discovery,[257–260] cell line development,[257,260–263] cell therapy development[257,263,264] and synthetic biology.[257]

Fig. 16 provides an overview of the Berkeley Lights platform, which uses ''Opto-Electro Positioning'' (OEP) technology, the company's commercial name for its proprietary OET technology. Fig. 16(a) shows a photograph of the Beacon instrument, developed by Berkeley Lights, and a microfluidic device to work with the Beacon instrument.[258,265] Berkeley Lights' microfluidic devices have up to 14 000 ''NanoPen'' chambers and a microfluidic channel that connects all the ''NanoPen'' chambers for loading/extracting cells, beads, *etc.* and delivering reagents. The volume of the NanoPens range from 250 pL to 2 nL depending on the application. This small volume enables the rapid phenotypic characterization of single cells. Fig. 16(b) demonstrates the manipulation of activated, individual T cells using the Berkeley Lights OEP technology and subsequent clonal expansion following 72 hours of culture.[262] Fig. 16(c) shows a typical workflow using the Beacon platform for cell analysis and selection.[262] Briefly, cells are loaded onto an OptoSelect Chip (OET-microfluidic chip) and positioned inside the NanoPens using light-induced dielectrophoresis. Following clonal expansion, reagents are selectively introduced onto the chip to characterize various phenotypic traits (*e.g.*, secreted proteins, cytokines, surface protein expression, *etc.*). After phenotypic characterization, selected clonal colonies are exported from the chip for further off-chip processing, including genomic analysis and/or downstream expansion in well plates. This process enables the user to precisely link the phenotypes of individual cells to a corresponding genotypic profile.

The flexibility of the Beacon system enables a variety of applications to run on the same system ranging from the discovery of antibody therapeutic candidates directly from B cells to developing powerful cellular therapeutics by selecting functional T cells.[257] Furthermore, the Beacon system can significantly accelerate the discovery and development of cell-based products.[260] For example, it usually requires 2–3 months to discover antibodies from B cells using traditional methods such as hybridoma. With the Beacon system, the screening time is reduced to several days. In addition, the Beacon system consumes less cells and reagents compared with traditional methods. Therefore, the Beacon system helps users find the best cells in a fraction of the time and cost of traditional methods. Recently, in response to the COVID-19 global health crisis, researchers have harnessed the Beacon system's flexibility and timeline compression to identify novel therapeutic and vaccine candidates.[266–268] The Beacon system is in active use in a growing number of research institutions and biopharmaceutical companies worldwide. While the Beacon system is aimed at high-throughput, high-automation applications, a smaller, less automated, but cheaper system, lightning, was recently released by Berkeley Lights to address needs in the research and academic markets.

In July 2020, Berkeley Lights executed an initial public offering raising gross proceeds of approximately 190 million USD, demonstrating strong market confidence in the company's future prospects (NASDAQ:BLI). In summary, with OET as the core technology, it is expected that Berkeley Lights will continue to grow and play important roles in the development of cellular therapeutics, biopharmaceuticals, and other cell-based products.

7. Future perspectives

Since the appearance in 2005, OET technology has attracted significant academic and commercial interest and has been used for different applications in a variety of fields and scenarios. This paper comprehensively reviews the working principles, experimental setups, applications and commercialization of the

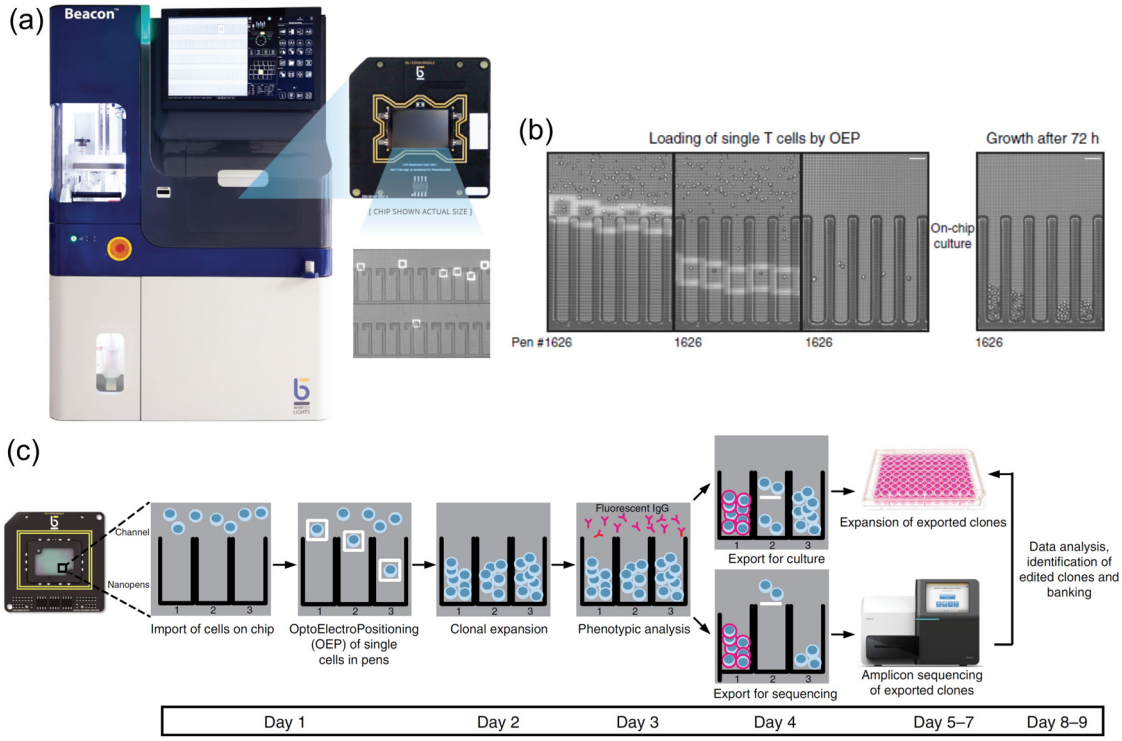

Fig. 16 Berkeley Lights' Beacon system for cell screening and selection. (a) Photograph of the Beacon system. The samples are loaded on a proprietary OET-microfluidic chip shown on the right. Reproduced from ref. 258 with permission from IEEE, copyright 2019. (b) Bright-field microscope images showing the loading and culturing of single T cells in NanoPen chambers using the Beacon system. (c) Workflow for cell manipulation, analysis and recovery using the Beacon system. (b and c) Reproduced from ref. 263 with permission from Springer Nature, copyright 2018.

OET technology. It is demonstrated in many aspects that OET is a powerful micromanipulation toolbox for scientific research. To date, most OET-based research focus on (1) the assembly of micro/nano devices and materials, (2) the manipulation, sorting and assay of chemicals, biomolecules and cells, (3) the acquisition and analysis of cellular properties, (4) the electroporation, fusion and lysis of cells, (5) the fabrication of cell-encapsulated biomaterials and biostructures, and (6) the development of optofluidic devices for fluid transport. These applications are summarized/classified in Table 1, which clearly demonstrates the superior performance and unique versatility and flexibility of the OET technology.

Although demonstrated for many useful applications, challenges do remain for OET to transform from a mainly lab-based technique to a one that is widely used in practical applications. Therefore, more improved approaches for overcoming some challenges of the current state of the art should be carried out. In the following text, we will discuss the major challenges of OET and some possible solutions to further improve the technology in the future. The search for new photoconductive materials and phototransistor structures is highly desirable for OET research. The performance of the OET device strongly relies on the quality of the photoconductive material. Until today, a-Si:H material is still a major choice to make a photoconductive layer OET device due to its high stability, good light adsorption, reusability and biocompatibility. However, the fabrication of a-Si:H materials is a laborious and expensive process, which requires well-trained personnel to use the PECVD machine in a cleanroom facility based on a well-developed recipe (*e.g.* optimized parameters for temperature, pressure, gas flow rate, *etc.*). Although other organic photoconductive materials such as P3HT/PCBM polymer and TiOPc have been developed to fabricate OET devices based on a simple spin-coating process. Their relatively short lifetime and poor stability after being exposed to water bring extra problems. Moreover, due to the limitation of the photoconductivity of the a-Si:H material, the liquid medium used in OET device must have a low electric conductivity. This is a major bottleneck for cell-related research, as OET devices based on a-Si:H cannot be used for direct cell manipulation in high-conductivity cell-friendly buffers. Although using patterned phototransistors as the photoconductive layer of OET device can effectively solve this problem, it is still an insurmountable challenge for most research groups to fabricate phototransistors that involves ion implantation, photolithography and multi-step plasma etching. To date only two research groups in the world have the experience and facility to fabricate phototransistor-based OET devices. It is worth mentioning that Berkeley Lights has successfully commercialized a fully automated OET instrument (*i.e.* the Beacon system and the Lightening system), along with phototransistor-based OET microfluidic chip matched to the instrument. The company's OET chip is for single use to avoid cross sample contamination. However, it may be impractical to use the phototransistor-based OET device

Table 1 Summary of OET for different applications

Device format	Application	Ref.
Phototransistor-based optoelectronic tweezers	Manipulation and separation of cells/particles	56–58
Vertical OET device	Manipulation/assembly of nanoscale objects	84, 86, 87, 100,1 14, 122, 126, 127 and 134
	Fabricate highly-conductive microelectrode and microelectronic devices	128–132
	Manipulation and assembly of microscale objects	44, 50, 53, 74–77, 96, 100, 127 and 143
	Manipulation of biomolecules and biochemical substances	152–155
	Manipulation and separation of cells	44, 74, 105, 137, 142 and 162
	Cell analysis	180, 191, 193 and 196
	Cell electroporation	202–204
	Cell fusion	205 and 206
	Cell lysis	209–213
	Bio-microfabrication	214–217
	Microfabrication	222
Lateral OET device	Manipulation/assembly of nanoscale and microscale objects	47–49
OET integration with channel microfluidics	Manipulation and separation of cells or particles	166, 170, 172, 195 and 231
OET integration with digital microfluidics and optoelectrowetting	Droplet control and micro-object manipulation	241, 245, 249 and 250
OET in combination with other micromanipulation technologies	Particle manipulation, microrobotics, and cell lysis	74, 233 and 253–256

for certain applications due to the high cost. Therefore, new photoconductive materials and phototransistors structures that can overcome these challenges would further evolve the field and broaden the applications of OET.

In addition, more studies should be carried out to investigate the underlying physics of OET to explain or predict target behaviors under various experimental conditions. Main OET working mechanisms including DEP, ACEO, ACET, and electrodeposition, which are induced by light illumination, have been extensively studied and well characterized for the case when each mechanism occurs alone or dominate over others. However, these mechanisms always occur in conjunction with each other, resulting in complex behaviors of targets in practice that are difficult to be explained using any of the current models. Therefore, it is necessary to develop a complete theoretical model that takes all mechanisms into consideration and can explain and predict the behaviors of targets under OET manipulation. Additionally, there are no conclusive explanations for some important phenomena observed in OET systems, such as self-rotation of certain species of cells, 3D movement of micro-objects, and electrohydrodynamic interactions between polarized micro-objects. More work need to be done to better understand the mechanisms for these phenomena, which is important for better use of OET in many applications.

Next, the capability of OET needs to be further explored in several areas. OET is mainly considered as a 2D manipulation technique, which has shown superior performance in many aspects as reviewed in this paper. However, OET cannot be used for reliable 3D manipulation, which is a major disadvantage compared with optical tweezers. Hence, it is necessary to develop new device or related technologies that support 3D manipulation in OET systems. In addition, 90% of the related research on OET to date have focused on vertical OET devices. There is still huge room to improve and explore the use of lateral OET devices, which have shown superior performance in the assembly of micro/nano optoelectronic components such as micro-disk lasers and nanowires. Apart from lateral OET devices, the research on OEW is insufficient and the capability of this technology is not fully explored. To date, OET is mainly used for manipulation and assembly in small areas ($\sim$less than 2 cm^2) and it is necessary to explore its capability for manipulation and assembly over large areas for manufacturing applications. Non-specific bonding of cells and micro-particles on surface of the OET device remains a problem for OET research. Therefore, relevant research needs to be carried out to develop suitable coatings that can reduce non-specific bonding but without harming the performance of OET. Moreover, it is of great importance to integrate OET with other devices/sensor/tools to detect, analyze, and measure micro/nano-objects. This requires systematically combining OET devices with other predominant characterization techniques, such as atomic force microscopy, confocal microscopy, and Raman microscopy to achieve multiparameter simultaneous acquisition, detection, and analysis of targeted samples. Finally, fully automated and cost-effective OET system is required. As mentioned previously, Berkeley Lights has commercialized a fully automatic OET system known as Beacon. However, the cost of this system is significant. Primarily for this reason, the Beacon system is mostly used in large pharmaceutical companies and the budgets of many labs make it a purchasing challenge. Therefore, it is necessary to develop a fully automatic cost-effective OET system for research and academic uses. More recently, Berkeley Lights developed another OET system known as the Lightning, which has less throughput and automation than the Beacon, but comes at a reduced price point. Such systems will be more affordable for smaller research labs and institutions. In addition, it is necessary

to develop supporting software and computer algorithms for the OET system to allow image acquisition, target identification, and automatic capture/manipulation of targets. It is expected that such a system with high-degree of automation will greatly benefit the OET research and attract more end users from various research fields.

In summary, we present in this article a comprehensive review of the OET technology, which offers tremendous research benefits by providing a programmable, flexible and versatile approach for parallel and multi-scaled micromanipulation. Thanks to the great efforts to improve this technology by worldwide researchers, we believe that OET research will continue to thrive in the near future and the technology will play an increasingly important role in materials/biological/pharmaceutical applications.

Conflicts of interest

Ming C. Wu is the co-founder of Berkeley Lights, Inc. and Justin K. Valley is the Vice President at Berkeley Lights, Inc. Other authors declare no competing interests.

Acknowledgements

This research was supported by the National Natural Science Foundation of China (Grant No. 62103050), Natural Sciences and Engineering Research Council of Canada (Grant No. LLRP 548593-19, CREATE 482073-16, RGPIN 2019-04867, and RTI-2019-00300) and the University of Toronto's Medicine by Design initiative, which receives funding from the Canada First Research Excellence Fund. A. R. W. acknowledges the Canada Research Chair (CRC) program.

References

1 A. Ashkin, J. M. Dziedzic, J. E. Bjorkholm and S. Chu, Observation of a single-beam gradient force optical trap for dielectric particles, *Opt. Lett.*, 1986, **11**(5), 288–290.
2 A. Ashkin, J. M. Dziedzic and T. Yamane, Optical trapping and manipulation of single cells using infrared laser beams, *Nature*, 1987, **330**(6150), 769–771.
3 A. Ashkin and J. M. Dziedzic, Optical trapping and manipulation of viruses and bacteria, *Science*, 1987, **235**(4795), 1517–1520.
4 L. Paterson, M. P. MacDonald, J. Arlt, W. Sibbett, P. E. Bryant and K. Dholakia, Controlled rotation of optically trapped microscopic particles, *Science*, 2001, **292**(5518), 912–914.
5 M. P. MacDonald, G. C. Spalding and K. Dholakia, Microfluidic sorting in an optical lattice, *Nature*, 2003, **426**(6965), 421–424.
6 D. G. Grier, A revolution in optical manipulation, *Nature*, 2003, **424**(6950), 810–816.
7 M. Padgett and R. Bowman, Tweezers with a twist, *Nat. Photonics*, 2011, **5**(6), 343–348.
8 K. Dholakia and T. Čižmár, Shaping the future of manipulation, *Nat. Photonics*, 2011, **5**(6), 335–342.
9 P. J. Pauzauskie, A. Radenovic, E. Trepagnier, H. Shroff, P. Yang and J. Liphardt, Optical trapping and integration of semiconductor nanowire assemblies in water, *Nat. Mater.*, 2006, **5**(2), 97–101.
10 D. B. Phillips, M. J. Padgett, S. Hanna, Y.-L. D. Ho, D. M. Carberry, M. J. Miles and S. H. Simpson, Shape-induced force fields in optical trapping, *Nat. Photonics*, 2014, **8**(5), 400–405.
11 M. Daly, M. Sergides and S. N. Chormaic, Optical trapping and manipulation of micrometer and submicrometer particles, *Laser Photonics Rev.*, 2015, **9**(3), 309–329.
12 A. Ashkin, History of optical trapping and manipulation of small-neutral particle, atoms, and molecules, *IEEE J. Sel. Top. Quantum Electron.*, 2000, **6**(6), 841–856.
13 D. T. Chiu and R. N. Zare, Biased diffusion, optical trapping, and manipulation of single molecules in solution, *J. Am. Chem. Soc.*, 1996, **118**(27), 6512–6513.
14 L. R. Liu, J. D. Hood, Y. Yu, J. T. Zhang, N. R. Hutzler, T. Rosenband and K. K. Ni, Building one molecule from a reservoir of two atoms, *Science*, 2018, **360**(6391), 900–903.
15 L. Anderegg, L. W. Cheuk, Y. Bao, S. Burchesky, W. Ketterle, K. K. Ni and J. M. Doyle, An optical tweezer array of ultracold molecules, *Science*, 2019, **365**(6458), 1156–1158.
16 S. M. Block, D. F. Blair and H. C. Berg, Compliance of bacterial flagella measured with optical tweezers, *Nature*, 1989, **338**(6215), 514–518.
17 H. Kress, J. G. Park, C. O. Mejean, J. D. Forster, J. Park, S. S. Walse, Y. Zhang, D. Wu, O. D. Weiner, T. M. Fahmy and E. R. Dufresne, Cell stimulation with optically manipulated microsources, *Nat. Methods*, 2009, **6**(12), 905–909.
18 T. Wu, T. A. Nieminen, S. Mohanty, J. Miotke, R. L. Meyer, H. Rubinsztein-Dunlop and M. W. Berns, A photon-driven micromotor can direct nerve fibre growth, *Nat. Photonics*, 2012, **6**(1), 62–67.
19 I. A. Favre-Bulle, A. B. Stilgoe, H. Rubinsztein-Dunlop and E. K. Scott, Optical trapping of otoliths drives vestibular behaviours in larval zebrafish, *Nat. Commun.*, 2017, **8**, 630.
20 R. Diekmann, D. L. Wolfson, C. Spahn, M. Heilemann, M. Schüttpelz and T. Huser, Nanoscopy of bacterial cells immobilized by holographic optical tweezers, *Nat. Commun.*, 2016, **7**, 13711.
21 M. C. Zhong, X. B. Wei, J. H. Zhou, Z. Q. Wang and Y. M. Li, Trapping red blood cells in living animals using optical tweezers, *Nat. Commun.*, 2013, **4**, 1768.
22 R. Berkowitz, Father of optical trapping awarded a share of the Nobel Prize in Physics, *Phys. Today*, 2018, **71**(12), 14–17.
23 L. Lin, M. Wang, X. Peng, E. N. Lissek, Z. Mao, L. Scarabelli, E. Adkins, S. Coskun, U. Sahin, H. E. Unalan, B. A. Korgel, L. M. Liz-Marzán, E. L. Florin and Y. Zheng, Opto-thermoelectric nanotweezers, *Nat. Photonics*, 2018, **12**(4), 195–201.
24 L. Lin, X. Peng, X. Wei, Z. Mao, C. Xie and Y. Zheng, Thermophoretic Tweezers for Low-Power and Versatile

Manipulation of Biological Cells, *ACS Nano*, 2017, **11**(3), 3147–3154.
25 L. Lin, J. Zhang, X. Peng, Z. Wu, A. C. H. Coughlan, Z. Mao, M. A. Bevan and Y. Zheng, Opto-Thermophoretic Assembly of Colloidal Matter, *Sci. Adv.*, 2017, **3**(9), e1700458.
26 Y. Liu, L. Lin, B. Bangalore Rajeeva, J. W. Jarrett, X. Li, X. Peng, P. Kollipara, K. Yao, D. Akinwande, A. K. Dunn and Y. Zheng, Nanoradiator-Mediated Deterministic Opto-Thermoelectric Manipulation, *ACS Nano*, 2018, **12**(10), 10383–10392.
27 F. Liu, Z. Zhang, Y. Wei, Q. Zhang, T. Cheng and X. Wu, Photophoretic trapping of multiple particles in tapered-ring optical field, *Opt. Express*, 2014, **22**(19), 23716–23723.
28 M. Esseling, P. Rose, C. Alpmann and C. Denz, Photophoretic trampoline—Interaction of single airborne absorbing droplets with light, *Appl. Phys. Lett.*, 2012, **101**(13), 131115.
29 M. L. Juan, M. Righini and R. Quidant, Plasmon nano-optical tweezers, *Nat. Photonics*, 2011, **5**(6), 349–356.
30 Y. Zhang, C. Min, X. Dou, X. Wang, H. P. Urbach, M. G. Somekh and X. Yuan, Plasmonic tweezers: for nanoscale optical trapping and beyond, *Light: Sci. Appl.*, 2021, **10**(1), 1–41.
31 K. Wang, E. Schonbrun, P. Steinvurzel and K. B. Crozier, Trapping and rotating nanoparticles using a plasmonic nano-tweezer with an integrated heat sink, *Nat. Commun.*, 2011, **2**, 469.
32 P. T. Lin, H. Y. Chu, T. W. Lu and P. T. Lee, Trapping particles using waveguide-coupled gold bowtie plasmonic tweezers, *Lab Chip*, 2014, **14**(24), 4647–4652.
33 Y. Zhao, A. A. E. Saleh and J. A. Dionne, Enantioselective optical trapping of chiral nanoparticles with plasmonic tweezers, *ACS Photonics*, 2016, **3**(3), 304–309.
34 P. Mestres, J. Berthelot, S. S. Aćimović and R. Quidant, Unraveling the optomechanical nature of plasmonic trapping, *Light: Sci. Appl.*, 2016, **5**(7), e16092.
35 Y. Xie, C. Zhao, Y. Zhao, S. Li, J. Rufo, S. Yang, F. Guo and T. J. Huang, Optoacoustic tweezers: a programmable, localized cell concentrator based on opto-thermally generated, acoustically activated, surface bubbles, *Lab Chip*, 2013, **13**(9), 1772–1779.
36 V. P. Zharov, T. V. Malinsky and R. C. Kurten, Photoacoustic tweezers with a pulsed laser: theory and experiments, *J. Phys. D: Appl. Phys*, 2005, **38**(15), 2662–2674.
37 M. C. Wu, Optoelectronic tweezers, *Nat. Photonics*, 2011, **5**(6), 322–324.
38 K. Dholakia, Optoelectronic tweezers, *Nat. Mater.*, 2005, **4**(8), 579–580.
39 H. Hwang and J. K. Park, Optoelectrofluidic platforms for chemistry and biology, *Lab Chip*, 2011, **11**(1), 33–47.
40 W. Liang, L. Liu, H. Zhang, Y. Wang and W. J. Li, Optoelectrokinetics-based microfluidic platform for bioapplications: A review of recent advances, *Biomicrofluidics*, 2019, **13**(5), 051502.
41 W. Liang, L. Liu, J. Wang, X. Yang, Y. Wang, W. J. Li and W. Yang, A Review on Optoelectrokinetics-Based Manipulation and Fabrication of Micro/Nanomaterials, *Micromachines*, 2020, **11**(1), 78.
42 Y. Huang, Z. Liang, M. Alsoraya, J. Guo and D. E. Fan, Light Gated Manipulation of Micro/Nanoparticles in Electric Fields, *Adv. Intell. Syst.*, 2020, **2**(7), 1900127.
43 M. Woerdemann, C. Alpmann, M. Esseling and C. Denz, Advanced optical trapping by complex beam shaping, *Laser Photonics Rev.*, 2013, **7**(6), 839–854.
44 P. Y. Chiou, A. T. Ohta and M. C. Wu, Massively parallel manipulation of single cells and microparticles using optical images, *Nature*, 2005, **436**(7049), 370–372.
45 S. L. Neale, M. Mazilu, J. I. B. Wilson, K. Dholakia and T. F. Krauss, The resolution of optical traps created by light induced dielectrophoresis (LIDEP), *Opt. Express*, 2007, **15**(20), 12619–12626.
46 J. K. Valley, A. T. Ohta, H. Y. Hsu, S. L. Neale, A. Jamshidi and M. C. Wu, Optoelectronic tweezers as a tool for parallel single-cell manipulation and stimulation, *IEEE Trans. Biomed. Circuits Syst.*, 2009, **3**(6), 424–431.
47 M. C. Tien, A. T. Ohta, K. Yu, S. L. Neale and M. C. Wu, Heterogeneous integration of InGaAsP microdisk laser on a silicon platform using optofluidic assembly, *Appl. Phys. A*, 2009, **95**(4), 967–972.
48 A. T. Ohta, A. Jamshidi, P. J. Pauzauskie, H. Y. Hsu, P. Yang and M. C. Wu, Trapping and transport of silicon nanowires using lateral-field optoelectronic tweezers, in 2007 Conference on Lasers and Electro-Optics (CLEO), Baltimore, MD, USA, 2007.
49 A. T. Ohta, S. L. Neale, H. Y. Hsu, J. K. Valley and M. C. Wu, Parallel assembly of nanowires using lateral-field optoelectronic tweezers, in 2008 IEEE/LEOS International Conference on Optical MEMs and Nanophotonics, Freiburg, Germany, 2008.
50 S. M. Yang, T. M. Yu, H. P. Huang, M. Y. Ku, L. Hsu and C. H. Liu, Dynamic manipulation and patterning of microparticles and cells by using TiOPc-based optoelectronic dielectrophoresis, *Opt. Lett.*, 2010, **35**(12), 1959–1961.
51 S. M. Yang, T. M. Yu, H. P. Huang, M. Y. Ku, S. Y. Tseng, C. L. Tsai, H. P. Chen, L. Hsu and C. H. Liu, Light-driven manipulation of picobubbles on a titanium oxide phthalocyanine-based optoelectronic chip, *Appl. Phys. Lett.*, 2011, **98**(15), 153512.
52 L. Y. Ke, Z. K. Kuo, Y. S. Chen, T. Y. Yeh, M. Dong, H. W. Tseng and C. H. Liu, Cancer immunotherapy μ-environment LabChip: taking advantage of optoelectronic tweezers, *Lab Chip*, 2018, **18**(1), 106–114.
53 W. Wang, Y. H. Lin, R. S. Guan, T. C. Wen, T. F. Guo and G. B. Lee, Bulk-heterojunction polymers in optically-induced dielectrophoretic devices for the manipulation of microparticles, *Opt. Express*, 2009, **17**(20), 17603–17613.
54 W. Wang, Y. H. Lin, T. C. Wen, T. F. Guo and G. B. Lee, Selective manipulation of microparticles using polymer-based optically induced dielectrophoretic devices, *Appl. Phys. Lett.*, 2010, **96**(11), 113302.
55 S. J. Lin, S. H. Hung, J. Y. Jeng, T. F. Guo and G. B. Lee, Manipulation of micro-particles by flexible polymer-based

optically-induced dielectrophoretic devices, *Opt. Express*, 2012, **20**(1), 583–592.
56 H. Y. Hsu, A. T. Ohta, P. Y. Chiou, A. Jamshidi, S. L. Neale and M. C. Wu, Phototransistor-based optoelectronic tweezers for dynamic cell manipulation in cell culture media, *Lab Chip*, 2010, **10**(2), 165–172.
57 A. Jamshidi, S. Shekarchian, W. Lam, J. K. Valley, S. N. Pei and M. C. Wu, Open-access phototransistor-based optoelectronic tweezers for long-term single cell heterogeneity study, in 2011 IEEE 24th International Conference on Micro Electro Mechanical Systems, Cancun, Mexico, 2011.
58 Y. Yang, Y. Mao, K. S. Shin, C. O. Chui and P. Y. Chiou, Self-locking optoelectronic tweezers for single-cell and microparticle manipulation across a large area in high conductivity media, *Sci. Rep.*, 2016, **6**, 22630.
59 H. A. Eggert, F. Y. Kuhnert, K. Buse, J. R. Adleman and D. Psaltis, Trapping of dielectric particles with light-induced space-charge fields, *Appl. Phys. Lett.*, 2007, **90**(24), 241909.
60 C. Arregui, J. B. Ramiro, Á. Alcázar, Á. Méndez, H. Burgos, Á. García-Cabañes and M. Carrascosa, Optoelectronic tweezers under arbitrary illumination patterns: theoretical simulations and comparison to experiment, *Opt. Express*, 2014, **22**(23), 29099–29110.
61 J. Villarroel, H. Burgos, Á. García-Cabañes, M. Carrascosa, A. Blázquez-Castro and F. Agulló-López, Photovoltaic versus optical tweezers, *Opt. Express*, 2011, **19**(24), 24320–24330.
62 M. Esseling, A. Zaltron, C. Sada and C. Denz, Charge sensor and particle trap based on z-cut lithium niobate, *Appl. Phys. Lett.*, 2013, **103**(6), 061115.
63 J. F. Muñoz-Martínez, M. Jubera, J. Matarrubia, A. García-Cabañes, F. Agulló-López and M. Carrascosa, Diffractive optical devices produced by light-assisted trapping of nanoparticles, *Opt. Lett.*, 2016, **41**(2), 432–435.
64 S. Glaesener, M. Esseling and C. Denz, Multiplexing and switching of virtual electrodes in optoelectronic tweezers based on lithium niobate, *Opt. Lett.*, 2012, **37**(18), 3744–3746.
65 J. F. Muñoz-Martínez, I. Elvira, M. Jubera, A. García-Cabañes, J. B. Ramiro, C. Arregui and M. Carrascosa, Efficient photo-induced dielectrophoretic particle trapping on Fe: $LiNbO_3$ for arbitrary two dimensional patterning, *Opt. Mater. Express*, 2015, **5**(5), 1137–1146.
66 I. Elvira, J. F. Muñoz-Martínez, Á. Barroso, C. Denz, J. B. Ramiro, A. García-Cabañes, F. Agulló-López and M. Carrascosa, Massive ordering and alignment of cylindrical micro-objects by photovoltaic optoelectronic tweezers, *Opt. Lett.*, 2018, **43**(1), 30–33.
67 M. Jubera, I. Elvira, A. García-Cabañes, J. L. Bella and M. Carrascosa, Trapping and patterning of biological objects using photovoltaic tweezers, *Appl. Phys. Lett.*, 2016, **108**(2), 023703.
68 A. Puerto, J. F. Muñoz-Martín, A. Méndez, L. Arizmendi, A. García-Cabañes, F. Agulló-López and M. Carrascosa, A Synergy between pyroelectric and photovoltaic effects for optoelectronic nanoparticle manipulation, *Opt. Express*, 2019, **27**(2), 804–815.
69 A. Puerto, A. Méndez, L. Arizmendi, A. García-Cabañes and M. Carrascosa, Optoelectronic Manipulation, Trapping, Splitting, and Merging of Water Droplets and Aqueous Biodroplets Based on the Bulk Photovoltaic Effect, *Phys. Rev. Appl.*, 2020, **14**, 024046.
70 A. Zaltron, D. Ferraro, A. Meggiolaro, S. Cremaschini, M. Carneri, E. Chiarello, P. Sartori, M. Pierno, C. Sada and G. Mistura, Optofluidic Platform for the Manipulation of Water Droplets on Engineered $LiNbO_3$ Surfaces, *Adv. Mater. Interfaces*, 2022, **9**, 2200345.
71 C. Sebastián-Vicente, E. Muñoz-Cortés, A. García-Cabañes, F. Agulló-López and M. Carrascosa, Real-Time Operation of Photovoltaic Optoelectronic Tweezers: New Strategies for Massive Nano-object Manipulation and Reconfigurable Patterning, *Part. Part. Syst. Charact.*, 2019, **36**(9), 1900233.
72 M. Carrascosa, A. García-Cabañes, M. Jubera, J. B. Ramiro and F. Agulló-López, $LiNbO_3$: A photovoltaic substrate for massive parallel manipulation and patterning of nano-objects, *Appl. Phys. Rev.*, 2015, **2**(4), 040605.
73 A. Blázquez-Castro, A. García-Cabañes and M. Carrascosa, Biological applications of ferroelectric materials, *Appl. Phys. Rev.*, 2018, **5**(4), 041101.
74 S. Zhang, N. Shakiba, Y. Chen, Y. Zhang, P. Tian, J. Singh, M. D. Chamberlain, M. Satkauskas, A. G. Flood, N. P. Kherani, S. Yu, P. W. Zandstra and A. R. Wheeler, Patterned optoelectronic tweezers: A new scheme for selecting, moving, and storing dielectric particles and cells, *Small*, 2018, **14**(45), 1803342.
75 S. Zhang, W. Li, M. Elsayed, P. Tian, A. W. Clark, A. R. Wheeler and S. L. Neale, Size-scaling effects for microparticles and cells manipulated by optoelectronic tweezers, *Opt. Lett.*, 2019, **44**(17), 4171–4174.
76 S. Zhang, Y. Liu, J. Juvert, P. Tian, J. C. Navarro, J. M. Cooper and S. L. Neale, Use of optoelectronic tweezers in manufacturing-accurate solder bead positioning, *Appl. Phys. Lett.*, 2016, **109**(22), 221110.
77 S. Zhang, J. Juvert, J. M. Cooper and S. L. Neale, Manipulating and assembling metallic beads with Optoelectronic Tweezers, *Sci. Rep.*, 2016, **6**, 32840.
78 N. Liu, Y. Lin, Y. Peng, L. Xin, T. Yue, Y. Liu, C. Ru, S. Xie, L. Dong, H. Pu, H. Chen, W. J. Li and Y. Sun, Automated Parallel Electrical Characterization of Cells Using Optically-Induced Dielectrophoresis, *IEEE Trans. Autom. Sci. Eng.*, 2020, **17**(2), 1084–1092.
79 Y. Li, S. H. Lai, N. Liu, G. Zhang, L. Liu, G. B. Lee and W. J. Li, Fabrication of high-aspect-ratio 3D hydrogel microstructures using optically induced electrokinetics, *Micromachines*, 2016, **7**(4), 65.
80 H. Hwang, Y. H. Park and J. K. Park, Optoelectrofluidic control of colloidal assembly in an optically induced electric field, *Langmuir*, 2009, **25**(11), 6010–6014.
81 M. Li, N. Liu, P. Li, J. Shi, G. Li, N. Xi, Y. Wang and L. Liu, Performance investigation of multilayer MoS2 thin-film transistors fabricated via mask-free optically induced electrodeposition, *ACS Appl. Mater. Interfaces*, 2017, **9**(9), 8361–8370.

82 S. Xie, X. Wang, N. Jiao, S. Tung and L. Liu, Programmable micrometer-sized motor array based on live cells, *Lab Chip*, 2017, **17**(12), 2046–2053.
83 S. Ota, S. Wang, Y. Wang, X. Yin and X. Zhang, Lipid bilayer-integrated optoelectronic tweezers for nanoparticle manipulations, *Nano Lett.*, 2013, **13**(6), 2766–2770.
84 A. Jamshidi, P. J. Pauzauskie, P. J. Schuck, A. T. Ohta, P. Y. Chiou, J. Chou, P. Yang and M. C. Wu, Dynamic manipulation and separation of individual semiconducting and metallic nanowires, *Nat. Photonics*, 2008, **2**(2), 86–89.
85 S. M. Yang, P. T. Harishchandra, T. M. Yu, M. H. Liu, L. Hsu and C. H. Liu, Concentration of magnetic beads utilizing light-induced electro-osmosis flow, *IEEE Trans. Magn.*, 2011, **47**(10), 2418–2421.
86 H. Hwang, D. Han, Y. J. Oh, Y. K. Cho, K. H. Jeong and J. K. Park, In situ dynamic measurements of the enhanced SERS signal using an optoelectrofluidic SERS platform, *Lab Chip*, 2011, **11**(15), 2518–2525.
87 M. B. Lim, J. L. Hanson, L. Vandsburger, P. B. Roder, X. Zhou, B. E. Smith, F. S. Ohuchi and P. J. Pauzauskie, Copper-and chloride-mediated synthesis and optoelectronic trapping of ultra-high aspect ratio palladium nanowires, *J. Mater. Chem. A*, 2018, **6**(14), 5644–5651.
88 A. T. Ohta, M. Garcia, J. K. Valley, L. Banie, H. Y. Hsu, A. Jamshidi, S. L. Neale, T. Lue and M. C. Wu, Motile and non-motile sperm diagnostic manipulation using optoelectronic tweezers, *Lab Chip*, 2010, **10**(23), 3213–3217.
89 A. H. Jeorrett, S. L. Neale, D. Massoubre, E. Gu, R. K. Henderson, O. Millington, K. Mathieson and M. D. Dawson, Optoelectronic tweezers system for single cell manipulation and fluorescence imaging of live immune cells, *Opt. Express*, 2014, **22**(2), 1372–1380.
90 A. Zarowna-Dabrowska, S. L. Neale, D. Massoubre, J. McKendry, B. R. Rae, R. K. Henderson, M. J. Rose, H. Yin, J. M. Cooper, E. Gu and M. D. Dawson, Miniaturized optoelectronic tweezers controlled by GaN micro-pixel light emitting diode arrays, *Opt. Express*, 2011, **19**(3), 2720–2728.
91 S. L. Neale, C. Witte and J. M. Cooper, Portable optoelectronic tweezers (OET), taking optical micromanipulation out of the optics lab, European Optical Society Annual Meeting, Aberdeen, UK, 2012.
92 W. Choi, S. H. Kim, J. Jang and J. K. Park, Lab-on-a-display: a new microparticle manipulation platform using a liquid crystal display (LCD), *Microfluid. Nanofluidics*, 2007, **3**(2), 217–225.
93 H. Hwang and J. K. Park, Rapid and selective concentration of microparticles in an optoelectrofluidic platform, *Lab Chip*, 2009, **9**(2), 199–206.
94 H. Hwang, Y. J. Choi, W. Choi, S. H. Kim, J. Jang and J. K. Park, Interactive manipulation of blood cells using a lens - integrated liquid crystal display based optoelectronic tweezers system, *Electrophoresis*, 2008, **29**(6), 1203–1212.
95 W. Choi, S. W. Nam, H. Hwang, S. Park and J. K. Park, Programmable manipulation of motile cells in optoelectronic tweezers using a grayscale image, *Appl. Phys. Lett.*, 2008, **93**(14), 143901.
96 K. W. Huang, T. W. Su, A. Ozcan and P. Y. Chiou, Optoelectronic tweezers integrated with lensfree holographic microscopy for wide-field interactive cell and particle manipulation on a chip, *Lab Chip*, 2013, **13**(12), 2278–2284.
97 H. Hwang, H. Chon, J. Choo and J. K. Park, Optoelectrofluidic sandwich immunoassays for detection of human tumor marker using surface-enhanced Raman scattering, *Anal. Chem.*, 2010, **82**(18), 7603–7610.
98 W. Yang, H. Yu, G. Li, Y. Wang and L. Liu, High-Throughput Fabrication and Modular Assembly of 3D Heterogeneous Microscale Tissues, *Small*, 2017, **13**(5), 1602769.
99 P. Y. Chu, C. J. Liao, C. H. Hsieh, H. W. Wang, W. P. Chou, P. H. Chen and M. H. Wu, Utilization of optically induced dielectrophoresis in a microfluidic system for sorting and isolation of cells with varied degree of viability: Demonstration of the sorting and isolation of drug-treated cancer cells with various degrees of anti-cancer drug resistance gene expression, *Sens. Actuators, B*, 2019, **283**, 621–631.
100 S. Zhang, Y. Zhai, R. Peng, M. Shayegannia, A. G. Flood, J. Qu, X. Liu, N. P. Kherani and A. R. Wheeler, Assembly of Topographical Micropatterns with Optoelectronic Tweezers, *Adv. Opt. Mater.*, 2019, **7**(20), 1900669.
101 W. Liang, S. Wang, Z. Dong, G. B. Lee and W. J. Li, Optical spectrum and electric field waveform dependent optically-induced dielectrophoretic (ODEP) micro-manipulation, *Micromachines*, 2012, **3**(2), 492–508.
102 X. Zhu, H. Yi and Z. Ni, Frequency-dependent behaviors of individual microscopic particles in an optically induced dielectrophoresis device, *Biomicrofluidics*, 2010, **4**(1), 013202.
103 J. K. Valley, A. Jamshidi, A. T. Ohta, H. Y. Hsu and M. C. Wu, Operational regimes and physics present in optoelectronic tweezers, *J. Microelectromech. Syst.*, 2008, **17**(2), 342–350.
104 R. Pethig, Review Article-Dielectrophoresis: Status of the theory, technology, and applications, *Biomicrofluidics*, 2010, **4**(2), 022811.
105 S. L. Neale, A. T. Ohta, H. Y. Hsu, J. K. Valley, A. Jamshidi and M. C. Wu, Trap profiles of projector based optoelectronic tweezers (OET) with HeLa cells, *Opt. Express*, 2009, **17**(7), 5231–5239.
106 C. Qian, H. Huang, L. Chen, X. Li, Z. Ge, T. Chen, Z. Yang and L. Sun, Dielectrophoresis for bioparticle manipulation. International journal of molecular sciences, *Int. J. Mol. Sci.*, 2014, **15**(10), 18281–18309.
107 J. Yang, Y. Huang, X. B. Wang, F. F. Becker and P. R. C. Gascoyne, Cell separation on microfabricated electrodes using dielectrophoretic/gravitational field-flow fractionation, *Anal. Chem.*, 1999, **71**(5), 911–918.
108 W. Liang, Y. Zhao, L. Liu, Y. Wang, Z. Dong, W. J. Li, G. B. Lee, X. Xiao and W. Zhang, Rapid and label-free separation of burkitt's lymphoma cells from red blood cells by optically-induced electrokinetics, *PLoS One*, 2014, **9**(3), e90827.

109 S. Zhang, A. Nikitina, Y. Chen, Y. Zhang, L. Liu, A. G. Flood, J. Juvert, M. D. Chamberlain, N. P. Kherani, S. L. Neale and A. R. Wheeler, Escape from an optoelectronic tweezer trap: Experimental results and simulations, *Opt. Express*, 2018, **26**(5), 5300–5309.

110 J. Juvert, S. Zhang, I. Eddie, C. J. Mitchell, G. T. Reed, J. S. Wilkinson, A. Kelly and S. L. Neale, Micromanipulation of InP lasers with optoelectronic tweezers for integration on a photonic platform, *Opt. Express*, 2016, **24**(16), 18163–18175.

111 S. Kumar and P. J. Hesketh, Interpretation of ac dielectrophoretic behavior of tin oxide nanobelts using Maxwell stress tensor approach modeling, *Sens. Actuators, B*, 2012, **161**(1), 1198–1208.

112 X. Wang, X. B. Wang and P. R. C. Gascoyne, General expressions for dielectrophoretic force and electrorotational torque derived using the Maxwell stress tensor method, *J. Electrostat.*, 1997, **39**(4), 277–295.

113 P. Y. Chiou, A. T. Ohta, A. Jamshidi, H. Y. Hsu and M. C. Wu, Light-actuated AC electroosmosis for nanoparticle manipulation, *J. Microelectromech. Syst*, 2008, **17**(3), 525–531.

114 A. Jamshidi, S. L. Neale, K. Yu, P. J. Pauzauskie, P. J. Schuck, J. K. Valley, H. Y. Hsu, A. T. Ohta and M. C. Wu, NanoPen: dynamic, low-power, and light-actuated patterning of nanoparticles, *Nano Lett.*, 2009, **9**(8), 2921–2925.

115 W. Liang, L. Liu, S. H. Lai, Y. Wang, G. B. Lee and W. J. Li, Rapid assembly of gold nanoparticle-based microstructures using optically-induced electrokinetics, *Opt. Mater. Express*, 2014, **4**(11), 2368–2380.

116 A. Kumar, J. S. Kwon, S. J. Williams, N. G. Green, N. K. Yip and S. T. Wereley, Optically modulated electrokinetic manipulation and concentration of colloidal particles near an electrode surface, *Langmuir*, 2010, **26**(7), 5262–5272.

117 S. J. Williams, A. Kumar and S. T. Wereley, Electrokinetic patterning of colloidal particles with optical landscapes, *Lab Chip*, 2008, **8**(11), 1879–1882.

118 A. Castellanos, A. Ramos, A. Gonzalez, N. G. Green and H. Morgan, Electrohydrodynamics and dielectrophoresis in microsystems: scaling laws, *J. Phys. D: Appl. Phys.*, 2003, **36**(20), 2584–2597.

119 A. N. Lau, A. T. Ohta, H. L. Phan, H. Y. Hsu, A. Jamshidi, P. Y. Chiou and M. C. Wu, Antifouling coatings for optoelectronic tweezers, *Lab Chip*, 2009, **9**(20), 2952–2957.

120 H. Hwang, Y. Oh, J. J. Kim, W. Choi, J. K. Park, S. H. Kim and J. Jang, Reduction of nonspecific surface-particle interactions in optoelectronic tweezers, *Appl. Phys, Lett.*, 2008, **92**(2), 024108.

121 H. Hwang, J. J. Kim and J. K. Park, Experimental investigation of electrostatic particle-particle interactions in optoelectronic tweezers, *J. Phys. Chem. B*, 2008, **112**(32), 9903–9908.

122 Y. H. Lin, K. S. Ho, C. T. Yang, J. H. Wang and C. S. Lai, A highly flexible platform for nanowire sensor assembly using a combination of optically induced and conventional dielectrophoresis, *Opt. Express*, 2014, **22**(11), 13811–13824.

123 S. Zhang, J. M. Cooper and S. L. Neale, *Assembling silver nanowires using optoelectronic tweezers*, Advanced Fabrication Technologies for Micro/Nano Optics and Photonics IX 2016, San Francisco, California, USA, 2016, vol. 9759, p. 97590S.

124 P. J. Pauzauskie, A. Jamshidi, J. K. Valley, J. J. H. Satcher and M. C. Wu, Parallel trapping of multiwalled carbon nanotubes with optoelectronic tweezers, *Appl. Phys. Lett.*, 2009, **95**(11), 113104.

125 M. J. Zheng, Y. L. Qu, Y. Z. Zhang and Z. L. Dong, Optically induced dielectrophoresis based automatic assembly of micro/nano-devices, *Integr. Ferroelectr.*, 2013, **145**(1), 24–31.

126 M. B. Lim, R. G. Felsted, X. Zhou, B. E. Smith and P. J. Pauzauskie, Patterning of graphene oxide with optoelectronic tweezers, *Appl. Phys. Lett.*, 2018, **113**(3), 031106.

127 S. Zhang, W. Li, M. Elsayed, J. Peng, Y. Chen, Y. Zhang, Y. Zhang, M. Shayegannia, W. Dou, T. Wang, Y. Sun, N. P. Kherani, S. L. Neale and A. R. Wheeler, Integrated Assembly and Photopreservation of Topographical Micropatterns, *Small*, 2021, **17**(37), 2103702.

128 N. Liu, W. Liang, J. D. Mai, L. Liu, G. B. Lee and W. J. Li, Rapid fabrication of nanomaterial electrodes using digitally controlled electrokinetics, *IEEE Trans. Nanotechnol.*, 2014, **13**(2), 245–253.

129 N. Liu, M. Li, L. Liu, Y. Yang, J. Mai, H. Pu, Y. Sun and W. J. Li, Single-step fabrication of electrodes with controlled nanostructured surface roughness using optically-induced electrodeposition, *J. Micromech. Microeng.*, 2018, **28**(2), 025011.

130 N. Liu, F. Wang, L. Liu, H. Yu, S. Xie, J. Wang, Y. Wang, G. B. Lee and W. J. Li, Rapidly patterning micro/nano devices by directly assembling ions and nanomaterials, *Sci. Rep.*, 2016, **6**, 32106.

131 N. Liu, F. Wei, L. Liu, H. S. Lai, H. Yu, Y. Wang, G. B. Lee and W. J. Li, Optically-controlled digital electrodeposition of thin-film metals for fabrication of nano-devices, *Opt. Mater. Express*, 2015, **5**(4), 838–848.

132 P. Li, N. Liu, H. Yu, F. Wang, L. Liu, G. B. Lee, Y. Wang and W. J. Li, Silver nanostructures synthesis via optically induced electrochemical deposition, *Sci. Rep.*, 2016, **6**, 28035.

133 Y. C. Tsai, Y. H. Hong, S. J. Zhang and J. N. Kuo, Frequency-selective electrokinetic manipulation of microparticles in gold nanofilm optically-induced dielectrophoretic device, *Microsyst. Technol.*, 2020, **26**, 1213–1222.

134 W. Liang, N. Liu, Z. Dong, L. Liu, J. D. Mai, G. B. Lee and W. J. Li, Simultaneous separation and concentration of micro-and nano-particles by optically induced electrokinetics, *Sens. Actuators, A*, 2013, **193**, 103–111.

135 I. F. Cheng, S. L. Liu, C. C. Chung and H. C. Chang, Stepwise gray-scale light-induced electric field gradient for passive and continuous separation of microparticles, *Microfluid. Nanofluidics*, 2012, **12**(1–4), 95–105.

136 S. Lee, H. J. Park, Y. S. Yoon and K. H. Kang, Optoelectrofluidic field separation based on light-intensity gradients, *Biomicrofluidics*, 2010, **4**(3), 034102.

137 A. T. Ohta, P. Y. Chiou, T. H. Han, J. C. Liao, U. Bhardwaj, E. R. McCabe, F. Yu, R. Sun and M. C. Wu, Dynamic cell and microparticle control via optoelectronic tweezers, *J. Microelectromech. Syst*, 2007, **16**(3), 491–499.

138 W. Y. Lin, Y. H. Lin and G. B. Lee, Separation of microparticles utilizing spatial difference of optically induced dielectrophoretic forces, *Microfluid. Nanofluidics*, 2010, **8**(2), 217–229.

139 S. Liang, Y. Cao, Y. Dai, F. Wang, X. Bai, B. Song, C. Zhang, C. Gan, F. Arai and L. Feng, A Versatile Optoelectronic Tweezer System for Micro-Objects Manipulation: Transportation, Patterning, Sorting, Rotating and Storage, *Micromachines*, 2021, **12**(3), 271.

140 S. Zhang, Y. Liu, Y. Qian, W. Li, J. Juvert, P. Tian, J. C. Navarro, A. W. Clark, E. Gu, M. D. Dawson, J. M. Cooper and S. L. Neale, Manufacturing with light - micro-assembly of opto-electronic microstructures, *Opt. Express*, 2017, **25**(23), 28838–28850.

141 J. R. Sperling, S. L. Neale and A. W. Clark, Bridging the gap: Rewritable electronics using real-time light-induced dielectrophoresis on lithium niobate, *Sci. Rep.*, 2017, **7**, 9660.

142 S. Liang, C. Gan, Y. Dai, C. Zhang, X. Bai, S. Zhang, A. R. Wheeler, H. Chen and L. Feng, Interaction between positive and negative dielectric microparticles/microorganism in optoelectronic tweezers, *Lab Chip*, 2021, **21**(22), 4379–4389.

143 S. Zhang, M. Elsayed, R. Peng, Y. Chen, Y. Zhang, S. L. Neale and A. R. Wheeler, Influence of light pattern thickness on the manipulation of dielectric microparticles by optoelectronic tweezers, *Photonics Res.*, 2022, **10**(2), 02000550.

144 D. H. Lee, H. Hwang and J. K. Park, Generation and manipulation of droplets in an optoelectrofluidic device integrated with microfluidic channels, *Appl. Phys. Lett.*, 2009, **95**(16), 164102.

145 S. H. Hung, Y. H. Lin and G. B. Lee, A microfluidic platform for manipulation and separation of oil-in-water emulsion droplets using optically induced dielectrophoresis, *J. Micromech. Microeng.*, 2010, **20**(4), 045026.

146 S. Park, C. Pan, T. H. Wu, C. Kloss, S. Kalim, C. E. Callahan, M. Teitell and E. P. Chiou, Floating electrode optoelectronic tweezers: light-driven dielectrophoretic droplet manipulation in electrically insulating oil medium, *Appl. Phys. Lett.*, 2008, **92**(15), 151101.

147 S. Y. Park, S. Kalim, C. Callahan, M. A. Teitell and E. P. Chiou, A light-induced dielectrophoretic droplet manipulation platform, *Lab Chip*, 2009, **9**(22), 3228–3235.

148 M. Esseling, A. Zaltron, W. Horn and C. Denz, Optofluidic droplet router, *Laser Photon. Rev.*, 2015, **9**(1), 98–104.

149 E. Muñoz-Cortés, A. Puerto, A. Blázquez-Castro, L. Arizmendi, J. L. Bella, C. López-Fernández, M. Carrascosa and A. García-Cabañes, Optoelectronic generation of bio-aqueous femtodroplets based on the bulk photovoltaic effect, *Opt. Lett.*, 2020, **45**(5), 1164–1167.

150 S. M. Yang, P. T. Harishchandra, T. M. Yu, M. H. Liu, L. Hsu and C. H. Liu, Concentration of magnetic beads utilizing light-induced electro-osmosis flow, *IEEE Trans. Magn.*, 2011, **47**(10), 2418–2421.

151 J. L. Hong, C. M. Yang, P. Y. Chu, W. P. Chou, C. J. Liao, C. H. Hsieh, M. H. Wu and P. H. Chen, The effect of operating conditions on the optically induced electrokinetic (OEK)-based manipulation of magnetic microbeads in a microfluidic system, *Sens. Actuators, B*, 2019, **296**, 126610.

152 M. Hoeb, J. O. Rädler, S. Klein, M. Stutzmann and M. S. Brandt, Light-induced dielectrophoretic manipulation of DNA, *Biophys. J.*, 2007, **93**(3), 1032–1038.

153 Y. H. Lin, C. M. Chang and G. B. Lee, Manipulation of single DNA molecules by using optically projected images, *Opt. Express*, 2009, **17**(17), 15318–15329.

154 H. Hwang and J. K. Park, Dynamic light-activated control of local chemical concentration in a fluid, *Anal. Chem.*, 2009, **81**(14), 5865–5870.

155 H. Hwang and J. K. Park, Measurement of molecular diffusion based on optoelectrofluidic fluorescence microscopy, *Anal. Chem.*, 2009, **81**(21), 9163–9167.

156 D. Han and J. K. Park, Optoelectrofluidic enhanced immunoreaction based on optically-induced dynamic AC electroosmosis, *Lab Chip*, 2016, **16**(7), 1189–1196.

157 D. Han and J. K. Park, Microarray-integrated optoelectrofluidic immunoassay system, *Biomicrofluidics*, 2016, **10**(3), 034106.

158 D. Han, H. Hwang and J. K. Park, Optoelectrofluidic behavior of metal–polymer hybrid colloidal particles, *Appl. Phys. Lett.*, 2013, **102**(5), 054105.

159 Y. S. Lu, Y. P. Huang, J. A. Yeh and C. Lee, Controllability of non-contact cell manipulation by image dielectrophoresis (iDEP), *Opt. Quantum Electron.*, 2005, **37**(13–15), 1385–1395.

160 P. Y. Chu, C. J. Liao, H. M. Wang and M. H. Wu, The Influence of Electric Parameters on the Manipulation of Biological Cells in a Microfluidic System Using Optically Induced Dielectrophoresis, *Int. J. Electrochem. Sci.*, 2019, **14**, 905–918.

161 X. Qu, L. Dong, J. Cai and Z. Wang, Manipulation of living cells by optically induced dielectrophoresis, in 2015 International Conference on Manipulation, Manufacturing and Measurement on the Nanoscale, Changchun, China 2015, pp. 259–262.

162 S. L. Neale, A. T. Ohta, H. Y. Hsu, J. K. Valley, A. Jamshidi and M. C. Wu, *Force versus position profiles of HeLa cells trapped in phototransistor-based optoelectronic tweezers*, Emerging Digital Micromirror Device Based Systems and Applications, San Jose, California, USA, 2009, vol. 7210, p. 721004.

163 H. Y. Hsu, A. T. Ohta, P. Y. Chiou, A. Jamshidi and M. C. Wu, Phototransistor-based optoelectronic tweezers for cell manipulation in highly conductive solution, TRANSDUCERS 2007-2007 International Solid-State Sensors, Actuators and Microsystems Conference, Lyon, France, 2007.

164 K. W. Huang, Y. C. Wu, J. A. Lee and P. Y. Chiou, Microfluidic integrated optoelectronic tweezers for single-cell

preparation and analysis, *Lab Chip*, 2013, **13**(18), 3721–3727.

165 T. K. Chiu, W. P. Chou, S. B. Huang, H. M. Wang, Y. C. Lin, C. H. Hsieh and M. H. Wu, Application of optically-induced-dielectrophoresis in microfluidic system for purification of circulating tumour cells for gene expression analysis-Cancer cell line model, *Sci. Rep.*, 2016, **6**, 32851.

166 C. J. Liao, C. H. Hsieh, T. K. Chiu, Y. X. Zhu, H. M. Wang, F. C. Hung, W. P. Chou and M. H. Wu, An Optically Induced Dielectrophoresis (ODEP)-Based Microfluidic System for the Isolation of High-Purity $CD45^{neg}/EpCAM^{neg}$ Cells from the Blood Samples of Cancer Patients—Demonstration and Initial Exploration of the Clinical Significance of These Cells, *Micromachines*, 2018, **9**(11), 563.

167 W. Hu, Y. Ma, Z. Zhan, D. Hussain and C. Hu, Robotic Intracellular Electrochemical Sensing for Adherent Cells, *Cyborg Bionic Syst.*, 2022, **2022**, 9763420.

168 S. B. Huang, J. Chen, J. Wang, C. L. Yang and M. H. Wu, A new optically-induced dielectrophoretic (ODEP) force-based scheme for effective cell sorting, *Int. J. Electrochem. Sci.*, 2012, **7**, 12656–12667.

169 M. Du, G. Li, Z. Wang, Y. Ge and F. Liu, Rapid isolation method of Saccharomyces cerevisiae based on optically induced dielectrophoresis technique for fungal infection diagnosis, *Appl. Opt.*, 2021, **60**(8), 2150–2157.

170 S. B. Huang, M. H. Wu, Y. H. Lin, C. H. Hsieh, C. L. Yang, H. C. Lin, C. P. Tseng and G. B. Lee, High-purity and label-free isolation of circulating tumor cells (CTCs) in a microfluidic platform by using optically-induced-dielectrophoretic (ODEP) force, *Lab Chip*, 2013, **13**(7), 1371–1383.

171 W. P. Chou, H. M. Wang, J. H. Chang, T. K. Chiu, C. H. Hsieh, C. J. Liao and M. H. Wu, The utilization of optically-induced-dielectrophoresis (ODEP)-based virtual cell filters in a microfluidic system for continuous isolation and purification of circulating tumour cells (CTCs) based on their size characteristics, *Sens. Actuators, B*, 2017, **241**, 245–254.

172 T. K. Chiu, A. C. Chao, W. P. Chou, C. J. Liao, H. M. Wang, J. H. Chang, P. H. Chen and M. H. Wu, Optically-induced-dielectrophoresis (ODEP)-based cell manipulation in a microfluidic system for high-purity isolation of integral circulating tumor cell (CTC) clusters based on their size characteristics, *Sens. Actuators, B*, 2018, **258**, 1161–1173.

173 S. B. Huang, S. L. Liu, J. T. Li and M. H. Wu, Label-free live and dead cell separation method using a high-efficiency Optically-Induced Dielectrophoretic (ODEP) force-based microfluidic platform, *Int. J. Autom. Smart Technol.*, 2014, **4**(2), 83–91.

174 A. T. Ohta, P. Y. Chiou, H. L. Phan, S. W. Sherwood, J. M. Yang, A. N. Lau, H. Y. Hsu, A. Jamshidi and M. C. Wu, Optically controlled cell discrimination and trapping using optoelectronic tweezers, *IEEE J. Sel. Top. Quantum Electron.*, 2007, **13**(2), 235–243.

175 H. Hwang, D. H. Lee, W. Choi and J. K. Park, Enhanced discrimination of normal oocytes using optically induced pulling-up dielectrophoretic force, *Biomicrofluidics*, 2009, **3**(1), 014103.

176 W. Liang, J. Liu, X. Yang, Q. Zhang, W. Yang, H. Zhang and L. Liu, Microfluidic-based cancer cell separation using active and passive mechanisms, *Microfluid. Nanofluidics*, 2020, **24**, 26.

177 L. Miccio, V. Marchesano, M. Mugnano, S. Grilli and P. Ferraro, Light induced DEP for immobilizing and orienting Escherichia coli bacteria, *Opt. Lasers Eng.*, 2016, **76**, 34–39.

178 H. Y. Wang, C. Y. Chen, P. Y. Chu, Y. X. Zhu, C. H. Hsieh, J. J. Lu and M. H. Wu, Application of an optically induced dielectrophoresis (ODEP)-based microfluidic system for the detection and isolation of bacteria with heterogeneity of antibiotic susceptibility, *Sens. Actuators, B*, 2020, **307**, 127540.

179 Y. S. Chen, C. P. Lai, C. Chen and G. B. Lee, Isolation and recovery of extracellular vesicles using optically-induced dielectrophoresis on an integrated microfluidic platform, *Lab Chip*, 2021, **21**(8), 1475–1483.

180 W. Liang, X. Yang, J. Wang, Y. Wang, H. Zhang, W. Yang and L. Liu, Label-free characterization of different kinds of cells using optoelectrokinetic-based microfluidics, *Opt. Lett.*, 2020, **45**(8), 2454–2457.

181 W. Liang, K. Zhang, X. Yang, L. Liu, H. Yu and W. Zhang, Distinctive translational and self-rotational motion of lymphoma cells in an optically induced non-rotational alternating current electric field, *Biomicrofluidics*, 2015, **9**(1), 014121.

182 L. H. Chau, W. Liang, F. W. Cheung, W. K. Liu, W. J. Li, S. C. Chen and G. B. Lee, Self-rotation of cells in an irrotational AC E-field in an opto-electrokinetics chip, *PLoS One*, 2013, **8**(1), e51577.

183 X. Yang, X. Niu, Z. Liu, Y. Zhao, G. Zhang, W. Liang and W. J. Li, Accurate extraction of the self-rotational speed for cells in an electrokinetics force field by an image matching algorithm, *Micromachines*, 2017, **8**(9), 282.

184 I. Turcu, Electric field induced rotation of spheres, *J. Phys. A: Math. Gen.*, 1987, **20**(11), 3301–3307.

185 C. Vaillier, T. Honegger, F. Kermarrec, X. Gidrol and D. Peyrade, Comprehensive analysis of human cells motion under an irrotational AC electric field in an electro-microfluidic chip, *PLoS One*, 2014, **9**(4), e95231.

186 M. Ouyang, W. K. Cheung, W. Liang, J. D. Mai, W. K. Liu and W. J. Li, Inducing self-rotation of cells with natural and artificial melanin in a linearly polarized alternating current electric field, *Biomicrofluidics*, 2013, **7**(5), 054112.

187 M. W. Rezanoor and P. Dutta, Combined AC electro-osmosis and dielectrophoresis for controlled rotation of microparticles, *Biomicrofluidics*, 2016, **10**(2), 024101.

188 X. Zhu, Manipulation of self-assembled microparticle chains by electroosmotic flow assisted electrorotation in an optoelectronic device, *Micromachines*, 2015, **6**(9), 1387–1405.

189 G. Zhang, M. Ouyang, J. Mai, W. J. Li and W. K. Liu, Automated rotation rate tracking of pigmented cells by a

customized block-matching algorithm, *SLAS Technol.*, 2013, **18**(2), 161–170.
190 Y. Zhao, D. Jia, X. Sha, G. Zhang and W. J. Li, Determination of the three-dimensional rate of cancer cell rotation in an optically-induced electrokinetics chip using an optical flow algorithm, *Micromachines*, 2018, **9**(3), 118.
191 W. Liang, Y. Wang, H. Zhang and L. Liu, Characterization of the self-rotational motion of stored red blood cells by using optically-induced electrokinetics, *Opt. Lett.*, 2016, **41**(12), 2763–2766.
192 C. H. Chuang, Y. M. Hsu and C. C. Yeh, The effects of nanoparticles uptaken by cells on electrorotation, *Electrophoresis*, 2009, **30**(9), 1449–1456.
193 W. Liang, Y. Zhao, L. Liu, Y. Wang, W. J. Li and G. B. Lee, Determination of cell membrane capacitance and conductance via optically induced electrokinetics, *Biophys. J.*, 2017, **113**(7), 1531–1539.
194 W. Liang, X. Yang, J. Wang, Y. Wang, W. Yang and L. Liu, Determination of Dielectric Properties of Cells using AC Electrokinetic-based Microfluidic Platform: A Review of Recent Advances, *Micromachines*, 2020, **11**(5), 513.
195 Y. Zhang, J. Zhao, H. Yu, P. Li, W. Liang, Z. Liu, G. B. Lee, L. Liu, W. J. Li and Z. Wang, Detection and isolation of free cancer cells from ascites and peritoneal lavages using optically induced electrokinetics (OEK), *Sci. Adv.*, 2020, **6**(32), eaba9628.
196 Y. Zhao, H. S. Lai, G. Zhang, G. B. Lee and W. J. Li, Rapid determination of cell mass and density using digitally controlled electric field in a microfluidic chip, *Lab Chip*, 2014, **14**(22), 4426–4434.
197 Y. Zhao, H. S. Lai, G. Zhang, G. B. Lee and W. J. Li, Measurement of single leukemia cell's density and mass using optically induced electric field in a microfluidics chip, *Biomicrofluidics*, 2015, **9**(2), 022406.
198 Y. Zhao, W. Liang, G. Zhang, J. D. Mai, L. Liu, G. B. Lee and W. J. Li, Distinguishing cells by their first-order transient motion response under an optically induced dielectrophoretic force field, *Appl. Phys. Lett.*, 2013, **103**(18), 183702.
199 J. K. Valley, P. Swinton, W. J. Boscardin, T. F. Lue, P. F. Rinaudo, M. C. Wu and M. M. Garcia, Preimplantation mouse embryo selection guided by light-induced dielectrophoresis, *PLoS One*, 2010, **5**(4), e10160.
200 L. Chang, L. Li, J. Shi, Y. Sheng, W. Lu, D. Gallego-Perez and L. J. Lee, Micro-/nanoscale electroporation, *Lab Chip*, 2016, **16**(21), 4047–4062.
201 S. Movahed and D. Li, Microfluidics cell electroporation, *Microfluid. Nanofluidics*, 2011, **10**(4), 703–734.
202 J. K. Valley, S. Neale, H. Y. Hsu, A. T. Ohta, A. Jamshidi and M. C. Wu, Parallel single-cell light-induced electroporation and dielectrophoretic manipulation, *Lab Chip*, 2009, **9**(12), 1714–1720.
203 C. H. Wang, Y. H. Lee, H. T. Kuo, W. F. Liang, W. J. Li and G. B. Lee, Dielectrophoretically-assisted electroporation using light-activated virtual microelectrodes for multiple DNA transfection, *Lab Chip*, 2014, **14**(3), 592–601.
204 G. B. Lee, C. J. Chang, C. H. Wang, M. Y. Lu and Y. Y. Luo, Continuous medium exchange and optically induced electroporation of cells in an integrated microfluidic system, *Microsyst. Nanoeng.*, 2015, **1**, 15007.
205 P. F. Yang, C. H. Wang and G. B. Lee, Optically-induced cell fusion on cell pairing microstructures, *Sci. Rep.*, 2016, **6**, 22036.
206 Y. C. Hsiao, C. H. Wang, W. B. Lee and G. B. Lee, Automatic cell fusion via optically-induced dielectrophoresis and optically-induced locally-enhanced electric field on a microfluidic chip, *Biomicrofluidics*, 2018, **12**(3), 034108.
207 W. He, L. Huang, Y. Feng, F. Liang, W. Ding and W. Wang, Highly integrated microfluidic device for cell pairing, fusion and culture, *Biomicrofluidics*, 2019, **13**(5), 054109.
208 A. M. Skelley, O. Kirak, H. Suh, R. Jaenisch and J. Voldman, Microfluidic control of cell pairing and fusion, *Nat. Methods*, 2009, **6**(2), 147–152.
209 Y. H. Lin and G. B. Lee, An optically induced cell lysis device using dielectrophoresis, *Appl. Phys. Lett.*, 2009, **94**(3), 033901.
210 C. Witte, C. Kremer, M. Chanasakulniyom, J. Reboud, R. Wilson, J. M. Cooper and S. L. Neale, Spatially selecting a single cell for lysis using light-induced electric fields, *Small*, 2014, **10**(15), 3026–3031.
211 Y. H. Lin and G. B. Lee, An integrated cell counting and continuous cell lysis device using an optically induced electric field, *Sens. Actuators, B*, 2010, **145**(2), 854–860.
212 S. H. Huang, L. Y. Hung and G. B. Lee, Continuous nucleus extraction by optically-induced cell lysis on a batch-type microfluidic platform, *Lab Chip*, 2016, **16**(8), 1447–1456.
213 C. Kremer, C. Witte, S. L. Neale, J. Reboud, M. P. Barrett and J. M. Coopr, Shape-dependent optoelectronic cell lysis, *Angew. Chem., Int. Ed.*, 2014, **126**(3), 861–865.
214 S. M. Yang, S. Y. Tseng, H. P. Chen, L. Hsu and C. H. Liu, Cell patterning via diffraction-induced optoelectronic dielectrophoresis force on an organic photoconductive chip, *Lab Chip*, 2013, **13**(19), 3893–3902.
215 W. Hu, K. Ishii and A. T. Ohta, Cell patterning in a hydrogel using optically induced dielectrophoresis, 2016 International Conference on Optical MEMS and Nanophotonics, 2016 International Conference on Optical MEMS and Nanophotonics (OMN), Singapore, 2016.
216 Y. H. Lin, Y. W. Yang, Y. D. Chen, S. S. Wang, Y. H. Chang and M. H. Wu, The application of an optically switched dielectrophoretic (ODEP) force for the manipulation and assembly of cell-encapsulating alginate microbeads in a microfluidic perfusion cell culture system for bottom-up tissue engineering, *Lab Chip*, 2012, **12**(6), 1164–1173.
217 H. J. Gi, D. Han and J. K. Park, Optoelectrofluidic printing system for fabricating hydrogel sheets with on-demand patterned cells and microparticles, *Biofabrication*, 2017, **9**(1), 015011.
218 J. Cui, H. P. Wang, Q. Shi and T. Sun, Pulsed Microfluid Force-Based On-Chip Modular Fabrication for Liver Lobule-Like 3D Cellular Models, *Cyborg Bionic Syst.*, 2021, **2021**, 9871396.

219 W. Yang, H. Yu, W. Liang, Y. Wang and L. Liu, Rapid fabrication of hydrogel microstructures using UV-induced projection printing, *Micromachines*, 2015, **6**(12), 1903–1913.
220 W. Yang, S. Cai, Y. Chen, W. Liang, Y. Lai, H. Yu, Y. Wang and L. Liu, Modular and Customized Fabrication of 3D Functional Microgels for Bottom-Up Tissue Engineering and Drug Screening, *Adv. Mater. Technol.*, 2020, **5**(5), 1900847.
221 N. Liu, W. Liang, L. Liu, Y. Wang, J. D. Mai, G. B. Lee and W. J. Li, Extracellular-controlled breast cancer cell formation and growth using non-UV patterned hydrogels via optically-induced electrokinetics, *Lab Chip*, 2014, **14**(7), 1367–1376.
222 S. Wang, W. Liang, Z. Dong, V. G. Lee and W. J. Li, Fabrication of micrometer-and nanometer-scale polymer structures by visible light induced dielectrophoresis (DEP) force, *Micromachines*, 2011, **2**(4), 431–442.
223 N. Liu, P. Li, L. Liu, H. Yu, Y. Wang, G. B. Lee and W. J. Li, 3-D non-UV digital printing of hydrogel microstructures by optically controlled digital electropolymerization, *J. Microelectromech. Syst.*, 2015, **24**(6), 2128–2135.
224 P. Li, H. Yu, N. Liu, F. Wang, G. B. Lee, Y. Wang, L. Liu and W. J. Li, Visible light induced electropolymerization of suspended hydrogel bioscaffolds in a microfluidic chip, *Biomater. Sci.*, 2018, **6**(6), 1371–1378.
225 G. Dai, W. Wan, Y. Zhao, Z. Wang, W. Li, P. Shi and Y. Shen, Controllable 3D alginate hydrogel patterning via visible-light induced electrodeposition, *Biofabrication*, 2016, **8**(2), 025004.
226 Y. Liu, C. Wu, H. S. Lai, Y. Y. Liu, W. J. Li and Y. J. Shen, Three-dimensional calcium alginate hydrogel assembly via tiopc-based light-induced controllable electrodeposition, *Micromachines*, 2017, **8**(6), 192.
227 F. Wang, H. Yu, N. Liu, J. D. Mai, L. Liu, G. B. Lee and W. J. Li, Non-ultraviolet-based patterning of polymer structures by optically induced electrohydrodynamic instability, *Appl. Phys. Lett.*, 2013, **103**(21), 214101.
228 F. Wang, L. Liu, G. Li, P. Li, Y. Wen, G. Zhang, Y. Wang, G. B. Lee and W. J. Li, Thermometry of photosensitive and optically induced electrokinetics chips, *Microsyst. Nanoeng.*, 2018, **4**, 26.
229 F. Wang, H. Yu, W. Liang, L. Liu, J. D. Mai, G. B. Lee and W. J. Li, Optically induced electrohydrodynamic instability-based micro-patterning of fluidic thin films, *Microfluid. Nanofluid.*, 2014, **16**(6), 1097–1106.
230 F. Wang, F. Fei, L. Liu, H. Yu, P. Yu, Y. Wang, G. B. Lee and W. J. Li, Exploring pulse-voltage-triggered optically induced electrohydrodynamic instability for femtolitre droplet generation, *Appl. Phys. Lett.*, 2014, **104**(26), 264103.
231 G. B. Lee, H. C. Wu, P. F. Yang and J. D. Mai, Optically induced dielectropheresis sorting with automated medium exchange in an integrated optofluidic device resulting in higher cell viability, *Lab Chip*, 2014, **14**(15), 2837–2843.
232 P. Y. Chu, C. H. Hsieh and M. H. Wu, The Combination of Immunomagnetic Bead-Based Cell Isolation and Optically Induced Dielectrophoresis (ODEP)-Based Microfluidic Device for the Negative Selection-Based Isolation of Circulating Tumor Cells (CTCs), *Front. Bioeng. Biotechnol.*, 2020, **8**, 921.
233 S. Zhang, E. Y. Scott, J. Singh, Y. Chen, Y. Zhang, M. Elsayed, M. D. Chamberlain, N. Shakiba, K. Adams, S. Yu, C. M. Morshead, P. W. Zandstra and A. R. Wheeler, The optoelectronic microrobot: A versatile toolbox for micromanipulation, *Proc. Natl. Acad. Sci. U. S. A.*, 2019, **116**(30), 14823–14828.
234 Y. H. Lin and G. B. Lee, Optically induced flow cytometry for continuous microparticle counting and sorting, *Biosens. Bioelectron.*, 2008, **24**(4), 572–578.
235 C. Witte, J. Reboud, J. M. Cooper and S. L. Neale, Channel integrated optoelectronic tweezer chip for microfluidic particle manipulation, *J. Micromech. Microeng.*, 2020, **30**(4), 045004.
236 S. M. Yang, T. M. Yu, M. H. Liu, L. Hsu and C. H. Liu, Moldless PEGDA-based optoelectrofluidic platform for microparticle selection, *Adv Optoelectron.*, 2011, **2011**, 1–8.
237 M. K. Raj and S. Chakraborty, PDMS microfluidics: A mini review, *J. Appl. Polym. Sci.*, 2020, **137**(27), 48958.
238 X. Xu, X. Huang, J. Sun, J. Chen, G. Wu, Y. Yao, N. Zhou, S. Wang and L. Sun, 3D-Stacked Multistage Inertial Microfluidic Chip for High-Throughput Enrichment of Circulating Tumor Cells, *Cyborg Bionic Syst.*, 2022, **2022**, 9829287.
239 K. W. Huang, S. Sattar, J. F. Zhong, C. H. Chou, H. K. Tsai and P. Y. Chiou, Electrodes for microfluidic integrated optoelectronic tweezers, *Adv. Optoelectron.*, 2011, **2011**, 1–10.
240 A. H. Ng, B. B. Li, M. D. Chamberlain and A. R. Wheeler, Digital microfluidic cell culture, *Annu. Rev. Biomed. Eng.*, 2015, **17**, 91–112.
241 G. J. Shah, A. T. Ohta, E. P. Chiou and M. C. Wu, EWOD-driven droplet microfluidic device integrated with optoelectronic tweezers as an automated platform for cellular isolation and analysis, *Lab Chip*, 2009, **9**(12), 1732–1739.
242 D. Baigl, Photo-actuation of liquids for light-driven microfluidics: state of the art and perspectives, *Lab Chip*, 2012, **12**(19), 3637–3653.
243 P. Y. Chiou, S. Y. Park and M. C. Wu, Continuous optoelectrowetting for picoliter droplet manipulation, *Appl. Phys. Lett.*, 2008, **93**(22), 221110.
244 S. N. Pei, J. K. Valley, Y. L. Wang and M. C. Wu, Distributed circuit model for multi-color light-actuated optoelectrowetting microfluidic device, *J. Lightwave Technol.*, 2015, **33**(16), 3486–3493.
245 J. K. Valley, S. NingPei, A. Jamshidi, H. Y. Hsu and M. C. Wu, A unified platform for optoelectrowetting and optoelectronic tweezers, *Lab Chip*, 2011, **11**(7), 1292–1297.
246 T. M. Yu, S. M. Yang, C. Y. Fu, M. H. Liu, L. Hsu, H. Y. Chang and C. H. Liu, Integration of organic optoelectrowetting and poly (ethylene) glycol diacrylate (PEGDA) microfluidics for droplets manipulation, *Sens. Actuators, B*, 2013, **180**, 35–42.
247 H. S. Chuang, A. Kumar and S. T. Wereley, Open optoelectrowetting droplet actuation, *Appl. Phys. Lett.*, 2008, **93**(6), 064104.

248 S. Y. Park, M. A. Teitell and E. P. Chiou, Single-sided continuous optoelectrowetting (SCOEW) for droplet manipulation with light patterns, *Lab Chip*, 2010, **10**(13), 1655–1661.
249 D. Jiang and S. Y. Park, Light-driven 3D droplet manipulation on flexible optoelectrowetting devices fabricated by a simple spin-coating method, *Lab Chip*, 2016, **16**(10), 1831–1839.
250 D. Jiang, S. Lee, S. W. Bae and S. Y. Park, Smartphone integrated optoelectrowetting (SiOEW) for on-chip sample processing and microscopic detection of water quality, *Lab Chip*, 2018, **18**(3), 532–539.
251 S. K. Thio, S. W. Bae and S. Y. Park, Plasmonic nanoparticle-enhanced optoelectrowetting (OEW) for effective light-driven droplet manipulation, *Sens. Actuators, B*, 2020, **308**, 127704.
252 M. A. Zaman, P. Padhy, Y. T. Cheng, L. Galambos and L. Hesselink, Optoelectronic tweezers with a non-uniform background field, *Appl. Phys. Lett.*, 2020, **117**(17), 171102.
253 C. Witte, R. Wilson, J. M. Cooper and S. L. Neale, *OET meets acoustic tweezing*, Optical Trapping and Optical Micromanipulation IX, San Diego, California, USA, 2012, vol. 8458, p. 84582I.
254 C. Witte, C. Kremer, J. M. Cooper and S. L. Neale, *Continuous cell lysis in microfluidics through acoustic and optoelectronic tweezers*, Microfluidics, BioMEMS, and Medical Microsystems XI, San Diego, California, United States, 2013, vol. 8615, p. 86150T.
255 C. Bendkowski, L. Mennillo, T. Xu, M. Elsayed, F. Stojic, H. Edwards, S. Zhang, C. Morshead, V. Pawar, A. R. Wheeler and D. Stoyanov, Autonomous object harvesting using synchronized optoelectronic microrobots, 2021 IEEE/RSJ International Conference on Intelligent Robots and Systems (IROS), Prague, Czech Republic, 2021, pp. 7498–7504.
256 S. Zhang, M. Elsayed, R. Peng, Y. Chen, Y. Zhang, J. Peng, W. Li, M. D. Chamberlain, A. Nikitina, S. Yu, X. Liu, S. L. Neale and A. R. Wheeler, Reconfigurable multi-component micromachines driven by optoelectronic tweezers, *Nat. Commun.*, 2021, **12**, 5349.
257 **https://www.berkeleylights.com/**.
258 M. C. Wu, Optoelectronic Tweezers – An Optofluidic Platform for Digital Cell Biology, 2019 International Conference on Optical MEMS and Nanophotonics, Daejeon, South Korea, 2019, pp. 94–95.
259 A. Winters, K. McFadden, J. Bergen, J. Landas, K. A. Berry, A. Gonzalez, H. Salimi-Moosavi, C. M. Murawsky, P. Tagari and C. T. King, Rapid single B cell antibody discovery using nanopens and structured light, *mAbs*, 2019, **11**(6), 1025–1035.
260 M. Jorgolli, T. Nevill, A. Winters, I. Chen, S. Chong, F. F. Lin, M. Mock, C. Chen, K. Le, C. Tan and P. Jess, Nanoscale integration of single cell biologics discovery processes using optofluidic manipulation and monitoring, *Biotechnol. Bioeng.*, 2019, **116**(9), 2393–2411.
261 K. Le, C. Tan, S. Gupta, T. Guhan, H. Barkhordarian, J. Lull, J. Stevens and T. Munro, A novel mammalian cell line development platform utilizing nanofluidics and optoelectro positioning technology, *Biotechnol. Prog.*, 2018, **34**(6), 1438–1446.
262 K. Le, C. Tan, H. Le, J. Tat, E. Zasadzinska, J. Diep, R. Zastrow, C. Chen and J. Stevens, Assuring Clonality on the Beacon Digital Cell Line Development Platform, *Biotechnol. J.*, 2020, **15**(1), 1900247.
263 A. Mocciaro, T. L. Roth, H. M. Bennett, M. Soumillon, A. Shah, J. Hiatt, K. Chapman, A. Marson and G. Lavieu, Light-activated cell identification and sorting (LACIS) for selection of edited clones on a nanofluidic device, *Commun. Biol.*, 2018, **1**, 41.
264 Y. Bronevetsky, Directly test individual T cell function with fewer cells on the berkeley lights lightning™ platform, *Cytotherapy*, 2020, **22**(5), S119.
265 M. Rienzo, K.-C. Lin and K. C. Mobilia, *et al.*, High-throughput optofluidic screening for improved microbial cell factories via real-time micron-scale productivity monitoring, *Lab Chip*, 2021, **15**(21), 2901–2912.
266 **https://www.berkeleylights.com/blog/racing-to-find-the-right-cells-our-covid-19-success-stories/**.
267 S. J. Zost, P. Gilchuk and R. E. Chen, *et al.*, Rapid isolation and profiling of a diverse panel of human monoclonal antibodies targeting the SARS-CoV-2 spike protein, *Nat. Med.*, 2020, **26**(9), 1422–1427.
268 H. Cho, K. K. Gonzales-Wartz and D. Huang, *et al.*, Bispecific antibodies targeting distinct regions of the spike protein potently neutralize SARS-CoV-2 variants of concern, *Sci. Transl. Med.*, 2021, **13**(616), eabj5413.

